DEVICES TO STUDY CANCER CELL BEHAVIOR

by

MOHAMMAD GHASSAN ABDALLAH

Presented to the Faculty of the Graduate School of

The University of Texas at Arlington

in Partial Fulfillment of the Requirements for the Degree of

DOCTOR OF PHILOSOPHY

THE UNIVERSITY OF TEXAS AT ARLINGTON

May 2018

Acknowledgments

Abstract

DEVICES TO STUDY CANCER CELL BEHAVIOR

Mohammad G. Abdallah, PhD

The University of Texas at Arlington, 2018

Supervising Professor: Samir Iqbal

Cancer is a major health concern that effects millions of people worldwide. The main contributing factor to the deadliness of the disease is cancer metastasis, where the cancer cells break away from the primary tumor site, transmigrate through the endothelium, and form secondary tumors in distant areas. Many studies have identified links between the mechanical properties of the cellular microenvironment and the behavior of cancer cells. Also, nanobiotechnology and bioMEMS have had a tremendous impact on biosensing in the areas of cancer cell detection and therapeutics, disease diagnostics, and DNA analysis. Most current technologies enable observation of only the population-level average and often ignore the vast degree of cell heterogeneity present even in clonal populations.

This research work focuses on four areas: 1) Simulation and Development of solid-state field-effect transistors with micropillared gates for sensing of cancer cell ion exchange; 2) Synthesis and surface functionalization of nanoporous PLGA microparticles; 3) Glioblastoma multiforme heterogeneity profiling with solid-state micropores; 4) Microfluidic approach to create microencapsulation for single cell confinements. This dissertation provides a new multidisciplinary approach to detect and analyze cancer cell in a population of background cells, and understanding the fundamental molecular

bioelectricity of cellular processes can open up a new cell sequencing and cytometry methods of research previously not perceived with older technologies.

These approaches showed an ability to isolate and study a single cell behavior and can be potentially used in the lab on a chip system. Overall, our novel approaches to study cell behavior are simple, reliable, low cost, and do not damage cells.

Table of Contents

Chapter 1

Introduction

For people with concerns about health issues, the physician's office is the first contact with healthcare. Physician's waiting room is usually busy with patients of all ages with different symptoms and reasons for being there. With a physician's competence and medical experience, they know what can be easily cured, what should be followed up and what needs to be referred to a specialist. The accurate testing of clinical parameters are the key for making important medical decisions. The dominant model of medical testing is a centralized laboratory; where analytical processes are done to manage large numbers of samples at relatively low cost (Figure 1.1). This trend is well established in biochemistry and hematology and is now extending to other disciplines including microbiology and anatomical pathology. However, healthcare is changing; partially because of economic pressures and the general recognition of that care needs to be less fragmented and more patient-centered. The need to make healthcare patient-centered is a global trend and based on the premise that healthcare should be organized more around the patient than the provider. The research projects presented in this dissertation focuses on the feasibility of development devices and methods to study cancer cells behavior. There are differences between the normal cell and tumor cells properties. The cell attributes of one type of tumor cells are also different from the other types of tumor. In addition, there are differences between cells of one type of tumor.
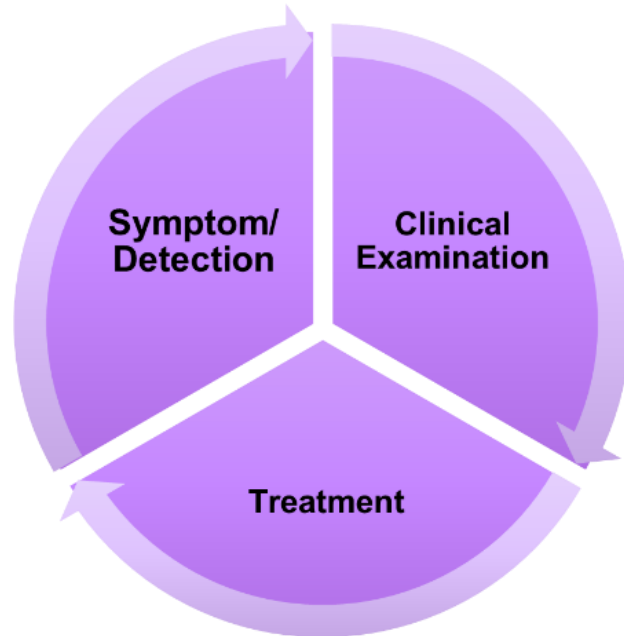
Figure 1.1 Patient's life cycle

1.1 Structure of Dissertation

The overall goal of this work is to introduce novel devices and approaches for studying cancer cell behavior that can help in designing a new class of techniques to study single cell. This dissertation is divided into 7 chapters. The breakdown of chapters is given below:

1.1.1 Introduction (Chapter 1)

This chapter is meant to introduce the reader to the drive and objective behind the entire research work. It also explains the advantages of using new engineered devices in medicine.

1.1.2 Background and Review (Chapter 2)

Chapter 2 reviews origin of cancer, cancer cell molecular biology and current methods to study single cell. It gives an overview of the research work done in this field and the challenges.

1.1.3 Simulation of Sensing Cancer Cell Ion Exchange as Biomarker (Chapter 3)

Inability to detect small concentrations of cancer cells in the early stages of disease is a major barrier for early diagnosis. Molecular bioelectricity, which depicts voltage gradients in non-excitable cells to coordinate morphogenesis, tissue development, repair, and cancer formation, is shown here as a novel modality to detect cancerous behavior. The design, simulation and electrical characterization of the ion-sensitive field-effective transistor, (ISFETs) are shown to detect cancer cells based on their molecular bioelectricity. ISFETs generate low impedance signals and consume a low amount of power. The small size of ISFETs enables miniature diagnosis devices. Therefore, ISFET allows for low sample requirements combined with a rapid response. ISFETs have the potential for selective detection of certain ions in complex samples efficiently and can lead the way for low-cost, lab-on-a-chip devices.

1.1.4 Synthesis and Surface Functionalization of Nanoporous PLGA Microparticles (Chapter 4)

Polylactic-co-glycolic acid (PLGA) microparticles are widely used for drug delivery. In cancer cell, ion channels have been recognized to play important roles in cancer pathology, as these regulate key events in cell proliferation and cancer initiation and progression. Ion channels are ideal drug targets as the respective small molecules may be effective from the extracellular space and do not need to enter the target cells. The development of cancer treatment using ion channel targeting compounds is still in early

13

stages, although some studies have shown that some voltage-gated ion channel (VGIC) blockers can inhibit cell behaviors associated with metastasis. We developed a simple and effective method to control the nanoporous formation, size, density and the surface functionalization of PLGA microparticles. PLGA microparticles were synthesized using water-in-oil-in-water (w/o/w) double emulsion method. The synthesis of nanoporous microparticles with this novel, rapid, inexpensive method, and easily controllable properties can be useful for applications in targeting one or multiple VGIC in cancer patients.

1.1.5 Cancer Heterogeneity Profiling with Solid-state Micropore (Chapter 5)

Glioblastoma multiforme (GBM) is the most common and lethal type of brain cancer. It is characterized by widespread heterogeneity at the cellular and molecular levels. The detection of this heterogeneity is valuable for patient's diagnosis. Herein, solid-state 20 μm diameter micropore made in thin suspended silicon dioxide membrane is used as cell sensor device. The device relies on cell's mechano-physical properties as an indicator to differentiate between the sub-types of GBM. A library of GBM cell lines (U251, U87, D54 EGFRviii and G55) was created by measuring the differences in cell's properties from their distinct electrical profiles. Each GBM sub-type has a distinct phenotype and this was depicted in their cell translocation behaviors. The library was used to distinguish cells from samples of brain tumor patients. The micropore device accurately detected sample cell sub-types by comparing data with the GBM library. The micropore approach is simple, can be implemented at low cost and can be used in the clinical setups and operation theaters to detect and identify GBM subtypes from patient samples.

1.1.6 Microfluidic Approach to Microencapsulate Single Cell (Chapter 6)

It is important to achieve complete cellular analysis at high throughput and screening so hundreds of thousands of cells can be analyzed within seconds. We present

novel microcapsules made of poly (lactic-co-glycolic acid) (PLGA) to encapsulate the cells and provide a single cell view. Cells in microcapsules were not masked by the intrinsic heterogeneity of the cell population. The cell microencapsulations were ~200 nl on average and provided 3D cell containment chambers. The hollow microcapsules were fabricated using a simple polydimethylsiloxane (PDMS) microfluidic device. The PDMS device had Y-shaped channels through which cells were focused between flowing PLGA solution. The microcapsule cores contained cells with PLGA acting as an encapsulating membrane. The shapes of the microcapsules were controlled by altering cells/PLGA flow rates. Using this design to encapsulate cells fulfilled several often-conflicting criteria, such as permeability, stability, and biocompatibility. The suitability of this novel microenvironment formulation for live cell encapsulation was evaluated using human glioblastoma multiforme (hGBM) cells. To demonstrate an efficient encapsulation for one and two cells, we varied the flow rate of cells and PLGA solutions and observed a significant effect of flow rate on encapsulation. The cell viability was evaluated post-encapsulation. The hollow PLGA microcapsule can be used for encapsulation of many cells and potentially developed into a point-of-care cell profiling device for diseases.

1.1.7 Future Research Directions (Chapter 7)

Chapter 7 covers future scopes and potential use of developed single-cell analysis platforms. It includes the direction of more work that could supplement/complement current work.

Chapter 2

Background and Literature Review

The medical diagnostic device field has seen exceptional growth and development in last few years. This field holds one of the greatest promises, drawing up contributions from biology, chemistry, physics, materials science, medicine, and engineering. The combination of biology and silicon at the micro and nanoscale offers tremendous opportunities for solving unmet medical needs and enables variety range of applications in diagnostics, sensing, therapeutics, and tissue engineering. The sensing and characterization of biological entities, processes, and interactions, by electrical means and novel solid-state devices will have an immediate impact in life sciences.

Cancer has a major societal impact in the United States (US) and across the globe. In 2018, an estimated 1,735,350 new cases of cancer are expected to be diagnosed in the United States, and 609,640 people are estimated to die of the disease. Figure 2.1 compares the projected number of cancer death in the US by 2020 versus the death rate. The very interesting observation that death rate is decreasing but cancer deaths are increasing. In Figure 2.2, the projected number of new cancer cases show almost ~2 million cases in the US by 2020. Also, the figure shows a constant incident rate per hundred thousand people. These two figures show that cancer is a disease scientists and researchers do not understand very well.

Therefore, it comes very clear for us that there is still improvement in each stage of a cancer patient from detection to treatment. It is summarized in Figure 2.3. First, there is a need to improve current methods of early cancer detection so patients can receive treatment when the cancer is in its early stages and has not metastasized to other areas of the body.

16
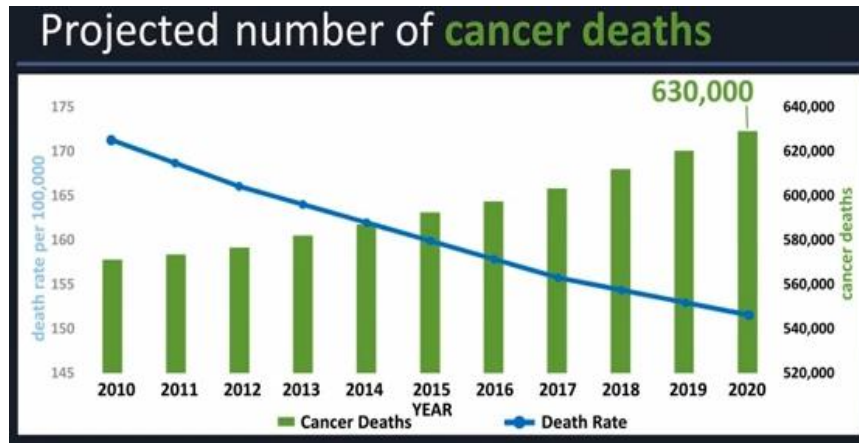
Figure 2.1 Recent cancer statistics number. Project number of cancer deaths in US by 2020 [1]
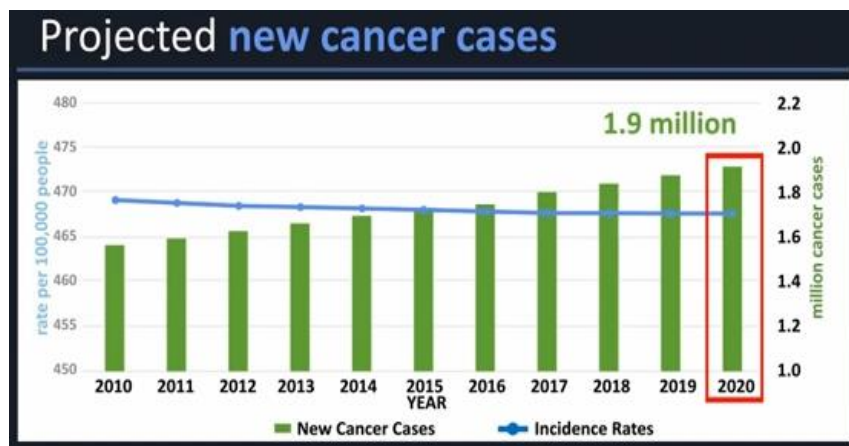
Figure 2.2 Recent cancer statistics number Projected new cancer cases in US by 2020 [1]

Second, every cell type has a characteristic profile based on its mechano-physical properties [2]. A cancer cell is well recognized for intratumoral and intertumoral heterogeneity. For example, Glioblastoma Multiforme the most common type of brain cancer. It is characterized by widespread heterogeneity at the cellular and molecular levels.

Figure 2.3. Improvement needed in current cancer patient life cycle

Finally, depending on the type and stage of cancer, treatments to eradicate the tumor or slow its growth may include some combination of surgery, radiation therapy, chemotherapy, hormone therapy or immunotherapy.

Many reports are available to document the growth in cancer diagnostic in vitro diagnostics (IVD) markets, including the point-of-care testing market. These markets were valued at USD 80.67 Billion in 2014 and expected to grow at during the forecast period (2014–2020), reaching USD 128.6 Billion by 2020 (Figure 2.4) [3].
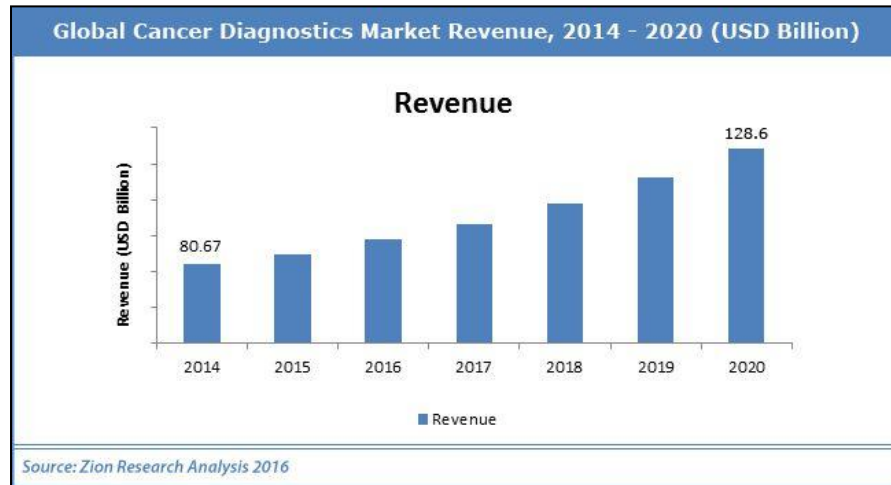
Figure 2.4 Cancer diagnostics Market forecast 2014-2020. Cancer diagnostics was valued at USD 80.67 billion in 2014 and expected to reach USD 128.6 billion in 2020 with 7.6% expecting to grow [3]

2.1 Molecular Bioelectricity

Several studies have contributed to the understanding of molecular mechanisms of cancers which range from genetic mutations to intricate biochemical and molecular pathways [4-5]. Although, cancer known for its complexity and heterogeneity and uncontrolled cell proliferation are critical for cancer initiation and progression [6-7].Recently, ion channels have been recognized to play an important role in cancer pathology as they are capable of regulating key events in cell proliferation and therefore, cancer initiation and progression [8–10]. The expression of specific ion channels has been linked with several stages of cancer and increased hostility. Furthermore, studies have shown manipulation of channel activity offers protection against several cancers. Thus, ion channels offer a novel strategy that can be potentially utilized to treat cancers. We introduce the role of voltage-gated ion channels in regulating cell proliferation, development, and progression of cancer.

Cell proliferation in normal cell is complex, well-synchronized event regulated by number of ions, molecules, and proteins associated with the cell cycle machinery including Ca^{2+}, ATP, cyclins, cyclin-dependent kinases and many other cell cycle regulators [11-12]. The cell cycle can be divided into phases (Figure 2.5), One of the most significant and dynamic factors that regulate cell cycle is the membrane potential (V_m; Voltage membrane) [13-14]. V_m is an electrical charge that is created by the difference in ionic concentration between the cell intracellular and extracellular environment. Ion channels and ion transporters play an essential role in generating V_m. They are selectively allowed ions cross the membrane according to chemical and/or electrical gradient. As a result of this movement, the V_m of a resting cell is negative. The cells are said to be depolarized (Figure 2.5) when the V_m is altered to relatively less negative state, whereas the cells are said to be hyperpolarized when the membrane potential is moved to more negative values than the resting membrane potential [15].

In a breast cancer cell line (MCF-7), it has been observed that the V_m during cell cycle progression correlates with the transition in each phase, such that, the MCF-7 cells in G1/S or G2/M transition enriches cells with hyperpolarized V_m while cells arrested in the G0/G1 and M Phases had enriched cells with depolarized V_m. [16]. Similarly, in neuroblastoma cell lines, cell cycle progression was observed to correlate with hyperpolarized V_m in G1-S transition and depolarized V_m at the M phase [17]. Thus, the progression of the cell cycle is accompanied by rhythmic oscillation of the V_m accompanied by transient hyperpolarization and depolarization [18–23]. Voltage-gated ion channels (VGICs) are group of ion channels that are selectively permeable to Na^+, K^+, Ca^{2+} or Cl^{1-} and respond to changes in the membrane potential [24–26]. VGICs generate potential in neurons or contraction in muscles in excitable cells. Also, VGICs play vital roles in non-
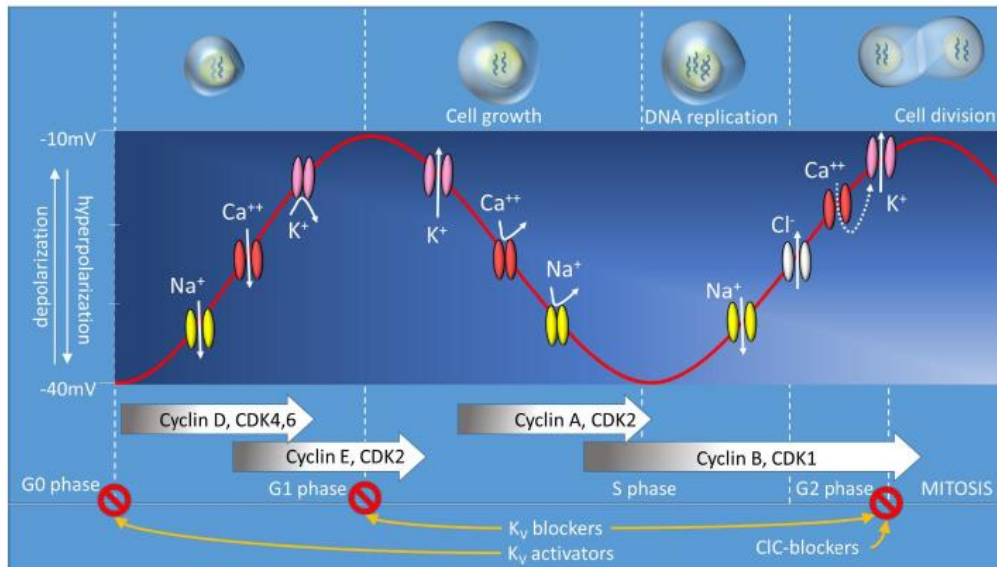
Figure 2.5. Schematic representation of possible involvement of different voltage-gated ion channels activity during the cell cycle of cancer cells. Reprinted by permission [27]

excitable cells including maintenance of cellular homeostasis by controlling ion transport, fluids, volume regulation and as well as proliferation.

2.2 Nano-Textured and Surfaces

PLGA is one of the most common polymers used for the development of drug delivery. It is biocompatible, biodegradable, non-toxic, and noninflammatory in the living environment, which are the foundations biomaterial and drug delivery applications. PLGA is hydrolyzed in acidic medium inside the body and gives two biodegradable monomers; glycolic acid and lactic acid as shown in Figure 2.6 [28]. The human body is known effectively to deal with these two monomers with no immune response is activated. Therefore, a minimal systemic toxicity is associated while using PLGA for drug delivery applications.
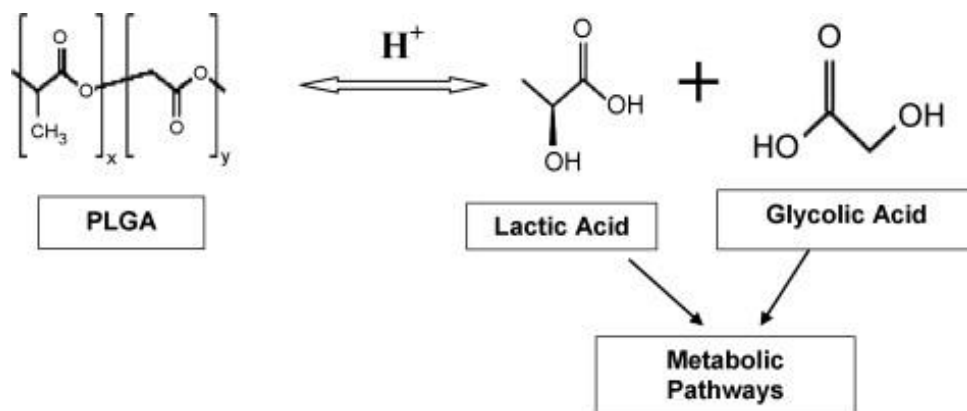
Figure 2.6 PLGA hydrolysis to produce lactic acid and glycolic monomers.

Reprinted with permission [28]

PLGA has been approved by Food and Drug Administration (FDA) for therapeutic use in humans. Thus, PLGA nanoparticles have been widely used to encapsulate various drugs. The PLGA nanoparticles protect unstable drugs loaded into these carriers from the biological surroundings and their small size facilitates them with capillary penetration and endosomal escape [29-30]. Furthermore, the high surface area offered by nanoparticles makes them exceedingly effective for targeted delivery to tumor cells or other tissues [31].

PLGA nanoparticles are mostly prepared by emulsion diffusion, solvent evaporation, interfacial deposition or nanoprecipitation methods [32-35]. Emulsion method starts with dissolving PLGA polymers in an organic solvent followed by separation in the aqueous phase. The aqueous phase contains a stabilizer, then homogenized to get nanoparticles. For solvent evaporation method, the PLGA polymers are dissolved in volatile organic solvents like methylene chloride, chloroform and acetonitrile, and acetone. The solution is then poured in a continuously stirring aqueous phase followed by sonication. The aqueous phase has a stabilizer in solvent evaporation technique. For

interfacial deposition method, nanoparticles are synthesized in the interfacial layer of water and the organic solvent. Then, sonication is used to separate the nanoparticles in this method of nanoparticles preparation. The most common method to prepare PLGA nanoparticles is nanoprecipitation. PLGA polymers are dissolved in a volatile organic solvent like acetone and the solution is added drop-wise into continuously stirring aqueous phase with stabilizer. Finally, the organic solvent is allowed to evaporate at low pressure. Figure 2.7 shows the synthesis schemes for PLGA nanoparticles.

PLGA nanoparticles generate acids during polymer erosion. These acids are neutralized by the bases in the human body or medium fluids. Slow diffusional mass transport across the nanoparticles results in a low pH within the drug carriers [36]. Such a drop in pH may affect drug stability and accelerates polymer degradation due to the autocatalytic effects which are the majors concerns in non-porous PLGA-based particles [37]. Porous drug delivery systems can overcome these autocatalytic effects by increasing the diffusivity of the molecules [38].
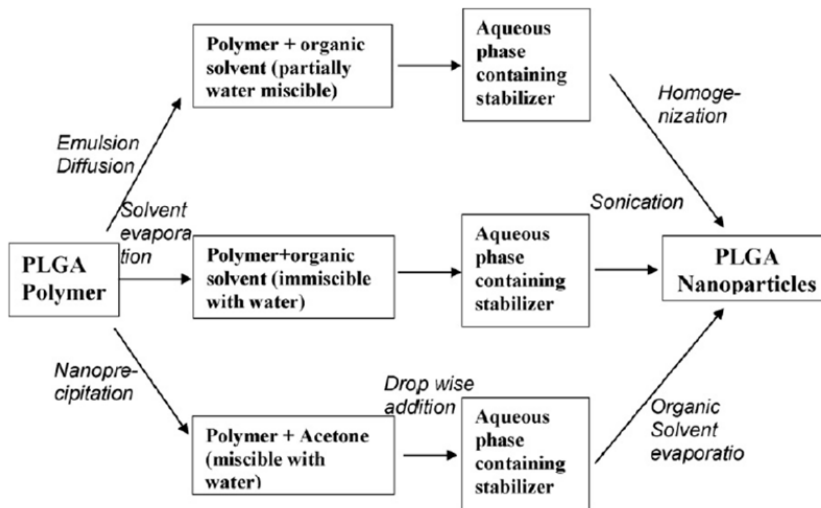
Figure 2.7 Schematic to show different methods for the synthesis of PLGA nanoparticles. Reprinted with permission [28]

23

Therefore, porous PLGA nanoparticles can be a much better carrier for controlled drug delivery systems. Drug release kinetics are directly controlled by the pore characteristics of porous PLGA nanoparticles so by controlling the pore morphology, highly controlled drug release systems can be designed [39].

Also, topographical surfaces at micro and nanoscale influence cell growth, orientation, adhesion and migration [40-41]. These features can be of any shape such as nanopores, nanotexture, micropillars, fibers, and ridges. The extracellular matrix (ECM) has porous structure at micro and nanoscale with fibrous collagen network [41]. Reproducing the ECM features can play serious rule to understand the cell behavior which would help in designing efficient treatment, artificial tissue, and implants. In biosensors applications, the nanostructures offer an increased surface area for molecule attachment which can increase the efficiency of systems sensing. It is well recognized the surface topography and substrate properties play important role in cell response. Microchannels are one feature used to study cell responses. These channels are patterned in an array form with certain orientation [42-44]. The orientation of the cells have been found to increase with increasing depth of the grooves, and it has been seen to decrease with increasing groove width [45]. It has been found that pore size played a key role in determining the tissue response and the primary cell line preferred rougher surfaces while transformed cells preferred wet etched smoother surfaces [46].

Also, the nanotextured surfaces show an effect on endothelial and smooth muscle cells by fabricating two type of substrates, one PLGA substrate and one NaOH treated PLGA substrate [47]. It has been reported that more smooth muscle cell growth on the NaOH treated PLGA substrate as compared with the PLGA substrate, while endothelial cells showed lesser growth on NaOH treated substrate as compared with the PLGA substrate [47].
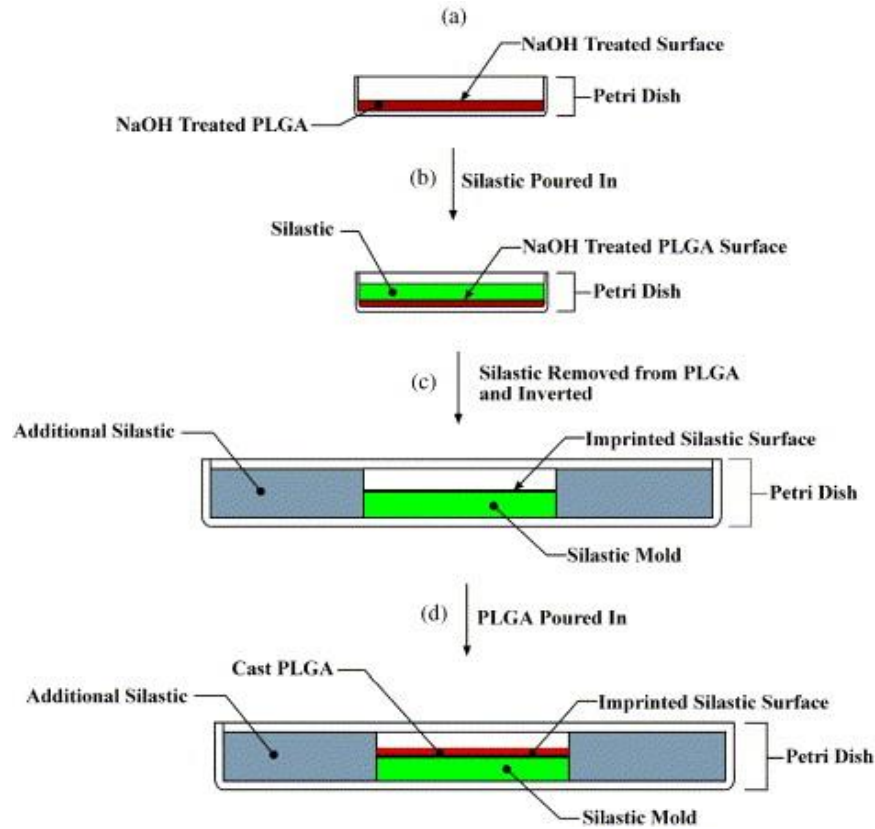
Figure 2.8 Nanotexture PLGA fabricating process flow. Reprinted by permission

[47]

Figure 2.8 shows nanotexture PLGA fabricating process flow polydimethylsiloxane (PDMS). They concluded that nano-texturing of PLGA substrate had increased the cell growth of both of the endothelial and smooth muscle cells [47].

2.3 Molecular heterogeneity of Glioblastoma Multiforme in Solid-state Micropore Sensor

Human solid tumors often have marked heterogeneity of both abnormal and normal cells on the histological, genetic, and gene expression levels. In cancer, not only tumors from different organs differ, but tumor located in the same organ is also different.

This heterogeneity among tumors is what is known as intertumor heterogeneity. Also, cells within a given tumor are different and this type of heterogeneity is known as intratumoral heterogeneity. The coexistence of different clones within the same tumor is apparently caused by stochastic events. The maintaining of existence is under pressure and can be favored or disfavored by the interaction with other cancer cells or host cells.

The concept of cancer heterogeneity is not new. Earlier in the nineteenth century, Rudolf Carl Virchow was the first to describe the pleomorphism of tumor cells [48]. Many observations have been made to describe differences within cancer cells morphology and protein expression in a tumor sample. The concept was limited due to cancer and host cells interaction, or random events within the cancer cells population. The differences were recognized to infiltrate of cancer cells in the surrounding tissue. However, there is the heterogeneity is one of the key feature of tumorigenesis responsible for tumor progression, resistance, metastatic potential, and relapse. The intratumor heterogeneity discusses an advantage in cancer cell environment fluctuations or selective pressure enforced by chemo/radiotherapy. The existence of cancer cells resistant to determined therapies has been demonstrated in various types of tumors before the treatment [49-50]. Thus, the study and understanding of cancer cells heterogeneity will characterize a new path to develop personalized therapies such as GBM, which is a type of tumor has known of intertumor and intratumor heterogeneity and resistance to treatment.

The clonal evolution model (Figure 2.9a), genetic mutations appear randomly and new phenotype is subjected to the pressure of natural selection. From this model, the clones will expand and outgrow the others, while heterogeneity would be explained as the presence of remaining weaker clones generated during tumor expansion. This variability would become significant in the case of environmental changes such as prompted by

26
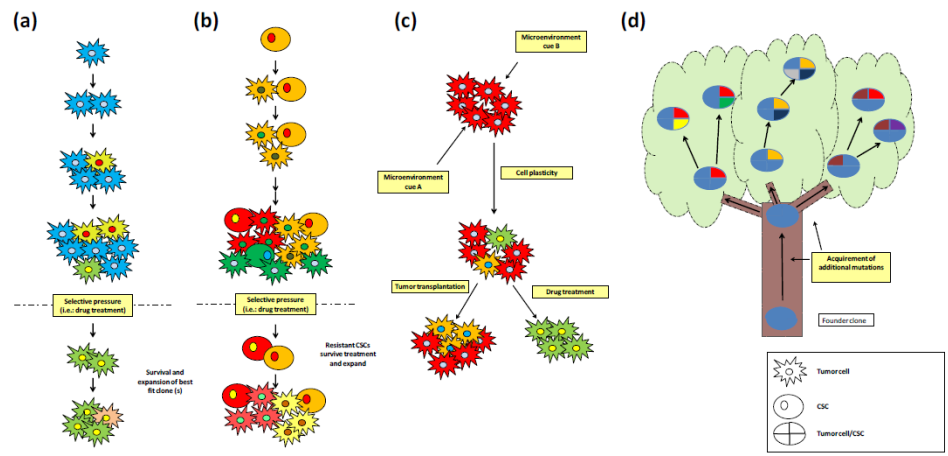
Figure 2.9 Models for the intratumor heterogeneity. (a) Clonal evolution. (b) CSC model. (c) Heterogeneity generated in response to the microenvironment. (d) Branched tree model

chemo/radiotherapy, when the previous acquisition of a resistant phenotype would allow a minor population to survive, expand, and become dominant [51].

Lately, cancer stem cell (CSC) theory (Figure 2.9b) became an accepted model of cancer initiation. This model suggests a hierarchical organization which tumor generates from cells with stem cell characteristics, known as CSCs. By division, these cells will maintain their population and generate more differentiated cells with proliferation properties that create the tumor. The heterogeneity is seen as the nature of CSCs (tumorigenic) and non CSCs with several degrees of differentiation regardless of their genetic background [52] most likely determined by epigenetic changes [53]. However, this model is based on assays of tumor transplantation that underestimate the tumorigenic potential of these cells depending on the mouse strain, conditions of the assay [53-54]. Glioblastoma CSCs were initially defined by the expression of the surface marker CD133, and cells not expressing this marker was thought to lack tumorigenic potential [55]. Recently, it has been shown that

27

a subpopulation of glioblastoma cells characterized by high expression of CD44 hold a stem-like a phenotype [56]. Also, it is been demonstrated that surface marker molecules can be used as CSC markers depending on the glioblastoma subtype. While CD133 seems to be expressed in proneural glioma CSCs, CD44 is highly expressed in mesenchymal glioma CSCs [57]. Other markers are under study and supporting the fact that some CD133 negative cells are able to form tumors in immunocompromised mice [58], suggesting that other markers are necessary for the identification of glioblastoma CSCs due to their heterogeneous nature. The clonal evolution and the CSC models have been considered as mutually exclusive, both models could be complementary as intraclonal heterogeneity has been observed in tumors in which CSCs were identified [59].

The microenvironment within a cancer cell is not homogeneous. Differences in oxygen, blood vessel density, growth factors, and composition of extracellular matrix are observed in human cancer cells. These differences affect cancer cells and might be the reason of phenotypic and genetic differences observed in tumor cells [54]. Cancer cell plasticity is a non-heritable source of heterogeneity that might explain some of the phenotypic differences between cancer cells and can be altered by the microenvironment [60] (Figure 2.9c).

The CSC model can be updated with the concept of various degrees of tumorigenic potential, determined either by the microenvironment cues or stochastic events [60-61]. Tumor cell plasticity might also be important in determining the drug resistance of tumor cells [62]. Based on results we obtained with current single-cell analysis approaches, the cancer clonal evolution as growing tree (Figure 2.9d) [63-64]. Other cancer clones, originating by the gain and the accumulation of new mutations, are represented as the branches of the growing tree. Hence, the branches represent heterogeneity observed in

cancer cells. The information of this tree structure of cancer cells would be predictive of the treatment.

The solid-state micropores have been used in a wide range of biosensor applications because of their chemical and thermal stability, mechanical strength. This type of biosensors have been used for patch clamp measurements, electroporation, the stability of lipid bilayers, bacterial activities monitoring, size-based discrimination, cell enumeration and electric characterization of cells [65-70]. The micropore sensors have also been deployed for determining the deformability of red blood cells (RBCs) where individual microscopic images of RBCs were processed to evaluate the cell's deformation while passing through the micropore [71]. Also, rectangular microscale slits and circular micropores have been used to study the deformation of RBCs while passing through them and concluded that the cells were more obstructed by circular micropores [71]. Therefore, circular shape micropores are remarkably sensitive to characterize the micro-organism passing through them.

There are several methods have been used to fabricate micropores in a simple, rapid and controlled environment. First, the heated probe tip has been used to drill a micropore in Teflon [67]. In this method, a heated Tungsten wire was used to make micropores in Teflon film. Ag/AgCl plate with a hole was attached to 12 μm thick Teflon film. A cover glass was used to clamp the Teflon film and the polished Tungsten tip. The tip was positioned at the center of the hole in Ag/AgCl plate by using a microscope as shown in Figure 2.10. The Tungsten wire tip was moved down to puncture a hole in the Teflon film at the point of contact. The process was characterized using Tungsten tips at different temperatures. It was observed that temperature gave optimum drilling of micropore without harming the Teflon film as shown in Figure 2.11. This is a simple and quick approach to fabricate micropores but is restricted by the material characteristics. This
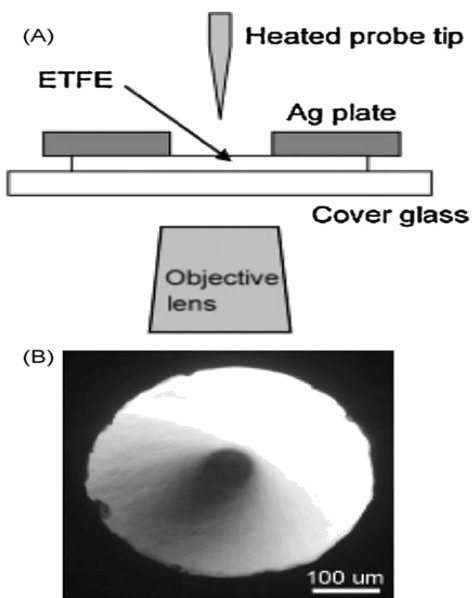
Figure 2.10 Fabrication of micropore using heated probe tip. (b) Placing the tip in

the middle of the opening in Ag/AgCl plat Reprinted by permission [67]
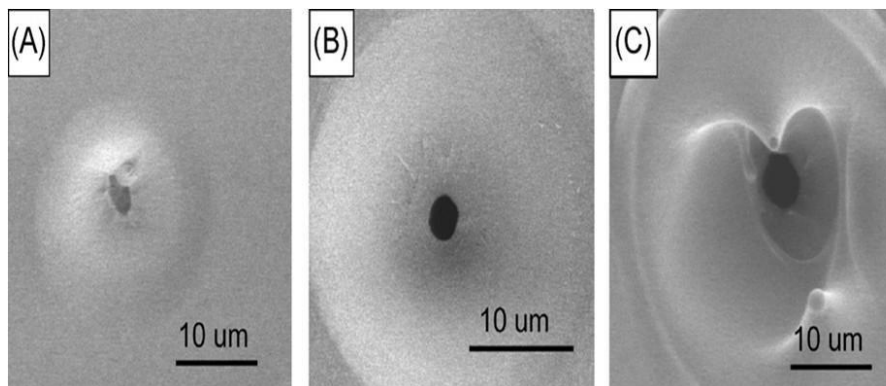
Figure 2.11 SEM images of fabricated micropore by using (A) Nonheated tip (B)

Moderately heated tip (C) Extremely heated tip. Reprinted by permission [67]

approach cannot be used to drill micropores in materials with a high melting point.

Therefore, solid-state micropores cannot be fabricated using this approach.

Photolithography approach followed by deep reactive ion etching (DRIE) can be used to fabricate solid-state micropores. This process has been used to manufacture silicon chip-based micropore devices [72]. Figure 2.12 shows the process flow for the fabrication of micropores. Herein, photolithography was used to define 2 µm circle shapes on the silicon substrate and DRIE was used to etch the silicon down to 20-40 µm. The photoresist was stripped off and the wafer was flipped for backside processing. Circles with 1 mm diameter centered on the 2 µm opening were defined and DRIE was used to etch down all the way to meet the 2 µm opening. Finally, silicon dioxide was deposited to isolate the two sides of the wafer. The oxide deposition reduced the micropore size and process could be used to decrease the diameter down to nano diameter. This method is limited by the fabrication process of DRIE and may result in irregular circular shapes of the fabricated pores.
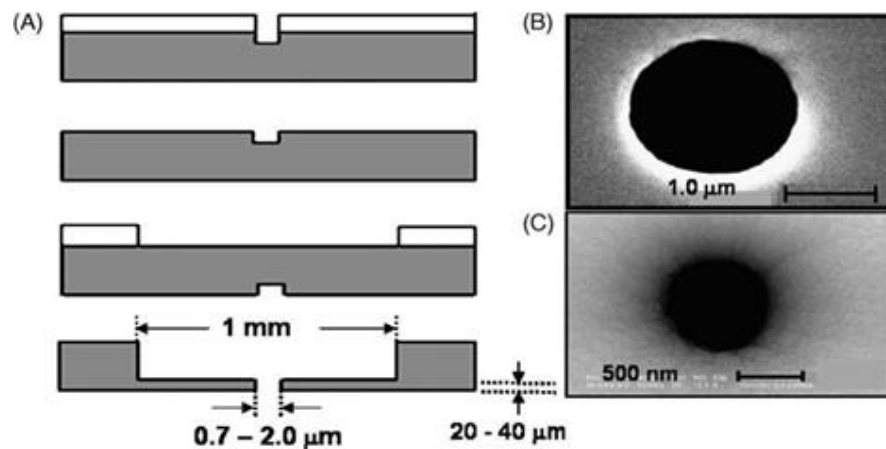
Figure 2.12 Fabrication process of micropores (a) Step by step fabrication process flow (b) SEM images of the micropore (C) SEM image of nanopore achieved by changing the oxide deposition process. Reprinted by permission [72]

2.4   Single Cell Microencapsulate

Polymers including nature and synthetic have been utilized for cell encapsulation. Natural polymers such as alginate, agarose, collagen, and hyaluronic acid more used because of their biocompatibility. On the other hand, synthetic polymers including poly(vinyl alcohol), poly(lactic-co-glycolic acid), polyacrylates, HEMA-MMA-MAA, polyphosphazines, and polyepoxides are widely used because of their consistent quality and characteristics compared to natural polymers. Alginate is a linear block polymer consisting of α-l-guluronic acid (G) and β-d-manuronic acid (M) blocks (Figure 2.13). Cations, such as Ca^{2+}, Ba^{2+}, and Sr^{2+}, link alginate molecules together through ionic cross-linking and forms alginate hydrogel capsules while encapsulating cells inside. The G and M contents of the alginate molecules can affect the gel properties including mechanical strength, biocompatibility, and permeability [73– 77].
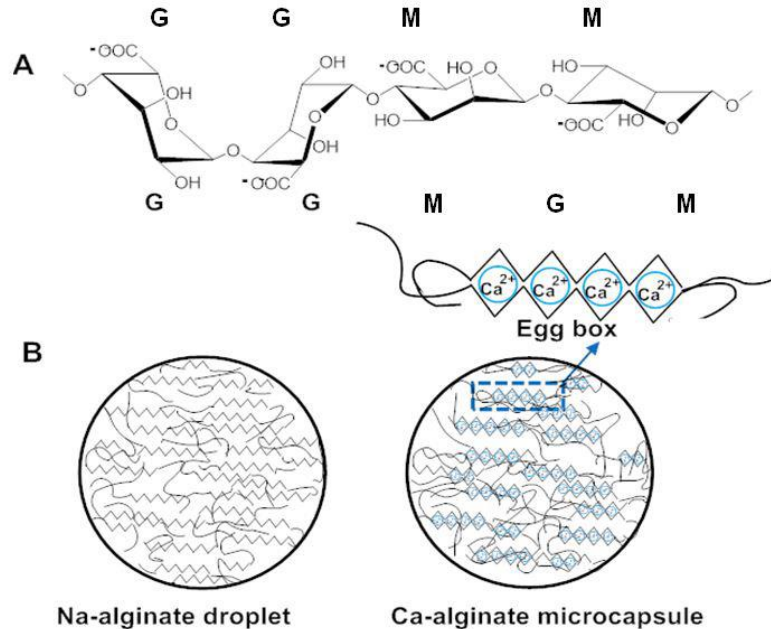
Figure 2.12 (a) Chemical structure of alginate (b) Alginate hydrogel formation

mechanism. Reprinted by permission [78]

32

Agarose is a thermal responsive polymer, consists of β-d-galactopyranose and 3,6-anhydro-α- l-galactopyranose which can undergo a sol-gel transition upon cooling through thermal crosslinking (Figure 2.13) at transition temperature close to body temperature. This transition stage makes Agarose a good candidate for cell encapsulation [79]. Polylactide-co-glycolide (PLGA) PLGA polymers belong is a biodegradable polymer (Figure 2.14). PLGA is dissolved in solvents and the second component is added to precipitate the polymer molecules [80-81] to prepare capsules.
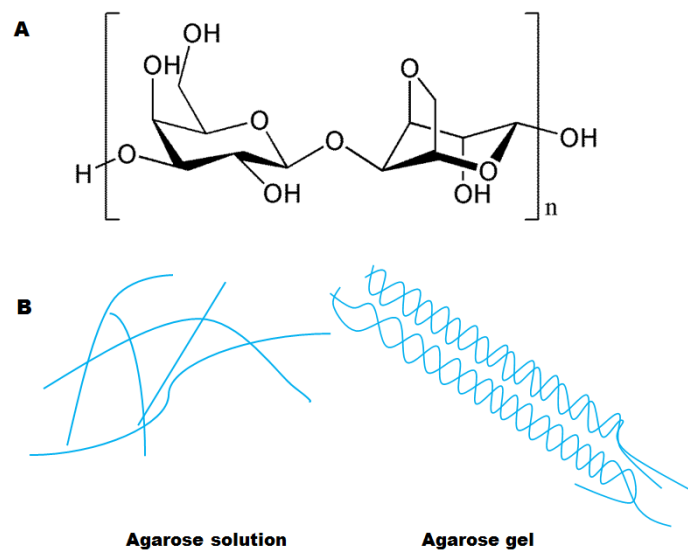
Figure 2.13 (a) Chemical structure of agarose (b) agarose hydrogel formation mechanism. Reprinted by permission [78]
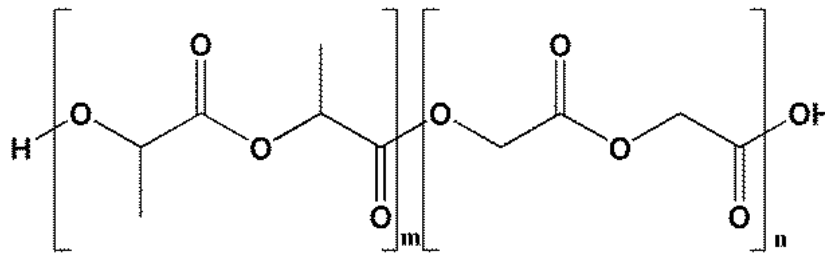
Figure 2.14 Chemical structure of PLGA. Printed by permission [78]

Different technologies have been used for cell encapsulation. The electrostatic spray method has a significant appeal because it is easy to use, capabilities to scale-up, no cell damage, and sterile operation conditions (Figure 2.15).[82]. A cell polymer mixture is pushed through a nozzle by using a pump. The droplets are broken into smaller ones under forces such as electrostatic, vibration..etc. Then, droplets collected in a gelling bath containing the crosslinkers, where cell encapsulated inside hydrogel form immediately through a reaction between ions and polymer molecules. Microfluidics devices can be used to generate microcapsules with a narrow size distribution and controlled morphology [83–85]. This method shows great promise for cell encapsulation, especially for single cell encapsulation [86].

Microcapsules are formed by allowing a core fluid to be surrounded by a flowing sheath stream [87]. Recently, these devices have also been successfully applied for the generation of cell loaded core-shell capsules (Figure 2.16) [85]. Beside the relatively low encapsulation efficiency, a significant drawback of the current microfluidic technologies is that the oil used for shearing may leave a residual adhesive oil layer on the capsule which affects subsequent coating processes.[82,88]
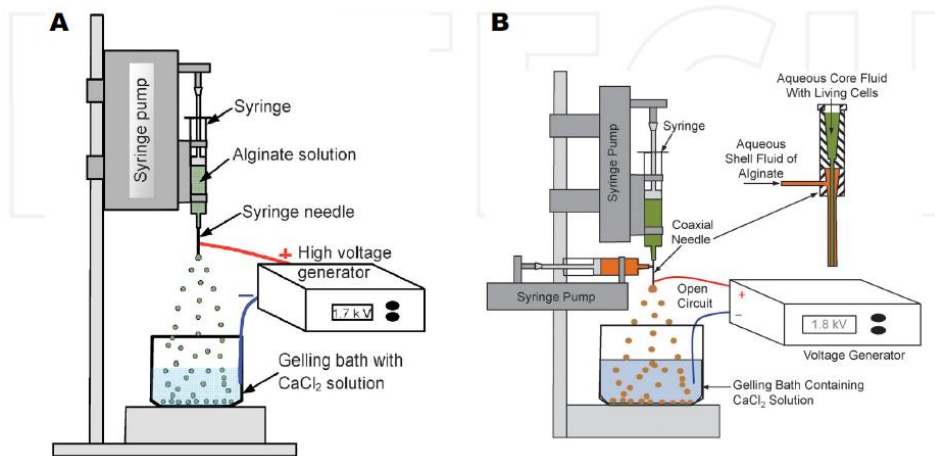
Figure 2.15 (a) electrostatic spray device used for generating polymeric hydrogel capsules. Printed by permission [82]. (b) Modified electrostatic spray for fabricating the hydrogel capsules. Printed by permission [89]
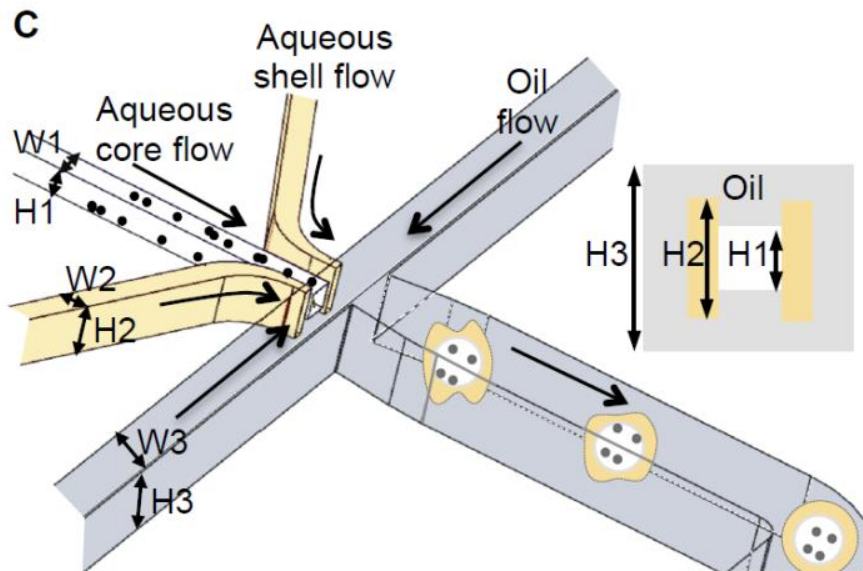
Figure 2.16 the microfluidics device for generating hydrogel capsules. Printed by permission [85]

2.5   References

1. CDC - Expected New Cancer Cases and Deaths in 2020. (2016, March 23).
    Retrieved from
    https://www.cdc.gov/cancer/dcpc/research/articles/cancer_2020.htm

2. Islam, M., Motasim Bellah, M., Sajid, A., Raziul Hasan, M., Kim, Y., & Iqbal, S. M.
    (2015). Effects of Nanotexture on Electrical Profiling of Single Tumor Cell and
    Detection of Cancer from Blood in Microfluidic Channels. Scientific Reports, 5(1).
    doi:10.1038/srep13031

3. Global Cancer Diagnostics Market Set for Rapid Growth, To Reach Around USD
    128.6 Billion by 2020. (2016, April 1). Retrieved from
    http://www.marketresearchstore.com/news/global-cancer-diagnostics-market-192

4. Pitot, H. (2007). The Biology of Cancer. By Robert A Weinberg. New York:
    Garland Science.. The Quarterly Review of Biology, 82(3), 311-311.
    doi:10.1086/523215

5. Pecorino, L. (2016). Molecular biology of cancer: Mechanisms, targets and
    therapeutics. Oxford: University Press.

6. Hanahan, D., & Weinberg, R. (2011). Hallmarks of Cancer: The Next Generation.
    Cell, 144(5), 646-674. doi:10.1016/j.cell.2011.02.013

7. Ouyang, L., Shi, Z., Zhao, S., Wang, F., Zhou, T., Liu, B., & Bao, J. (2012).
    Programmed cell death pathways in cancer: a review of apoptosis, autophagy
    and programmed necrosis. Cell Proliferation, 45(6), 487-498. doi:10.1111/j.1365-
    2184.2012.00845.

8. Calcium-permeable ion channels involved in glutamate receptor-independent
    ischemic brain injury. (2011). Acta Pharmacologica Sinica, 32(6), 734-740.
    doi:10.1038/aps.2011.47

9. Pedersen, S. F., & Stock, C. (2013). Ion Channels and Transporters in Cancer: Pathophysiology, Regulation, and Clinical Potential. Cancer Research, 73(6), 1658-1661. doi:10.1158/0008-5472.can-12-4188

10. Djamgoz, M. B., Coombes, R. C., & Schwab, A. (2014). Ion transport and cancer: from initiation to metastasis. Philosophical Transactions of the Royal Society B: Biological Sciences, 369(1638), 20130092-20130092. doi:10.1098/rstb.2013.0092

11. Golias, C., Charalabopoulos, A., & Charalabopoulos, K. (2004). Cell proliferation and cell cycle control: a mini review. International Journal of Clinical Practice, 58(12), 1134-1141. doi:10.1111/j.1742-1241.2004.00284.

12. Vermeulen, K., Van Bockstaele, D. R., & Berneman, Z. N. (2003). The cell cycle: a review of regulation, deregulation and therapeutic targets in cancer. Cell Proliferation, 36(3), 131-149. doi:10.1046/j.1365-2184.2003.00266.

13. Yang, M., & Brackenbury, W. J. (2013). Membrane potential and cancer progression. Frontiers in Physiology, 4. doi:10.3389/fphys.2013.00185

14. Blackiston, D. J., McLaughlin, K. A., & Levin, M. (2009). Bioelectric controls of cell proliferation: Ion channels, membrane voltage and the cell cycle. Cell Cycle, 8(21), 3527-3536. doi:10.4161/cc.8.21.9888

15. Wright, S. H. (2004). Generation of resting membrane potential. Advances in Physiology Education, 28(4), 139-142. doi:10.1152/advan.00029.2004

16. Wonderlin, W. F., Woodfork, K. A., & Strobl, J. S. (1995). Changes in membrane potential during the progression of MCF-7 human mammary tumor cells through the cell cycle. Journal of Cellular Physiology, 165(1), 177-185. doi:10.1002/jcp.1041650121

17. Boonstra, J., Mummery, C. L., Tertoolen, L. G., Van Der Saag, P. T., & De Laat, S. W. (1981). Cation transport and growth regulation in neuroblastoma cells. Modulations of K+ transport and electrical membrane properties during the cell cycle. Journal of Cellular Physiology, 107(1), 75-83. doi:10.1002/jcp.1041070110

18. Stillwell, E.F.; Cone, C.M.; Cone, C.D., Jr. Stimulation of DNA synthesis in CNS neurones by sustained depolarization. Nat. New Biol. 1973, 246, 110–111.

19. Boonstra, J.; Mummery, C.L.; Tertoolen, L.G.; van der Saag, P.T.; de Laat, S.W. Cation transport and growth regulation in neuroblastoma cells. Modulations of K+ transport and electrical membrane properties during the cell cycle. J. Cell. Physiol. 1981, 107, 75–83. [CrossRef]

20. Cone, C.D., Jr.; Cone, C.M. Induction of mitosis in mature neurons in central nervous system by sustained depolarization. Science 1976, 192, 155–158.

21. Sachs, H.G.; Stambrook, P.J.; Ebert, J.D. Changes in membrane potential during the cell cycle. Exp. Cell. Res. 1974, 83, 362–366.

22. Sundelacruz, S.; Levin, M.; Kaplan, D.L. Role of membrane potential in the regulation of cell proliferation and differentiation. Stem Cell Rev. 2009, 5, 231–246.

23. Huang, X.; Jan, L.Y. Targeting potassium channels in cancer. J. Cell Biol. 2014, 206, 151–162.

24. Bezanilla, F. Voltage-gated ion channels. IEEE Trans. Nanobioscience 2005, 4, 34–48.

25. Catterall, W.A. Structure and function of voltage-gated ion channels. Annu. Rev. Biochem. 1995, 64, 493–531.

26. Armstrong, C.M.; Hille, B. Voltage-gated ion channels and electrical excitability. Neuron 1998, 20, 371–380.

27. Rao, V., Perez-Neut, M., Kaja, S., & Gentile, S. (2015). Voltage-Gated Ion Channels in Cancer Cell Proliferation. Cancers, 7(2), 849-875. doi:10.3390/cancers7020813

28. Kumari, A., Yadav, S. K., & Yadav, S. C. (2010). Biodegradable polymeric nanoparticles based drug delivery systems. Colloids and Surfaces B: Biointerfaces, 75(1), 1-18. doi:10.1016/j.colsurfb.2009.09.001

29. K. S. Soppimath, T. M. Aminabhavi, A. R. Kulkarni, and W. E. Rudzinski, "Biodegradable polymeric nanoparticles as drug delivery devices," Journal of controlled release, vol. 70, pp. 1-20, 2001.

30. [112] J. Panyam, W.-Z. Zhou, S. Prabha, S. K. Sahoo, and V. Labhasetwar, "Rapid endo-lysosomal escape of poly (DL-lactide-co-glycolide) nanoparticles: implications for drug and gene delivery," The FASEB Journal, vol. 16, pp. 1217-1226, 2002.

31. L. Nobs, F. Buchegger, R. Gurny, and E. Allémann, "Poly (lactic acid) nanoparticles labeled with biologically active Neutravidin„¢ for active targeting," European journal of pharmaceutics and biopharmaceutics, vol. 58, pp. 483-490, 2004.

32. M. F. Zambaux, F. Bonneaux, R. Gref, E. Dellacherie, and C. Vigneron, "Preparation and characterization of protein C-loaded PLA nanoparticles," Journal of controlled release, vol. 60, pp. 179-188, 1999.

33. D. K. Sahana, G. Mittal, V. Bhardwaj, and M. N. V. Kumar, "PLGA nanoparticles for oral delivery of hydrophobic drugs: Influence of organic solvent on nanoparticle formation and release behavior in vitro and in vivo using estradiol as a model drug," Journal of pharmaceutical sciences, vol. 97, pp. 1530-1542, 2008.

34. [115] J. M. Barichello, M. Morishita, K. Takayama, and T. Nagai, "Encapsulation of hydrophilic and lipophilic drugs in PLGA nanoparticles by the nanoprecipitation method," Drug development and industrial pharmacy, vol. 25, pp. 471-476, 1999.

35. [116] C. Pinto Reis, R. J. Neufeld, A. n. J. Ribeiro, and F. Veiga, "Nanoencapsulation I. Methods for preparation of drug-loaded polymeric nanoparticles," Nanomedicine: Nanotechnology, Biology and Medicine, vol. 2, pp. 8-21, 2006.

36. L. Li and S. P. Schwendeman, "Mapping neutral microclimate pH in PLGA microspheres," Journal of controlled release, vol. 101, pp. 163-173, 2005.

37. J. Siepmann, K. Elkharraz, F. Siepmann, and D. Klose, "How autocatalysis accelerates drug release from PLGA-based microparticles: a quantitative treatment," Biomacromolecules, vol. 6, pp. 2312-2319, 2005

38. L. Fan and S. K. Singh, Controlled release: A quantitative treatment: Springer-Verlag Berlin, 1989.

39. D. Klose, F. Siepmann, K. Elkharraz, S. Krenzlin, and J. Siepmann, "How porosity and size affect the drug release mechanisms from PLGA-based microparticles," International journal of pharmaceutics, vol. 314, pp. 198-206, 2006.

40. Y. J. Oh, J. Lee, J. Y. Seo, T. Rhim, S. H. Kim, H. J. Yoon, and K. Y. Lee, "Preparation of budesonide-loaded porous PLGA microparticles and their therapeutic efficacy in a murine asthma model," Journal of Controlled Release, vol. 150, pp. 56-62, 2011.

41. J. A. Straub, D. E. Chickering, C. C. Church, B. Shah, T. Hanlon, and H. Bernstein, "Porous PLGA microparticles: AI-700, an intravenously administered

ultrasound contrast agent for use in echocardiography," Journal of controlled release, vol. 108, pp. 21-32, 2005.

42. J. G. M. Klijn, P. Berns, P. I. M. Schmitz, and J. A. Foekens, "The clinical significance of epidermal growth factor receptor (EGF-R) in human breast cancer: a review on 5232 patients," Endocrine reviews, vol. 13, p. 3, 1992.

43. T. J. Lynch, D. W. Bell, R. Sordella, S. Gurubhagavatula, R. A. Okimoto, B. W. Brannigan, P. L. Harris, S. M. Haserlat, J. G. Supko, and F. G. Haluska, "Activating mutations in the epidermal growth factor receptor underlying responsiveness of non-small-cell lung cancer to gefitinib," The New England journal of medicine, vol. 350, p. 2129, 2004.

44. A. M. F. Kersemaekers, G. J. Fleuren, G. G. Kenter, L. Van den Broek, S. M. Uljee, J. Hermans, and M. J. Van de Vijver, "Oncogene alterations in carcinomas of the uterine cervix: overexpression of the epidermal growth factor receptor is associated with poor prognosis," Clinical Cancer Research, vol. 5, p. 577, 1999.

45. K. Mellon, C. Wright, P. Kelly, C. H. Horne, and D. E. Neal, "Original Articles: Bladder Cancer: Long-Term Outcome Related to Epidermal Growth Factor Receptor Status in Bladder Cancer," The Journal of urology, vol. 153, pp. 919-925, 1995.

46. S. Inada, T. Koto, K. Futami, S. Arima, and A. Iwashita, "Evaluation of malignancy and the prognosis of esophageal cancer based on an immunohistochemical study (p53, E-cadherin, epidermal growth factor receptor)," Surgery today, vol. 29, pp. 493-503, 1999.

47. J. Fischer-Colbrie, A. Witt, H. Heinzl, P. Speiser, K. Czerwenka, P. Sevelda, and R. Zeillinger, "EGFR and steroid receptors in ovarian carcinoma: comparison with

prognostic parameters and outcome of patients," Anticancer research, vol. 17, pp. 613-619, 1997.

48. Brown, T.M.; Fee, E. Rudolf Carl Virchow: Medical scientist, social reformer, role model. Am. J. Public Health 2006, 96, 2104–2105.

49. Nguyen, K.S.; Kobayashi, S.; Costa, D.B. Acquired resistance to epidermal growth factor receptor tyrosine kinase inhibitors in non-small-cell lung cancers dependent on the epidermal growth factor receptor pathway. Clin. Lung Cancer 2009, 10, 281–289.

50. Nickel, G.C.; Barnholtz-Sloan, J.; Gould, M.P.; McMahon, S.; Cohen, A.; Adams, M.D.; Guda, K.; Cohen, M.; Sloan, A.E.; LaFramboise, T. Characterizing mutational heterogeneity in a glioblastoma patient with double recurrence. PLoS One 2012, 7, e35262.

51. Nowell, P.C. The clonal evolution of tumor cell populations. Science 1976, 194, 23–28.

52. Shibata, M.; Shen, M.M. The roots of cancer: Stem cells and the basis for tumor heterogeneity. Bioessays 2012, 35, 253–260.

53. Magee, J.A.; Piskounova, E.; Morrison, S.J. Cancer stem cells: Impact, heterogeneity, and uncertainty. Cancer Cell 2012, 21, 283–296.

54. Quintana, E.; Shackleton, M.; Foster, H.R.; Fullen, D.R.; Sabel, M.S.; Johnson, T.M.; Morrison, S.J. Phenotypic heterogeneity among tumorigenic melanoma cells from patients that is reversible and not hierarchically organized. Cancer Cell 2010, 18, 510–523.

55. Singh, S.K.; Hawkins, C.; Clarke, I.D.; Squire, J.A.; Bayani, J.; Hide, T.; Henkelman, R.M.; Cusimano, M.D.; Dirks, P.B. Identification of human brain tumour initiating cells. Nature 2004, 432, 396–401.

56. Anido, J.; Saez-Borderias, A.; Gonzalez-Junca, A.; Rodon, L.; Folch, G.; Carmona, M.A.; Prieto-Sanchez, R.M.; Barba, I.; Martinez-Saez, E.; Prudkin, L.; et al. TGF-beta receptor inhibitors target the CD44(high)/Id1(high) glioma-initiating cell population in human glioblastoma. Cancer Cell 2010, 18, 655–668.

57. Mao, P.; Joshi, K.; Li, J.; Kim, S.H.; Li, P.; Santana-Santos, L.; Luthra, S.; Chandran, U.R.; Benos, P.V.; Smith, L.; et al. Mesenchymal glioma stem cells are maintained by activated glycolytic metabolism involving aldehyde dehydrogenase 1A3. Proc. Natl. Acad. Sci. USA 2013, 110, 8644–8649.

58. Nitta, M.; Kozono, D.; Kennedy, R.; Stommel, J.; Ng, K.; Zinn, P.O.; Kushwaha, D.; Kesari, S.; Inda, M.D.; Wykosky, J.; et al. Targeting EGFR induced oxidative stress by PARP1 inhibition in glioblastoma therapy. PLoS One 2010, 5, e10767.

59. Greaves, M. Cancer stem cells: Back to Darwin? Semin. Cancer Biol. 2010, 20, 65–70.

60. Marusyk, A.; Polyak, K. Tumor heterogeneity: Causes and consequences. Biochim. Biophys. Acta 2010, 1805, 105–117.

61. Hill, R.P. Identifying cancer stem cells in solid tumors: Case not proven. Cancer Res. 2006, 66, 1891–1895.

62. Spencer, S.L.; Gaudet, S.; Albeck, J.G.; Burke, J.M.; Sorger, P.K. Non-genetic origins of cell-to-cell variability in TRAIL-induced apoptosis. Nature 2009, 459, 428–432.

63. Gerlinger, M.; Rowan, A.J.; Horswell, S.; Larkin, J.; Endesfelder, D.; Gronroos, E.; Martinez, P.; Matthews, N.; Stewart, A.; Tarpey, P.; et al. Intratumor heterogeneity and branched evolution revealed by multiregion sequencing. N. Engl. J. Med. 2012, 366, 883–892.

64. Yap, T.A.; Gerlinger, M.; Futreal, P.A.; Pusztai, L.; Swanton, C. Intratumor heterogeneity: Seeing the wood for the trees. Sci. Transl. Med. 2012, 4, doi:10.1126/scitranslmed.3003854.

65. A. ul Haque, M. Zuberi, R. E. Diaz-Rivera, and D. Marshall Porterfield, "Electrical characterization of a single cell electroporation biochip with the 2-D scanning vibrating electrode technology," Biomedical microdevices, vol. 11, pp. 1239-1250, 2009.

66. [32] B. Matthews and J. W. Judy, "Design and fabrication of a micromachined planar patch-clamp substrate with integrated microfluidics for single-cell measurements," Journal of Microelectromechanical Systems, vol. 15, pp. 214-222, 2006.

67. [33] M. Kitta, H. Tanaka, and T. Kawai, "Rapid fabrication of Teflon micropores for artificial lipid bilayer formation," Biosensors and Bioelectronics, vol. 25, pp. 931-934, 2009.

68. [34] X. Niu and Z. Yan, "The expression of red blood cell deformability in micropore filtration tests," Journal of Biomedical Engineering, vol. 18, p. 615, 2001.

69. [35] H. Chang, A. Ikram, F. Kosari, G. Vasmatzis, A. Bhunia, and R. Bashir, "Electrical characterization of micro-organisms using microfabricated devices," Journal of Vacuum Science & Technology B: Microelectronics and Nanometer Structures, vol. 20, pp. 2058-2064, 2002.

70. [36] W. Asghar, Y. Wan, A. Ilyas, R. Bachoo, Y. Kim, and S. M. Iqbal, "Electrical fingerprinting, 3D profiling and detection of tumor cells with solid-state micropores," Lab on a Chip, vol. 12, pp. 2345-2352, 2012.

71. E. Ogura, B. Kusumoputro, and T. Moriizumi, "Passage time measurement of individual and blood cells through arrayed micropores on Si3N4 membrane," Journal of biomedical engineering, vol. 13, pp. 503-506, 1991.

72. R. Pantoja, J. M. Nagarah, D. M. Starace, N. A. Melosh, R. Blunck, F. Bezanilla, and J. R. Heath, "Silicon chip-based patch-clamp electrodes integrated with PDMS microfluidics," Biosensors and Bioelectronics, vol. 20, pp. 509-517, 2004.

73. De Vos P, Faas MM, Strand B, Calafiore R. Alginate-based microcapsules for immunoisolation of pancreatic islets. Biomaterials 2006, 27:5603–5617.

74. Morch YA, Donati I, Strand BL, Skjak-Braek G. Effect of Ca2+, Ba2+, and Sr2+ on alginate microbeads. Biomacromolecules 2006, 7:1471–1480.

75. Smidsrød O, Skjåk-Braek G. Alginate as immobilization matrix for cells. Trends in Biotechnology 1990, 8:71–78.

76. Zhang W, He X. Microencapsulating and banking living cells for cell-based medicine. Journal of Healthcare Engineering 2011, 2:427–446.

77. Zimmermann H, Zimmermann D, Reuss R, Feilen PJ, Manz B, Katsen A, Weber M, Ihmig FR, Ehrhart F, Gessner P, Behringer M, Steinbach A, Wegner LH, Sukhorukov VL, Vásquez JA, Schneider S, Weber MM, Volke F, Wolf R, Zimmermann U. Towards a medically approved technology for alginate-based microcapsules allowing long-term immunoisolated transplantation. Journal of Materials Science: Materials in Medicine 2005, 16:491–501.

78. Wujie Zhang. (2015). Encapsulation of Transgenic Cells for Gene Therapy. InTech.

79. Gasperini L, Mano JF, Reis RL. Natural polymers for the microencapsulation of cells. Journal of The Royal Society Interface 2014, 11:20140817.

80. Olabisi RM. Cell microencapsulation with synthetic polymers. Journal of Biomedical Materials Research Part A. DOI: 10.1002/jbm.a.35205.

81. Abalovich A, Jatimliansky C, Diegex E, Arias M, Altamirano A, Amorena C, Martinez B, Nacucchio M. Pancreatic islets microencapsulation with polylactide-co-glycolide. Transplantation Proceedings 2001, 33:1977–1979.

82. Zhang W, He X. Encapsulation of living cells in small (approximately 100 microm) alginate microcapsules by electrostatic spraying: a parametric study. Journal of Biomechanical Engineering 2009, 131:074515.

83. Wan J. Microfluidic-based synthesis of hydrogel particles for cell microencapsulation and cell-based drug delivery. Polymers 2012, 4:1084–1108.

84. Mazzitelli S, Capretto L, Quinci F, Piva R, Nastruzzi C. Preparation of cell-encapsulation devices in confined microenvironment. Advanced Drug Delivery Reviews 2013, 65:1533–1555.

85. Agarwal P, Zhao S, Bielecki P, Rao W, Choi JK, Zhao Y, Yu J, Zhang W, He X. Onestep microfluidic generation of pre-hatching embryo-like core-shell microcapsules for miniaturized 3D culture of pluripotent stem cells. Lab on a Chip 2013, 13:4525–4533

86. Wu L, Chen P, Dong Y, Feng X, Liu BF. Encapsulation of single cells on a microfluidic device integrating droplet generation with fluorescence-activated droplet sorting. Biomedical Microdevices 2013, 15:553–560.

87. Kang A, Park J, Ju J, Jeong GS, Lee SH. Cell encapsulation via microtechnologies. Biomaterials 2014, 35:2651–2663.

88. Tendulkar S, Mirmalek-Sani SH, Childers C, Saul J, Opara EC, Ramasubramanian MK. A three-dimensional microfluidic approach to scaling up microencapsulation of cells. Biomedical Microdevices 2012, 14:461–469.

89. Zhao S, Agarwal P, Rao W, Huang H, Zhang R, Liu Z, Yu J, Weisleder N, Zhang W, He X. Coaxial electrospray of liquid core-hydrogel shell microcapsules for encapsulation and miniaturized 3D culture of pluripotent stem cells. Integrative Biology (Camb) 2014, 6:874–884

Chapter 3

Ion-sensitive Field-effect Transistors with Micropillared gates for Sensing of Cancer

Cell Ion Exchange as a Biomarker

3.1 Introduction

Cancer has a major societal impact in the United States and across the globe. In 2018, an estimated 1,735,350 new cases of cancer are expected to be diagnosed in the United States, and 609,640 people are estimated to die of the disease. There is an unmet medical need to improve current methods of early cancer detection so patients can receive treatment when the cancer is in its early stages and has not metastasized to other areas of the body. Every cell type has a characteristic profile based on its mechano-physical properties [1]. Cells are highly organized living microstructures. They contain high concentrations of chemicals, including enzymes, nucleic acids, ions, many types of proteins, and small organic molecules. Moreover, they process multiple incoming information signals using parallel activation of different signaling pathways and respond with appropriate reaction patterns according to the types of input from physical or chemical stimuli. For cancer diagnostics, detection of cells with the correct physical, chemical, electrical, and biological properties are very important.

Cone's theory proposed a general correlation between proliferation and membrane potential (V_m) [2]. The value of the resting membrane potential varies from cell to cell and ranges from about −20 mV to −100 mV. The molecular bioelectricity of cells is regulated through K^+, Na^+, Cl^-, and Ca^{+2} channels [3]. In cancer cells, several ion channels have been recognized to play important roles in cancer pathology, as these regulate key events in cell proliferation, cancer initiation, and its progression [4-6]. Ion- selective field effect transistors are used to detect methylated nucleotides in a DNA sample, which is a critical step in tumorigenesis for most types of cancer [7]. A direct role of molecular bioelectricity, such as V_m can be used to detect and to differentiate tumor cells.

The microscale and nanoscale environments are known to modulate cellular behavior [8]. Studies on micropatterned and nanopatterned engineered surfaces have

49

demonstrated the influence of topography on a variety of cellular functions, like the migration of endothelial cells and fibroblasts [9-10], osteogenic differentiation of stem cells [11-14], mechano-sensitive gene expressions in fibroblast cells [15-18], directional polarization of neurons [19-24], immobilization of tumor cells [25-26], etc. Researchers have utilized micro/nanostructures and nanotextured surfaces for a wide range of applications to modulate the cellular responses. Small diameter nanowires with high aspect ratios are known to penetrate the cell membrane. Therefore, these have been used for applications requiring intracellular access, such as for drug delivery [27-32]. Silicon micropillar arrays have been used for the efficient isolation and capture of circulating tumor cells through enhanced local topographic interactions [33-34].

Here, we introduce an ISFET sensor concept to record cell molecular changes, and in particular the enhanced ion exchange that occurs during the diseased cell proliferation. Proliferation is the mechanism by which ions can impel it to divide, differentiate, or die (Figure. 1). A surface engineering approach with 3D features enhances the device's electrical properties in comparison to a flat surface device. Introducing an innovative 3D micropillar surface at gate area improves tumor cell detection. The array of silicon dioxide micropillars was made on top of 10 µm doped silicon channel area. The effect of the micropillar's physical diameter on device performance was also studied here.

The cells were in contact with micro features. The trenches between micropillars were filled with ionic liquid and allowed an ion influx between the cell membrane and extracellular environment. The ions diffused out of the cell and accumulated on the outside surface of the cell membrane, making it more positive or negative than inside the membrane. This resulted in a separation of charges across the cell membrane and created an electrical potential across the cell membrane. The drain current measurements of this ISFET were affected by the cell membrane potential. Surface engineering and use of
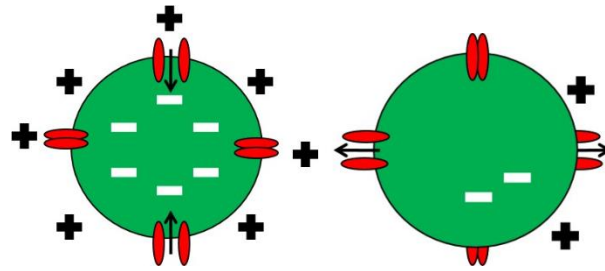
(a)
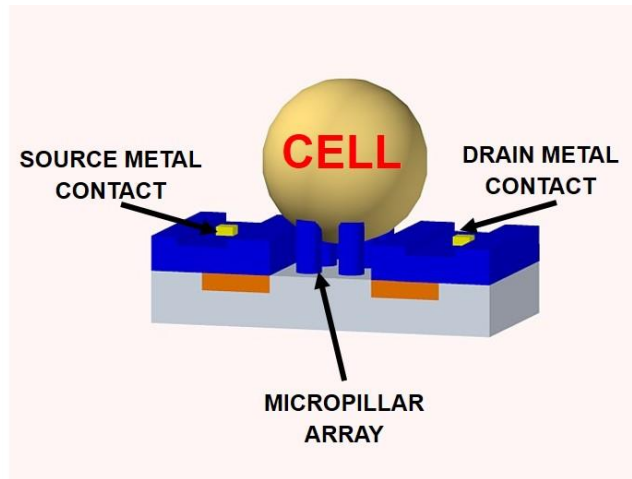
(b)

Figure 1 ISFET with micropillared gates. (a) Schematic illustration of cell ion channels. Cells are depolarized or hyperpolarized (b) 3D schematic of ISFET device. This shows a cell on top of micropillar array

microstructures, specifically micropillars, enhanced the sensitivity of ISFETs and made them suitable for detecting tumor cells in a real-time diagnostics environment.

3.2   Methods and procedures

3.2.1   Cell-Ion Exchange Model

The 3D geometric model was designed in COMSOL (Fig. 1(b)). In this model, the n-type substrate was defined with a donor doping concentration of 1.5×10^{16}/cm³. Both the source and drain were p-type (doping 1×10^{18}/cm³). For the electrostatic model, two

terminals were used for source and drain. The source terminal voltage was set to zero and the drain terminal was set to −10 mV. The third terminal was used for the applied voltage at the gate area and at the edges of the micropillars to simulate cell membrane potential while the cell was in contact with the micropillars. In the semiconductor model, two metal contacts were used as source and drain. A third metal contact was placed in between the source and drain to the gate area, which was separated from the channel by a thin 5 nm layer of silicon dioxide (SiO_2). A fourth metal contact was used to simulate the interface between the micropillars and the substrate.

3.2.2   Variation in Micropillar Diameter

In order to study the physical parameters of the design, the diameter of the micropillars was varied. First, a 2 µm diameter was modeled and simulated. Next, 1 µm diameter was modeled and simulated. The simulation provided the DC electrical characteristics of both devices.

3.2.3   Electrostatic Potential

The semiconductor and electrostatic models were executed simultaneously to capture the effects of electrostatic potential and to simulate the DC characteristics of ISFET. A plot of the drain current was used to determine the turn-on voltage of the device. A small voltage (−10 mV) was applied to the drain. The voltages at the gate and edges of the micropillars (device surface) were swept from −200 mV to +100 mV. Then, drain voltage was swept from −100 to 0 mV while the surface voltage was swept from −200 mV to −100 mV. The drain current versus drain voltage was plotted at several values of surface voltage (i.e. voltage at the gate and edges of the micropillars). The electrostatic model solved the MOS capacitor effect from the micropillars, where the substrate was taken to be grounded. The gate and the micropillar's edges were biased with a voltage. The electrical scalar potential (V_{ES}) satisfied Poisson's equation.

The semiconductor model solved the Poisson's equation for the charge carriers. Equation (1) defines the Poisson's equation in which the electric field term is shown on the left-hand side, and space charge densities are shown on the right-hand side. The **q** is the charge of the carrier, and the electron and hole surface concentrations are denoted by **n** and **p**, respectively. N_a^- and N_d^+ are the acceptor and donor ion concentrations. In the steady state, the total charge contributions of the carriers can be calculated from the following:

$$\nabla.(-\epsilon \nabla V_{Semi}) = q(p - n + N_d^+ - N_a^-) \tag{1}$$

3.2.4 Charge Distribution

The micropillars were modeled as ideal MOS capacitors; thus, the semiconductor areas under SiO$_2$ micropillars had equal charges as in the metal contact. The charge, due to accumulation and inversion, resulted in a very narrow charge distribution near the interface. The charges, due to depletion bias resulted in a depletion width (W_{dep}). Thus, the hole concentration near the interface equaled the donor concentration. This entailed:

$$\frac{1}{C} = \frac{1}{C_{ox}} + \frac{1}{C_{dep}} \tag{2}$$

$$\frac{1}{C_{dep}} = \frac{W_{dep}}{\varepsilon \times Area} \tag{3}$$

$$p_{interface} = N_d = n_i \, e^{[\frac{E_{i-interface} - E_f}{kT}]} = n_i \, e^{[\frac{E_f - E_i}{kT}]} \tag{4}$$

In the semiconductor model, metallic contacts were considered between Si-SiO$_2$ to simulate electrical potential generated from the MOS capacitor. The voltage of the metal contacts was set to the electrostatic voltage output from the electrostatic model ($V = V_{ES}$). As a result of (2)-(4), p-type doping was applied to the area on silicon substrate under SiO$_2$ micropillars. The electrical insulation was assumed throughout the device boundary.

3.3   Results and Discussion

The results of the simulations were plotted to obtain DC characteristics for the ISFET sensor. The data clearly depicted the change in membrane potential at the interfaces of the micropillars.

3.3.1   Analyzing ISFET characteristics

The ISFET worked on the basic principle of measuring surface charge changes in the interface of the insulator layer and the overlying layer. This was simulated by an applied voltage. Changes in surface charges resulted in changes in the work function that in turn was measured as a shift in transistor threshold voltage. Figure 2 shows the device electric potential for 2 µm x 3 µm and 1 µm x 3 µm array of micropillars. The electrical field is depicted by the arrow lines. Poisson's equation can be applied to the oxide since there are no charges in the oxide:

$$\frac{dE_{oxide}}{dx} = \rho = 0, \quad E_{oxide} = \text{constant} \tag{5}$$

$$V_{ES} = \iint E_{oxide} \, dx \, dy \tag{6}$$

The potential varied linearly. It was seen going outward through the micropillars, and the maximum electric potential was seen at the device gate and Si-SiO$_2$ interface. The ISFET design allowed the achievement of a physiological response to ion exchange activity (cell molecular bioelectricity) toward cancer cell characterization.

The micropillar diameter impacted the electric field direction as shown in Figure 2 (a, b). The 2 µm diameter micropillar shows electrical field direction covering the entire micropillars. However, 1 µm diameter shows electric field direction is only part of the micropillar for the same conditions ($V_d = -10$ mV, $V_g = -100$ mV). Micropillar diameter imposes a higher effect on the electric field when in contact with cells. The 2 µm x 3 µm device shows a total higher electrical field effect than 1 µm x 3 µm device.
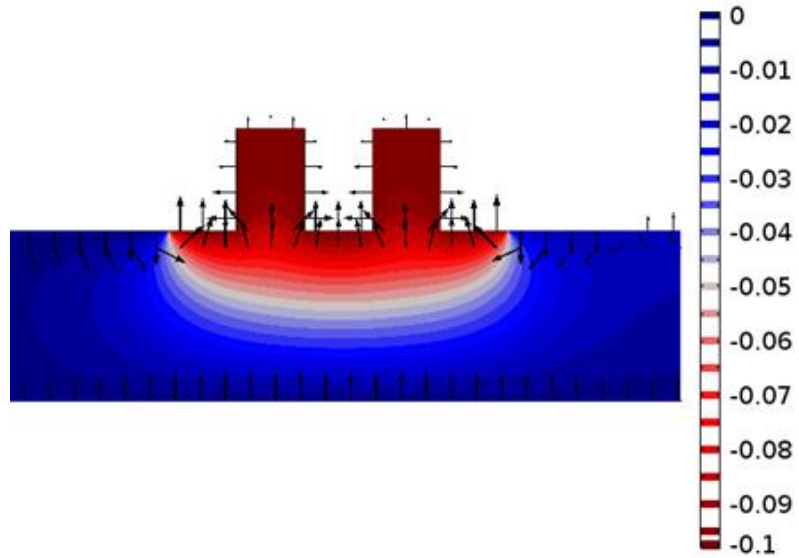
(a)
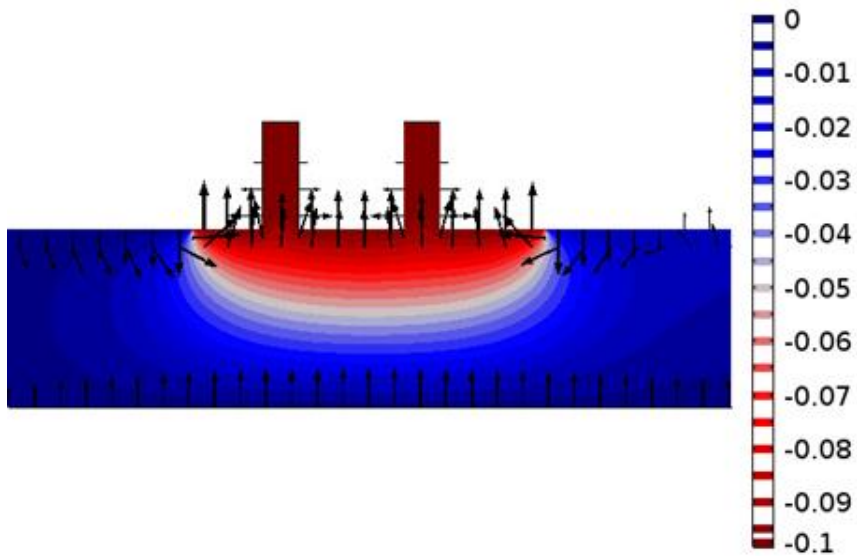
(b)

Figure 2 Device electrical potential results with micropillar sizes of (a) 2 μm x 3 μm device, and (b) 1 μm x 3 μm. The color depicts the electrical potential magnitude as depicted in the color scale on the right. Arrows depict electrical field direction in x-y direction.

Figure. 3 (a) shows the ISFET drain current with respect to the surface voltage at a small fixed drain voltage of -10 mV for 2 µm x 3 µm and 1 µm x 3 µm devices. The threshold voltage (V_T) of the devices was extracted from a log scale plot of $I_d - V_g$ by plotting and extrapolating to find V_T. The I_{dsat} was extracted from $I_d - V_d$ graph where ($V_g < V_T$, $V_d < V_g + |V_T|$) (Table I).The micropillar diameters show a correlation with V_T and I_{dsat} parameters. The V_T of the device is lower when micropillar diameter is larger, which increased the drain channel current. The micropillar diameter controls the device turn on/off voltage.

(a)

(b)
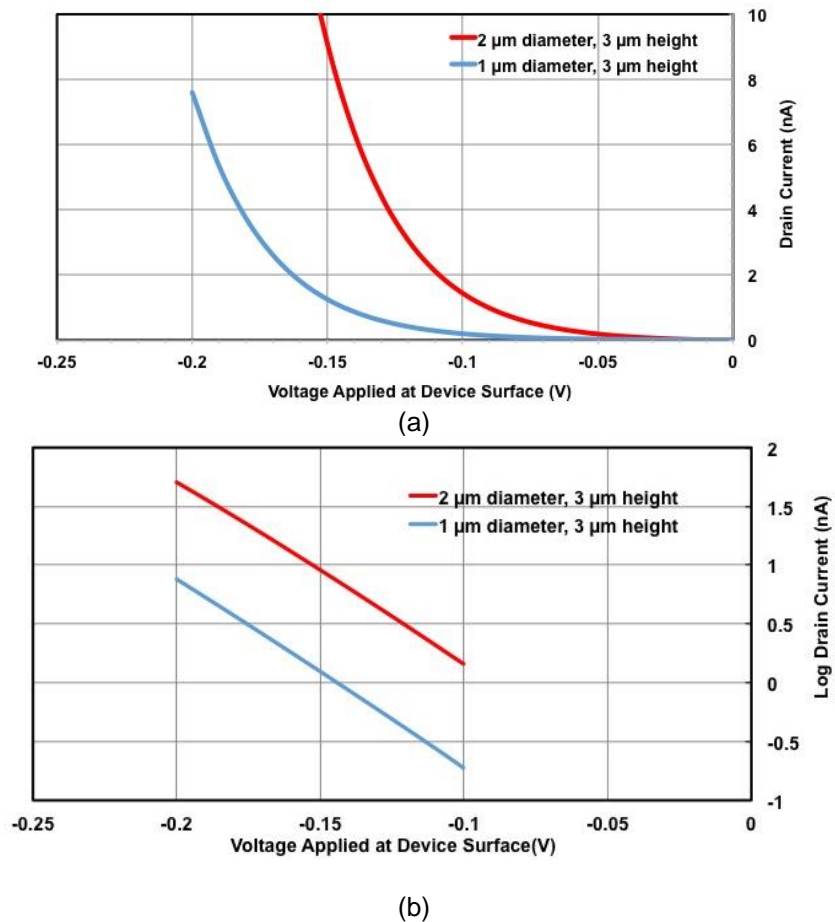
Figure 3 Drain current vs. surface voltage ($V_d = -10$ mV). (a) Linear plot, and (b) Drain current plotted in log scale to extract V_T.

56

TABLE I ISFET DC CHARACTERISTICS SUMMARY

Device (Diameter x Height)	V_T (mV)	I_{dsat} (nA)	g_m (µS)
2 µm x 3 µm	-90	0.96	10.62
1 µm x 3 µm	-140	0.85	6.06

3.3.2   Drain Current vs. Drain Voltage at Various Gate Voltages

The drain current vs. drain voltage simulation of ISFET without the effect of micropillars is shown in Figure. 4 (a). The value of the linear current (I_{LIN}) was defined as a drain current that passed through the device at $V_d = -10$ mV. The I_{LIN} was extracted from the plot of the drain current at ($V_d = -10$ mV) versus the surface voltage. A linear response of 16.5 pA/dec was seen between −70 mV and −30 mV.

Two sets of micropillar diameters were simulated to study the effect of diameter on device surface charge. The drain current output curves were recorded at different voltages of gate and edges of each micropillar. (Figure. 4 (b, c)). With decreasing surface voltage (on gate and micropillar edges), the output curve shifted more toward a positive drain current through the device. To quantify the shift, the linear current was extracted from the curves. The value of I_{LIN} was 42 nA/dec and 34 nA/dec for 2 µm and 1 µm diameter, respectively.

The results showed the impact of the physical diameter of a micropillar on I_{LIN}. The current was higher when the diameter was larger. Here, a 2 µm diameter showed ~ 1.2 timesmore I_{LIN} than that for 1 µm diameter micropillars.
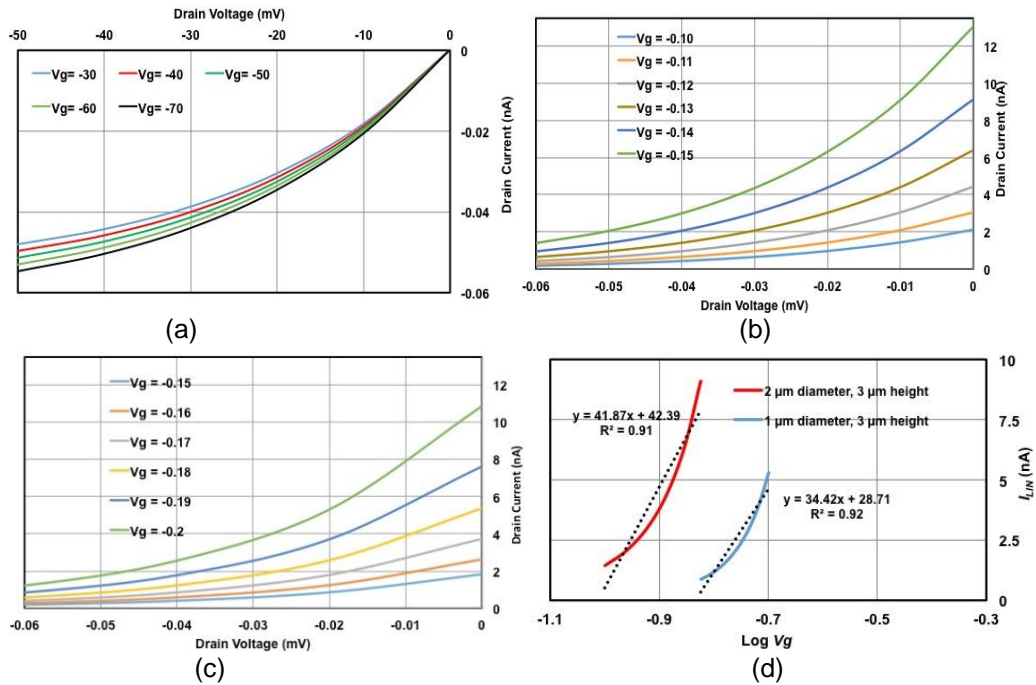
Figure 4 Drain current vs. drain voltage simulation analysis. (a) Drain current vs. drain voltage without micropillar effect (b) Drain current vs. drain voltage for device with 2 μm x 3 μm micropillar (c) Drain current vs. drain voltage for device with 1 μm x 3 μm (d) I_{LIN} vs. log values of the voltage applied to device surface micropillar and gate.

3.3.3 Capacitance-Voltage (C–V) Characteristics

The *C-V* measurement of MOS capacitor structure provides device information, which is significant for this work. The MOS structure is modeled as a series connection of two capacitors: capacitance of the oxide and capacitance of depletion layer. The device capacitance depends on three operating modes: accumulation capacitance, which is oxide capacitor with no depletion layer, depletion capacitance, which is equal to series connection of oxide and depletion layer capacitance and inversion capacitance, which becomes independent of voltage at the gate and edges of the micropillar (surface voltage).

For this simulation, all metal contacts were set to ground and surface voltage was swept from −1 V to +1 V to record device capacitance from gate to bulk. The device capacitance behavior was recorded for the two micropillar diameters. The results show that the two behaviors depend on the micropillar diameters (Figure 5). When micropillar diameter increased, device capacitance lowered. Accordingly, the device flat band voltage changed, and we captured the change in V_T. The 2 μm x 3 μm device capacitance simulation showed lower capacitance when compared with 1 μm x 3 μm and this described lower $|V_T|$.
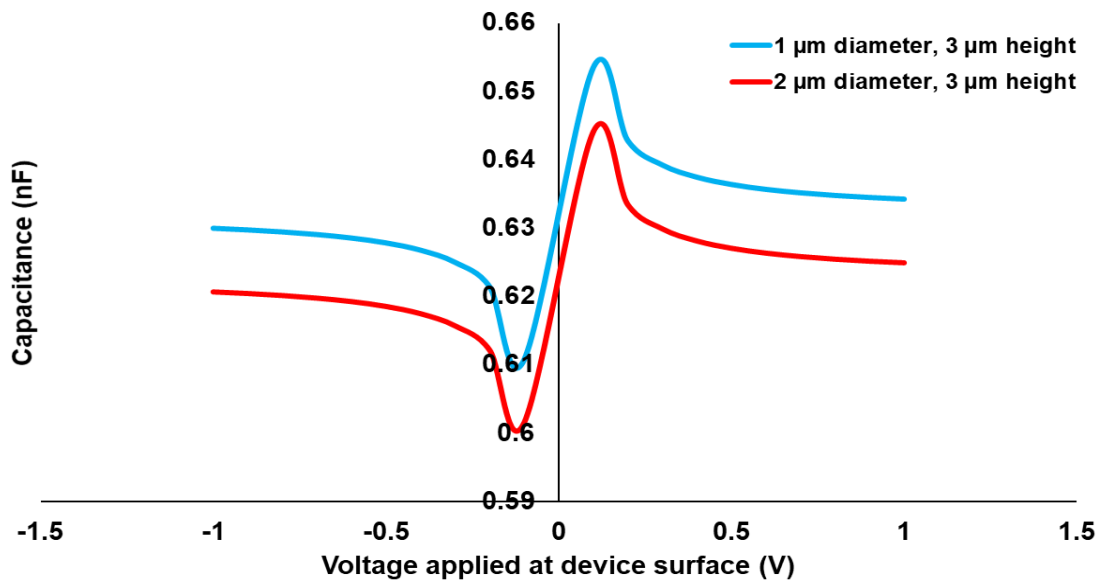
Figure 5 Device simulated capacitance behavior vs. surface voltage. Red line depicts the data for the 2 μm x 3 μm micropillar device, and the blue line shows the behavior of the 1 μm x 3 μm micropillar device.

3.3.4 Electron and hole concentrations

The hole concentration for the device was captured at the initial value ($T = 0$) and no channel had been formed. When $Vg > 0$, the charge model for n-type silicon substrate

indicated that negative charge must have been created in the semiconductor near the interface. This charge was in the form of electrons. The electron concentration in the semiconductor near the interface increased (accumulation: n-type became more "n"). At $Vg < 0$, the charge model indicated that positive charge must be created in the semiconductor near the interface: this charge was in the form of ionized donors. Hence, electron concentration in the semiconductor near the interface decreased (depletion). For higher magnitudes of bias ($Vg << 0$), the charge model indicated that positive charges must be created in the semiconductor nears the interface. These charges were now in the form of ionized donors and holes. Accordingly, electron concentration decreased as the applied surface voltage on the device became more negative. The area under SiO_2 micropillar at the end of the simulation was inspected for electron concentration. Table. II shows electron concentration versus the applied voltage on the device surface. The electron concentration decreased as applied voltage became more negative, which is expected from the semiconductor charge model (6). The electrons were replaced by holes and created an inversion channel of holes from source to drain.

TABLE II LOG OF ELECTRON CONCENTRATION UNDER MICROPILLARS

Gate Voltage (mV)	Log of Electron Concentration
100	10.82
80	10.58
60	10.37
40	10.17
20	10.00
-20	9.76
-40	9.69
-60	9.65
-80	9.62
-100	9.61

3.4   CONCLUSION

A simulation of the cell membrane potential effect has been done on ISFET with high aspect ratio micropillars in the gate area, where charges were present on micropillar surfaces. The simulation of the micropillars' physical diameter was done (2 μm x 3 μm and 1 μm x 3 μm). It was observed that the drain current changed as the potential was applied. The ISFET sensing mechanism could be attributed to a change in the threshold current due to surface charges, which changed the effective potential of the semiconductor channel. The micropillars' diameters played a key role in controlling device DC characteristics and performance. We observed an enhancement of device performance when micropillar diameter was 2 μm. The results showed that the ISFET sensor could be used to characterize cancer cells, based on their enhanced ion concentrations in the solution. The simulations showed promising results in which micropillars enhanced the sensitivity of the ISFET devices in detecting ion exchange activity of diseased cells. ISFET chips can be manufactured at low cost and would be affordable for point of care application.

3.5   Acknowledgment

3.6   References

[1] M. Islam, *et al*. "Effects of nanotexture on electrical profiling of single tumor cell and detection of cancer from blood in microfluidic channels." *Scientific Reports*, vol. 5, 13031, 2015.

[2] C. D. Cone, "Unified theory on the basic mechanism of normal mitotic control and oncogenesis." *Journal of Theoretical Biology*, vol. 30, no. 1 pp. 151-181, 1971.

[3] V. R. Rao, M. Perez-Neut, S. Kaja, and S. Gntile, "Voltage-gated ion channels in cancer cell proliferation." *Cancers*, vol. 7, no. 2, pp. 849-875, 2015.

[4] M. Yang and W. J. Brackenbury, "Membrane potential and cancer progression." *Frontiers in Physiology,* vol. 4, 185, 2013.

[5] M. B. Djamgoz, R. C. Coombes, and A. Schwab, "Ion transport and cancer: from initiation to metastasis." *Philosophical Transactions of the Royal Society B: Biological Sciences*, vol. 369, no. 1638, pp. 20130092, 2014.

[6] X. Huang and L. Y. Jan, "Targeting potassium channels in cancer." *J. Cell Biol*, vol. 206, no. 2, pp. 151–162, 2014.

[7] M. B. Kalofonou, and C. C. Toumazou, " Semiconductor technology for early detection of DNA methylation for cancer: From concept to practice." *Sensors and Actuators*, vol. 178, pp. 572-580, 2013.

[8] D. H. Kim, P. P. Provenzano, C. L. Smith, and A. Levchenko, "Matrix nanotopography as a regulator of cell function." *J. Cell Biol*, vol. 197, no. 3, pp. 351−360, 2012.

[9] X. Jiang, D. Bruzewicz, A. P. Wong, M. Piel, and G. M. Whitesides, "Directing cell migration with asymmetric micropatterns." *Proc. Natl. Acad. Sci. U. S. A*, vol. 102, no. 4, pp. 975−978, 2005.

[10] G. Mahmud, *et al.* "Directing cell motions on micropatterned ratchets." *Nat. Phys*, vol. 5, no. 8, pp. 606−612, 2009.

[11] R. McBeath, D. M. Pirone, C. M. Nelson, K. Bhadriraju, and C. S. Chen, "Cell shape, cytoskeletal tension, and rhoA regulate stem cell lineage commitment." *Dev. Cell*, vol. 6, no. 4, pp. 483−495, 2004.

[12] E. Avizienyte and M. C. Frame, "Src and FAK signalling controls adhesion fate and the epithelial-to-mesenchymal transition." *Curr. Opin. Cell Biol.*, vol. 17, no. 5, pp. 542-547, 2005.

[13] K. C. Popat, *et al.* "Osteogenic differentiation of marrow stromal cells cultured on nanoporous alumni surfaces." *J. Biomed. Mater. Res.,* vol. 80A, no. 4, pp. 955−964, 2007.

[14] R. A. Gittens, *et al.* "Differential responses of osteoblast lineage cells to nanotopographically-modified, microroughened titanium- aluminum-vanadium alloy surfaces." *Biomaterials*, vol. 33, no. 35, pp. 8986−8994, 2012.

[15] L. E. McNamara, *et al.* "The role of microtopography in cellular mechanotransduction." *Biomaterials,* vol. 33, no. 10, pp. 2835−2847, 2012.

[16] M.J. Dalby, N. Gadegaard, M. O. Riehle, C. D. Wilkinson, and A. S. Curtis, "Investigating filopodia sensing using arrays of defined nano-pits down to 35 nm diameter in size." *Int. J. Biochem. Cell Biol.*, vol. 36, no. 10, pp. 2005−2015, 2004.

[17] M. Dalby, "Use of nanotopography to study mechanotransduction in fibroblasts− methods and perspectives." *Eur. J. Cell Biol*, vol. 83, no. 4, pp. 159−169, 2004.

[18] M. J. Dalby, "Topographically induced direct cell mechanotransduction, " *Eng. Phys,* vol. 27, no. 9, pp. 730−742, 2005.

[19] A. M. Rajnicek, S. Britland, and C. McCaig, "Contact guidance of CNS neurites on grooved quartz: influence of groove dimensions, neuronal age and cell Type." *J. Cell Sci,* vol. 110, pp. 2905−2913, 1997.

[20] D. Fozdar, S. Chen, and C. Schmidt, "Selective axonal growth of embryonic hippocampal neurons according to topographic features of various sizes and shapes." *Int. J. Nanomed*, vol. 6, no.1, pp. 45−57, 2010.

[21] N. Gomez, J. Lee, J. Nickels, and C. Schmidt, "Micropatterned polypyrrole: a combination of electrical and topographical characteristics for the stimulation of cells." *Adv. Funct. Mater*, vol. 17, no. 10, pp. 1645−1653, 2007.

[22] N. Gomez, S. Chen, and C. E. Schmidt, "Polarization of hippocampal neurons with competitive surface stimuli: contact guidance cues are preferred over chemical ligands." *J. R. Soc., Interface,* vol. 4, no. 13, pp. 223−233, 2007.

[23] N. Gomez, Y. Lu, S. Chen, and C. E. Schmidt, "Immobilized nerve growth factor and microtopography have distinct effects on polarization versus axon elongation in hippocampal cells in culture." *Biomaterials*, vol. 28, no. 2, pp. 271−284, 2007.

[24] A. Ferrari, *et al.* "Neuronal polarity selection by topography-induced focal adhesion control." *Biomaterials*, vol. 31, no. 17, pp. 4682−4694, 2010.

[25] S. Wang, Y. Wan, and Y. Liu, "Effects of nanopillar array diameter and spacing on cancer cell capture and cell behaviors." *Nanoscale*, vol. 6, no. 21, pp. 12482−12489, 2014.

[26] S. Wang, *et al.* "Three-dimensional nanostructured substrates toward efficient capture of circulating tumor cells." *Angew. Chem., Int. Ed,* vol. 48, no. 47, pp. 8970−8973, 2009.

[27] X. Xie, *et al.* "Nanostraw-electroporation system for highly efficient intracellular delivery and transfection." *ACS Nano,* vol. 7, no. 5 pp. 4351−4358, 2013.

[28] C. Chiappini, *et al.* "Biodegradable nanoneedles for localized delivery of nanoparticles in vivo: exploring the biointerface." *ACS Nano*, vol. 9, no. 5, pp. 5500−5509, 2015.

[29] A. K. Shalek, *et al.* "Nanowire-mediated delivery enables functional interrogation of primary immune cells: application to the analysis of chronic lymphocytic leukemia." *Nano Lett.,* vol. 12, no. 12, pp. 6498−6504, 2012.

[30] H. Persson, *et al.* "Fibroblasts cultured on nanowires exhibit low motility, impaired cell division, and DNA damage." *Small,* vol. 9, no. 23, pp. 4006−4016, 2013.

[31] A. K. Shalek, *et al.* "Vertical silicon nanowires as a universal platform for delivering biomolecules into living cells." *Proc. Natl. Acad. Sci. U. S. A.,* vol. 107, no. 5, pp. 1870−1875, 2010.

[32] J. J. VanDersarl, A. M. Xu, and N. A. Melosh, "Nanostraws for direct fluidic intracellular access." *Nano Lett.,* vol. 12, no. 8, pp. 3881−3886, 2012.

[33] F. Zhang, *et al.* "Hierarchical nanowire arrays as three-dimensional fractal nanobiointerfaces for high efficient capture of cancer cells." *Nano Lett.,* vol. 16, no. 1, pp. 766− 772, 2016.

[34] S. Nagrath, *et al.* "Isolation of rare circulating tumour cells in cancer patients by microchip technology." *Nature,* vol. 450, no. 7173, pp. 1235−1239, 2007.

Chapter 4

Surface Functionalization of Nanoporous PLGA Microparticles

4.1   Introduction

Polymeric particles from synthetic PLGA have been widely used for controlling delivery of drugs and *in vivo* studies. PLGA blocks are built from lactic and glycolic acid monomers that can be metabolized by the cell. Therefore, PLGA is safe, non-toxic and used to deliver a drug in a stable and protective form. Moreover, hydrophilic and hydrophobic small molecule drugs, DNA and proteins can be encapsulated [1]. Due to the excellent biocompatibility [2-3], the release of encapsulated molecules is achieved via degradation and erosion of the polymer matrix [4-6].

However, nanotechnology offers unique and fascinating approaches in the area of nanomedicine and healthcare application [7-8]. Among these are the nanoporous microparticles for bioseparation, drug release and tissue engineering. In bioseparation, highly nanoporous microspheres have been extensively commercialized in chromatography, such as size exclusion chromatography (SEC) and high-performance chromatography (HPLC) [9-11]. In drug release, nanoporous microspheres can be designed to be multifunctional carriers for efficiently loading drugs, specifically targeting drug delivery and controllable release [12-13]. In tissue engineering and regenerative medicine, nanoporous microspheres are one of the best candidates for regenerative, repair and tissue engineering [14-15]. These nanoporous microparticles exhibit significant advantages in many practical applications. Ion channels are ideal drug targets as the respective small molecules may be effective from the extracellular space and do not need to enter the target cells. In addition, it is becoming increasingly clear that the inhibition of ion channels is effective in halting tumor growth and metastasis [16-18]. The use of channel inhibitors is limited by side effects.

In this study, we present surface modification of nanoporous PLGA microparticles (Figure. 1) at the monolayer level, specifically, the covalent bonding between the carboxylic groups in PLGA with an amine targeting ligand group. Also, the effect of salt concentration on the formation of nanoporous and microparticles porosity is measured. Consequently, we introduce an approach that can be used to block VGIC activity; whereas, channel blockers on PLGA microparticles can act like a cork in a bottle, preventing the flow of ions until it slowly diffuses off. A targeted approach blocking VGIC activity will provide less toxicity and a better-tolerated treatment.
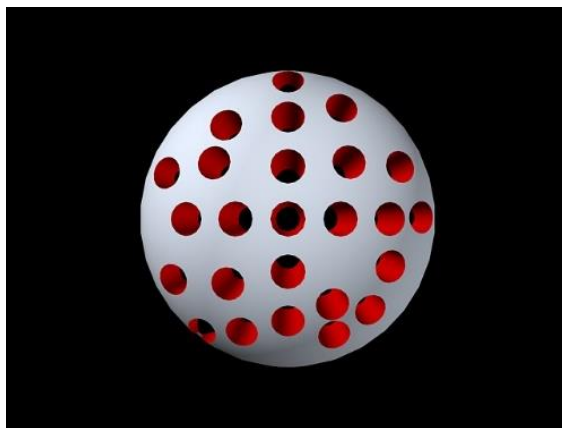
Figure 1.   3D sketch of nanoporous PLGA microparticles

4.2   Material and Methods

4.2.1   Chemicals

Poly (D, L-lactide-*co*-glycolide) 75:25 molar ratio with a carbocyclic group (uncapped) was obtained from Resomer® (Darmstadt, Germany). 1, 2-Dichloroethane (ACS reagent, ≥99%), polyvinylpyrrolidone (PVP-k90), 1-(3-dimethylaminopropyl) -3-ethylcarbodimide hydrochloride (EDC), *N*-hydroxysuccinimide (NHS), L-Lysine and sodium bicarbonate (NaHCO$_3$) were purchased from Sigma-Aldrich (St. Louis, Missouri, USA).

Micro BCA protein assay kit was purchased from Thermo-Scientific, Rockford, Illinois, USA.

4.2.2 Synthesis of nanoporous PLGA microparticles

PLGA microparticles were synthesized using w/o/w double emulsion method. Specifically, 3% (w/v) of PLGA solution was prepared by dissolving 30 mg PLGA in 1 ml of dichloroethane. Then, 350 mg of PVP-k90 was dissolved in 7 ml of deionized (DI) water to make 5% solution of PVP-k90. Next, 200 µl DI water was added to PLGA solution and vortexed for 30 s to create water-in-oil phase. To form nanoporous microparticles, solutions of 3%, 0.5% and 0.1% (w/v) $NaHCO_3$ were prepared and added to three different water-in-oil phase samples. The solution was vortexed for 1 min to ensure well mixing. This step of adding $NaHCO_3$ solution was skipped for the preparation of nonporous microparticles as shown by the schematic flowchart in Figure. 2. It was then added drop wise to the stirring beaker of PVP-k90 solution. TABLE I shows the formed w/o/w phase batches. Next, the solution vial was kept on stir plate overnight in a chemical hood, allowing dichloroethane to evaporate. Once the dichloroethane evaporated completely, the solution was transferred into a 15 ml tube and centrifuged at 4000 rpm for 15 min. The pellets were collected and suspended in PBS, then freeze-dried at -80 °C.

The freeze-dried microparticles were taken in a plastic tube, washed with DI water and centrifuged at 4,000 rpm for 15 min three times to perform salt leaching to get nanoporous PLGA microparticles and to completely remove the trapped salt. Iterative washing in DI water after centrifugation is known to remove the water- soluble salts completely [19-21]. The pellets were suspended in 5 ml PBS.
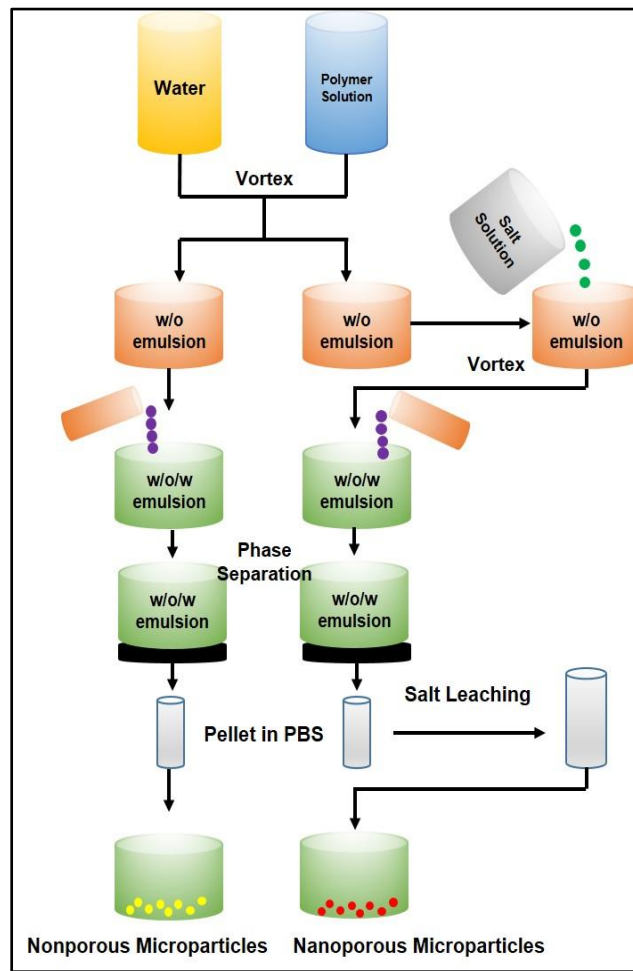
Figure 2.   Schematic flowchart. Procedure to synthesize nanoporous and nonporous

microparticles

Table I.   Percent composition (w/v) of nanoporous PLGA microparticles

Batch No.	Components % (w/v)		
	PLGA	PVP-k90	NaHCO$_3$
A	3.0	1.0	3.0

B	3.0	1.0	0.5
C	3.0	1.0	0.1
D	3.0	1.0	n/a

4.2.3 Surface functionalization

The carbodiimide crosslinker chemistry has been used to surface functionalization PLGA microparticles. EDC/NHS protocol forms an NHS ester that is considerably more stable while allowing for efficient conjugation to primary amines at physiologic pH [22]. The NHS and EDC were added to the nanoporous PLGA microparticles to modify the surface. The sample was incubated for 15 min, then washed with DI water to remove excess of EDC/NHS. The sample was suspended in DI water prepared for analysis.

4.2.4 Preparation of nanoporous PLGA microparticles for scanning electron microscope (SEM) imaging

A 10 mg freeze-dried microparticle were suspended in 1.5 ml DI water, the sample was diluted to better imaging in SEM. DI water was used instead of PBS to avoid crystallization and imaging artifacts stemming from the salts. The sample was then sputter coated with 50 Å thick gold to prevent the surface from getting charged during SEM. The thin layer of gold coating made sure that the coverslip surface was conductive enough to image with SEM.

4.2.5 Preparation of Nanoporous PLGA Microparticles for X-ray Photoelectron Spectroscopy (XPS)

A 1 mg sample size has been placed on a glass slide and kept on chemical hood overnight to dry. The first sample was nanoporous microparticles with no surface functionalization (control), and the second sample with EDC/NHS surface functionalization. XPS has been used to confirm the chemical change on the PLGA microparticles and calculate atomic percent concentrations.

4.2.6   Covalent attachment of protein with Nanoporous PLGA Microparticles

The surface functionalized nanoporous PLGA microparticles were suspended in PBS for covalent attachment of l-lysine. The microparticles underwent the process of conjugation followed by PBS washing. For each sample in Table I, 10 mg was suspended in 5 ml PBS, then 30 mg of l-lysine was added to each sample and incubated for 30 min. The excess of l-lysine was removed by centrifugation followed by PBS washes (x 2) to obtain nanoporous microparticles surface conjugated with l-lysine. Hence, amide bonds were formed between the primary amine groups of l-lysine with amine-reactive Sulfo-NHS ester on functionalized nanoporous PLGA microparticles.

4.3   Results and Discussion

The shape of nanoporous PLGA microparticles is a critical feature in the success of targeting VGIC on cancer cell. The movement of spherical shape microparticles is easier due to their symmetry. The shape of particles also influences their surface area available for surface functionalization. The nanoporous microparticles were prepared using w/o/w double emulsion method with $NaHCO_3$ as a pores foaming agent. The morphology of synthesized nanoporous PLGA microparticles was found to be spherical from SEM micrographs (Figure. 3).

The nanoporous formation was regulated by varying $NaCHO_3$ concentration. The pore size of PLGA microparticles increased with an increase in $NaHCO_3$ concentration. Images have been taken in SEM were used to calculate the microparticles diameter. The mean diameter of the nonporous PLGA microparticles was 1.05 ± 0.34 µm (n = 3). The diameter of nanoporous PLGA microparticles prepared with 0.1%, 0.5% and 3% $NaHCO_3$ was 1.53± 0.17 µm, 1.30 ± 0.50 and 1.34 ± 0.75 µm (n = 3), respectively (Figure. 4).

(a)

(b)

(c)
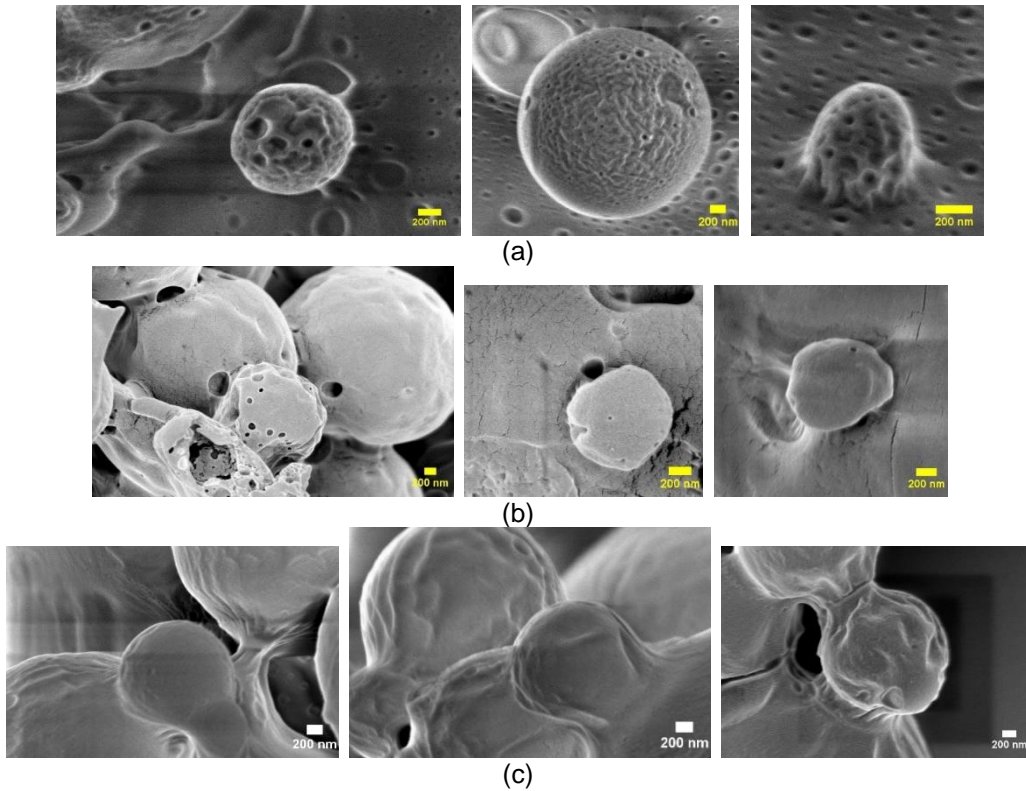
Figure 3 Nanoporous PLGA Microparticles. (a) 3% NaHCO$_3$ (b) 0.5% NaHCO$_3$

(c) 0.1% NaHCO$_3$
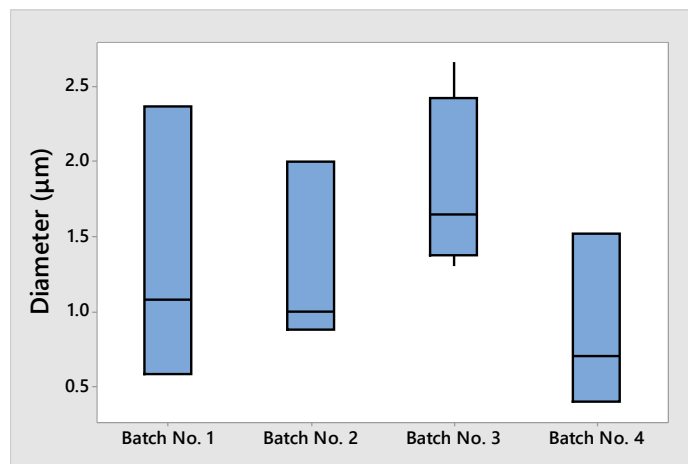
Figure 4 Diameter of nanoporous PLGA microparticles

The mean diameter of the PLGA microparticles increased with the addition of NaHCO$_3$. In this regard, microparticles size needed to be very close to platelet size (2- 3 μm) [23]; which they known to promote metastasis by protecting cancer cells against natural killer cells in the blood, because of direct contact between platelets and cancer cells. Controlling the nanoporous PLGA microparticles diameter size could assist the physical attachment to a cancer cell surface.

Selective targeting approaches require ligands that specifically interact with receptors expressed on the cell surface. Therefore, this requires multiple copies of the ligand on the carrier surface to stimulate multivalent binding effects, in which results in enhanced affinity. PLGA microparticles porosities of the samples have been calculated using *ImageJ* software (National Institutes of Health, Bethesda, Maryland, USA), where the percentage of pixels in the image have been highlighted using image threshold adjustment. Figure 5 & 6 show pore size and porosity percentage for batch 1, 2 and 3 (n = 3). The analysis showed an increase with porosity (%) as NaHCO$_3$ concentration was increased (see TABLE. II).
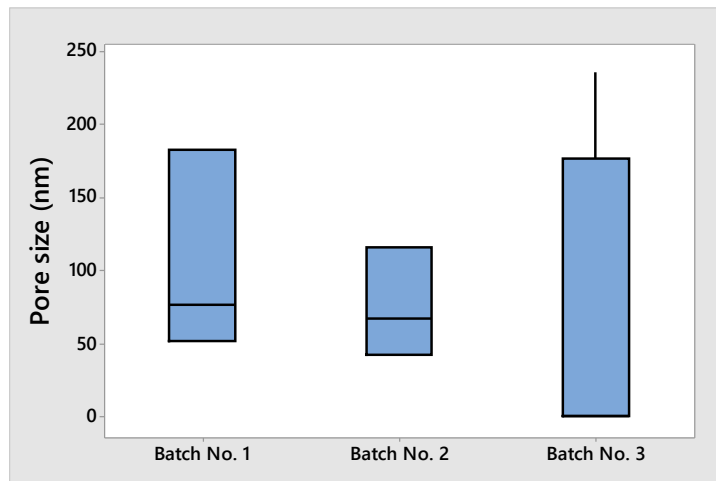
Figure 5 Pore size of nanoporous PLGA microparticles

74
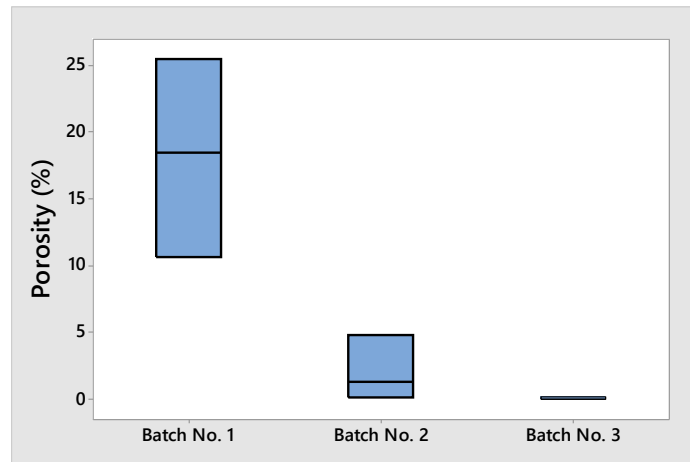
Figure 6 Porosity of nanoporous PLGA microparticles

Table II.   Sample Characterization (n = 3)

Sample	Pore Size (nm)	Porosity (%)	Diameter (µm)
A	103 ± 56	18.2 ± 6.1	1.34 ± 0.75
B	75 ± 31	2.1 ± 2.0	1.30 ± 0.50
C[a]	59 ± 102	0.07 ± 0.12	1.53± 0.17
D	n/a	n/a	1.05 ± 0.34

([a]n = 4 sample size)

The XPS chromatography was used to confirm the surface functionalization at the monolayer level. The surface modification sample had a new peak appeared that did not appear on control sample (Figure 7). The surface quantification of the O, C and N for both samples has been calculated based on the atomic percentage (Table III).

The micro BCA assay kit has been used for colorimetric detection and quantitation of total l-lysine molecules have attached to nanoporous PLGA microparticles surfaces. The absorbance of samples at 562 nm that was linear with increasing protein concentrations was measured on plate reader (n =3). The study showed a correlation between the

75
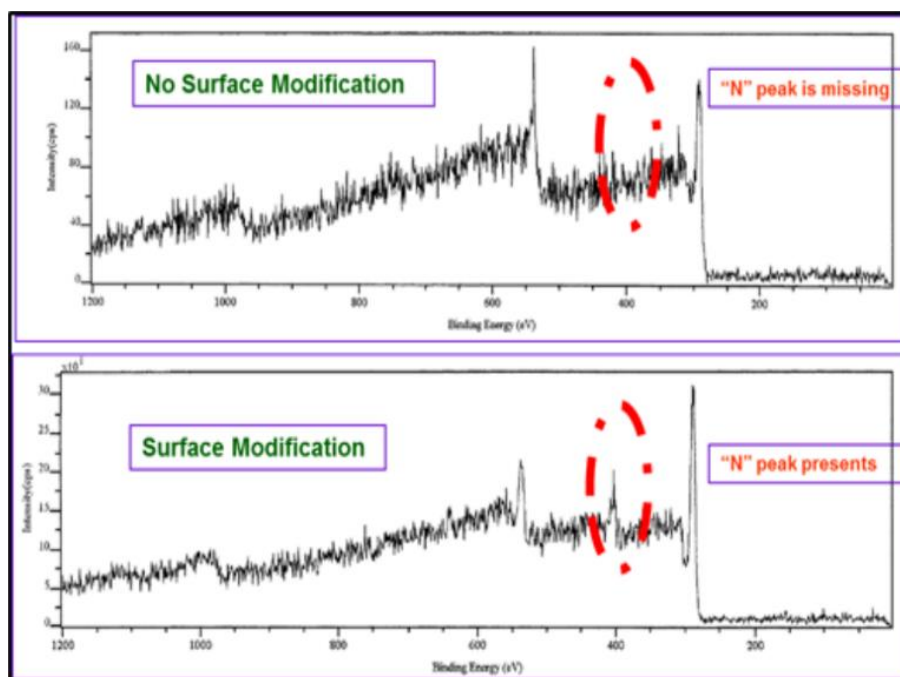
Figure 7 XPS chromatograph of sample with surface modification and no surface

modification

Table III.   XPS surface atomic concentration (%)

Sample	Peak	Atomic Concentration (%)
No surface Modification particles (control)	C (1s)	94.60
	O (1s)	5.40
Surface modified particles	C (1s)	80.50
	O (1s)	13.70
	N (1s)	5.80

amounts of l-lysine found in the sample with different batches prepared in Table I. The l-

lysine assay value for each batch and control sample of l-lysine in PBS.
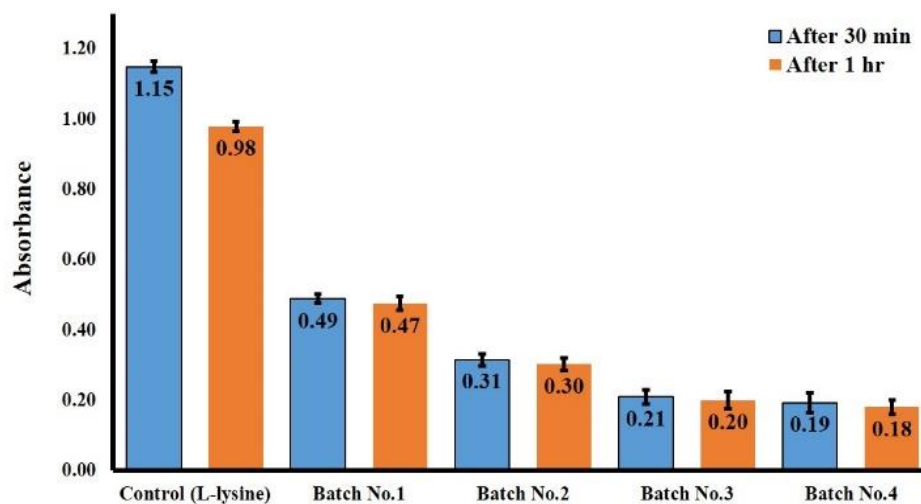
Figure 8 L-lysine assay

The batch with higher porosity showed higher l-lysine concentration. The results showed a promising a method to control the density of ligand that could conjugate on the carrier surface to stimulate multivalent binding effects, in which results in enhanced affinity. Measurement has been run after 30 min and after 1 hour from sample preparation. The results showed a very stable covalent attachment of l-lysine to nanoporous PLGA microparticles (Figure 8).

4.4   Conclusion

This paper demonstrates the synthesis of controlled porosity of nanoporous PLGA microparticles, which are functionalized to form a stable amide bond with primary amine groups. The w/o/w double emulsion technique has been used to synthesize the particles. The EDC/NHS crosslinker chemistry has been used to functionalize the nanoporous PLGA microparticles surface. Owing to the enhanced surface area, the functionalization of microparticles can maximize selectively targeting VGIC in cancer cells, which are a potentially advanced therapeutic for cancer. In fact, a higher density of VGIC blocker would

be available for specific binding PLGA microparticles have been used to load and deliver drug molecules. This work shows that the nanoporous PLGA microparticles platform can be designed to carry out multifunctional purposes.

4.5 Acknowledgments

4.6 References

[1] W. Zheng, "A water-in-oil-in-oil-in-water (W/O/O/W) method for producing drug-releasing, double-walled microspheres." International Journal of Pharmaceutics, vol. 374, no. 1-2, pp. 90-95 2009.

[2] W. Barrow, "Microsphere Technology for Chemotherapy of Mycobacterial Infections." Current Pharmaceutical Design, vol. 10, no. 26, pp. 3275-3284, 2004.

[3] D. N. Kapoor, et al. "PLGA: a unique polymer for drug delivery." Therapeutic Delivery, vol. 6, no. 1, pp. 41-58, 2015.

[4] J. M. Anderson and M. S. Shive, "Biodegradation and biocompatibility of PLA and PLGA microspheres." Advanced Drug Delivery Reviews, vol. 28, no. 1, pp. 5-24, 1997.

[5] J. M. Anderson and M. S. Shive, "Biodegradation and biocompatibility of PLA and PLGA microspheres." Advanced Drug Delivery Reviews, vol. 28, no. 1, pp. 5-24, 1997.

[6] S. Fredenberg, et al. "The mechanisms of drug release in poly(lactic-co-glycolic acid)-based drug delivery systems—A review." International Journal of Pharmaceutics, vol. 415, no. 1-2, pp. 34-52, 2011.

[7] M. Cegnar, et al. "Nanoscale polymer carriers to deliver chemotherapeutic agents to tumours." Expert Opinion on Biological Therapy, vol. 5, no. 12, pp. 1557-1569, 2005.

[8] L. Juillerat-Jeanneret and F. Schmitt, "Chemical Modification of Therapeutic Drugs or Drug Vector Systems to Achieve Targeted Therapy: Looking for the Grail." ChemInform, vol. 27, no. 4, pp.574-590, 2009.

[9] I. Halasz and C. Horvath, "Porous Layer Glass Bead Column Packing in Gas Adsorption Layer Chromatography." Analytical Chemistry, vol. 36, no. 12, pp. 2226-2229, 1964.

[10] I. Halasz and C. Horvath, "Micro Beads Coated with a Porous Thin Layer as Column Packing in Gas Chromatography. Some Properties of Graphitized Carbon Black as the Stationary Phase." Analytical Chemistry, vol. 36, no. 7, pp. 1178-1186, 1964.

[11] J. Kirkland, "Porous silica microspheres for high-performance size exclusion chromatography." Journal of Chromatography, vol. 125, no. 1, pp. 231-250, 1976.

[12] D. A. LaVan, T. McGuire and R. Langer, "Small-scale systems for in vivo drug delivery." Nature Biotechnology, vol. 21, no. 10, pp.1184-1191, 2003

[13] F. Mohamed and C. F. Van der Walle, "Engineering Biodegradable Polyester Particles with Specific Drug Targeting and Drug Release Properties." Journal of Pharmaceutical Sciences, vol. 97, no. 1, pp. 71-87, 2008

[14] D. W. Hutmacher, "Scaffolds in tissue engineering bone and cartilage." Biomaterials, vol. 21, no. 24, pp. 2529-2543, 2000.

[15] H. J. Chung and T. G. Park, "Surface engineered and drug releasing pre-fabricated scaffolds for tissue engineering." Advanced Drug Delivery Reviews, vol. 59, no. 4-5, pp. 249-262, 2007.

[16] S. M. Huber, "Oncochannels." Cell Calcium, vol. 53, no. 4, pp. 241-255, 2013.

[17] K. L. Turner and H. Sontheimer, "Cl- and K+ channels and their role in primary brain tumour biology." Philosophical Transactions of the Royal Society B: Biological Sciences, vol. 369, no. 1638, pp. 20130095-20130095, 2014.

[18] C. D. Bortner and J. A. Cidlowski, "Ion channels and apoptosis in cancer." Philosophical Transactions of the Royal Society B: Biological Sciences, vol. 369, no. 1638, pp. 20130104-20130104, 2014.

[19] S. B. Lee, et al. "Study of gelatin-containing artificial skin V: fabrication of gelatin scaffolds using a salt-leaching method." Biomaterials, vol. 26, no. 14, pp. 1961-1968, 2005.

[20] T. G. Kim, H. J. Chung and T. G. Park, "Macroporous and nanofibrous hyaluronic acid/collagen hybrid scaffold fabricated by concurrent electrospinning and deposition/leaching of salt particles." Acta Biomaterialia, vol. 4, no. 6, pp. 1611-1619 2008.

[21] Ilyas, Azhar, et al. "Salt-Leaching Synthesis of Porous PLGA Nanoparticles." IEEE Transactions on Nanotechnology, vol. 12, no. 6, pp. 1082-1088. 2013.

[22] S. Sam, et al. "Semiquantitative Study of the EDC/NHS Activation of Acid Terminal Groups at Modified Porous Silicon Surfaces." Langmuir, vol. 26, no. 2, pp. 809-814, 2010.

[23] P. Kocbek, N. Obermajer, M. Cegnar, J. Kos, J. Kristl, "Targeting cancer cells using PLGA nanoparticles surface modified with monoclonal antibody." J Control Release, vol. 120, no. 1-2, pp. 18-26 2007.

Chapter 5

Glioblastoma Multiforme Heterogeneity Profiling with Solid-state Micropores

5.1   Introduction

Glioblastoma multiforme (GBM) is the most common form of brain cancer in adults. Survival for most GBM patients has remained low for decades[1]. GBM is characterized by uncontrolled cellular proliferation, intense resistance to cell death, diffuse infiltration, and robust angiogenesis.   It is also well recognized for intratumoral heterogeneity. The heterogeneous nature of GBM stems from mixed cytological subtypes, regional differences in gene expression, and nonuniform representation of key gene mutations and genomic alterations[2-4]. It remains unclear whether such intratumoral heterogeneity is the result of an inherent interactivity between tumor cells, genomic instability, stochastic noise at the level of transcription, translation, or post-translational modifications. Patients with GBM have a uniformly poor prognosis, with a median survival of one year[5]. Advanced approaches on scientific and clinical fronts are needed that can help identify tumor sub-types in a quick and robust manner.

Histopathology remains the gold standard for the diagnosis and classification of glioblastoma. The World Health Organization (WHO) classification of glioblastoma depends on cellular morphology to determine tumor grade, testing the presence or absence of nuclear atypia, mitotic activity, and microvascular proliferation[6]. This classification system is depended on inter-observer subjectivity, which is replete with errors[7]. Tumors with the same histopathological classification also show usually variable clinical presentation. The primary glioblastoma forms most commonly in old patients. In contrast, secondary glioblastoma occurs in younger patients. The molecular analysis shows GBM arises from different genomic alterations[8].

A technology-based surgery is necessary to resect tumor from patient's brain with an adequate margin. Tumors have a distinct borderline where they stop and the normal brain mass begins. The surgeons must be able to identify the area between tumor and

neighboring brain tissue to remove only the tumor. Optical techniques are useful for brain tumor surgery in providing real-time intraoperative information[9]. The introduction of computed tomography (CT) scanning, magnetic resonance imaging (MRI) and image-guided neuronavigation allow accurate resection of the tumor. The new optical microscopy techniques that use nonlinear light-matter interactions have been developed to generate signal contrast [10]. Two-photon microscopy (TPM) has been widely used for translational and clinical cancer research[11, 12]. TPM uses either exogenous markers or endogenous contrasts including auto-fluorescence[13]. It has been used for clinical application but it is limited due to biocompatibility issues of the markers. Coherent anti-Stokes Raman scattering (CARS) microscopy is another nonlinear imaging modality that can be used for chemically-selective imaging of brain tumors. CARS microscopy is based on intrinsic vibrational properties of the molecules and thus does not require staining or labeling[14]. Overall, it has been challenging to differentiate tumor margin due to the limited resolution of these techniques[15].

Many groups have used high dimensional profiling studies such as gene expression profiling to identify signatures associated with receptor proteins such as epidermal growth factor receptor (EGFR) overexpression[16-20]. Despite its aggressive nature, GBM rarely forms clinically evident metastases, with only 0.4% of cases having metastases to visceral organs, including liver, spleen, kidney, and skin[21]. It is unclear whether GBM cells are incapable of invading into the vasculature, or invasive GBM cells circulate in the blood but are unable to proliferate in tissues outside of the brain.

We report a simple and efficient electrical detection approach using solid-state micropores to create database of GBM cell lines translocation behavior and identifying GBM cell types in patient samples. The database provided us a library to map the behavior of cells from patient samples. A single micropore setup works on the principle of cell

counter, where any physical blockage of the micropore channel causes a dip in the ionic current[22]. Previously, a similar device was used to detect lung cancer cells[23], differentiate between metastatic and non-metastatic tumor cells[24], and size-based detection of circulating tumor cells (CTCs) from the whole blood of a cancer patient[25]. The approach provides rapid detection of cell subtype based on their size and mechano-physical properties like elasticity, viscosity, and stiffness. The use of a single micropore device enables the detection of GBM cells and maps cells to the library. Although on-site histopathology provides an accurate diagnosis, it is time-consuming and expensive. Thus, there exists a clinical demand of better approaches for precise tumor margin delineation with advanced optical imaging modality. This approach provides an inexpensive instrument that can be used for brain delineation in a lab-on-a-chip setting.

5.2   Materials and methods

5.2.1   Micropore Device Fabrication

The fabrication process started with p-type double side polished, silicon wafer of (100) crystallographic orientation. First, wafer was cleaned in a piranha solution (H_2SO_4: H_2O_2 at 3:1). Then, 500 nm silicon dioxide (SiO_2) was thermally grown on the wafer. Positive photoresist (Shipley S1813) was coated on both sides of the wafer. A standard g-line photolithography process and dark field mask were used to transfer a square pattern on to the wafer. The wafer was developed for 40 seconds in MF-319 developer solution to obtain square windows patterned on one side of the wafer. The buffered hydrofluoric (BHF) acid was used to etch away SiO_2 film and transfer square window patterns to reveal bare silicon wafer underneath. Then, acetone was used to remove the residual photoresist from both sides of the wafer.

Tetramethyl ammonium hydroxide (TMAH) is anisotropic silicon etchant. It was used to make membranes through the square window. Wafer was dipped in BHF for 30 seconds to remove native oxide from opened areas, then immersed in 25% TMAH solution at 90 °C with steady stirring at 200 rpm (etch rate: ~1 μm min^{-1})[32]. The etching stopped when silicon got etched through the whole thickness and thin SiO_2 membrane was reached on the other side of the wafer.

A micropore of 20 μm diameter was drilled in 200 nm thin SiO_2 membrane using focused ion beam (FIB). The size of the drilled micropore depended on the FIB milling current, thickness of SiO_2 membrane and drilling time[26, 33-35]. The higher the exposure time or the milling current, the larger was the diameter of the resulting micropore. FIB dose (30 kV acceleration voltage, 1 nA milling current and 300 seconds exposure time) was used to drill 20 μm pore in SiO_2 membrane. After drilling, each chip was annealed at a high temperature for 5 minutes to smoothen the walls of the micropore and to relieve stresses on the oxide membranes[34].

5.2.2   Glioblastoma Multiforme (GBM) Cancer Cell Line Culture

All methods were carried out in accordance with relevant guidelines and regulations. The culture of GBM cell lines (G55, D54 EGFRviii, U87, and U251) has been reported before[36]. Briefly, these cells were cultured in DMEM/F-12 (Cellgro) with 10% fetal bovine serum. Gentamycin and L-glutamine (Invitrogen) were added to the cell culture medium and plated at a density of 3×10^6 live cells per 60 mm plate.

5.2.3   Human Astrocyte Cell Culture

Human astrocyte cells were obtained from consenting patients at the University of Oklahoma Health Science Center (OK, USA). The collected human astrocyte cells were cultured in DMEM/F-12 (Cellgro) with 10% fetal bovine serum. Gentamycin and L-

glutamine were added to the cell culture medium. Standard cell culture conditions i.e. a sterile, humidified, 95% air, 5% CO_2, and 37 °C were maintained.

5.2.4   GBM Patient Samples

GBM cancer cells (Case 8 and 25) found in brain tissue were obtained from consenting patients at the University of Oklahoma Health Science Center (OK, USA). The collected brain tissue containing GBM cancer cells were collected in ice-cold Hanks medium and were chemically dissociated with papain and dispase (both 2%). The cells were cultured in chemically defined, serum-free Dulbecco's Modified Eagle's Medium (DMEM)/ F-12 medium supplemented with 20 ng ml^{-1} mouse EGF (from Peprotech, Rocky Hill, NJ), 1× B27 supplement (Invitrogen, Carlsbad, CA), 1 × insulin-transferrin-selenium-X (ITS-X, Invitrogen), and penicillin:streptomycin (100 U ml^{-1} : 100 µg ml^{-1}) (HyClone, Wilmington, DE, USA). CD133p GBM cancer cells were provided by the University of Texas Southwestern medical center with the approval of IRB[37].

5.2.5   Measurement of GMB Cancer Cell Diameter

GBM cancer cell lines and GBM cells collected from patients samples were dissociated with Trypsin-EDTA (0.05%) and seeded on a hemocytometer to measure the cell diameters. The dissociated cancer cells were imaged and their diameters were measured by ImageJ software (National Institutes of Health, Bethesda, Maryland, USA). For statistical analysis, ANOVA analysis was carried out. The averages and standard deviations were calculated.

5.3   Results

5.3.1   Micropore Measurements

The fabrication of micropore is listed in detail in methods section. Figure. 1(a-d) give a summary of the solid-state micropore fabrication process. Two Teflon blocks were

used to clamp the micropore chip. Polydimethylsiloxane (PDMS) gaskets were used to hold the chip in between Teflon blocks and to prevent leakage of solution during the experiments. Each block had a channel ending in 1 mm opening, which aligned with gaskets and micropore chip when the blocks were assembled together.The two Teflon blocks formed the inlet and outlet chambers. Inlet and outlet tubes were connected to the Teflon blocks. The inlet chamber was connected to syringe pump through a tube adapter. Ag/AgCl electrode pair was used to bias the chip and to record ionic current. One electrode was dipped in each chamber and these were connected to data acquisition cards of a computer.

The syringe pump injected the cell suspension made up of 0.85% NaCl solution through the inlet chamber while the other chamber was filled with just 0.85% NaCl. The ionic current through the micropore was monitored and when a cell translocated through the micropore, physical blockage resulted in a unique pulse in the current traces. Pulse magnitude, width, and shape indicated the mechano-physical property of the translocating cell. This data for all the cells in the samples provided the quantitative behavior of each single cell, which specifically correlated to the physiological status of the cell. When a cell translocated through the micropore, the physical blockage of the micropore increased resistance to the ionic current flow.

(a)

(b)

(c)

(d)
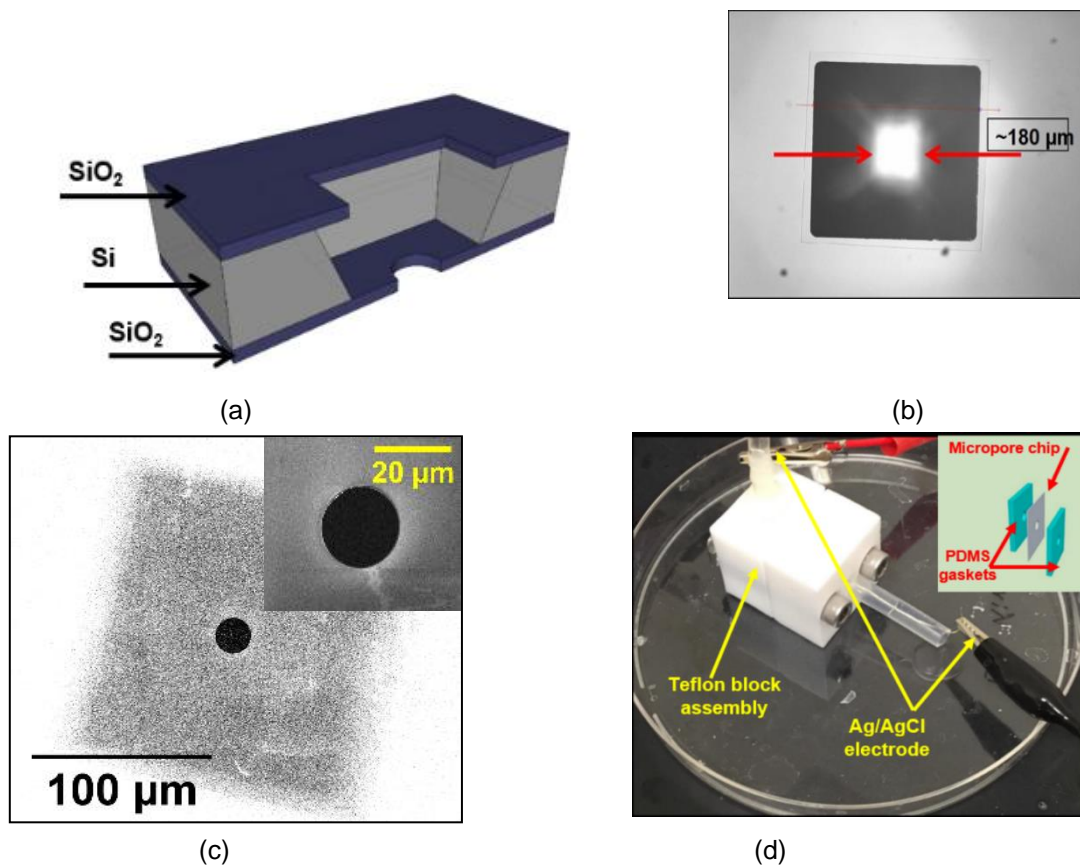
Figure 1. Solid-state micropore fabrication process and experiment setup. (a) 3D cross-section sketch of micropore in SiO_2 membrane. (b) Photolithography to open a window in photoresist and BHF etch to transfer square pattern to oxide. The TMAH solution wet etches silicon all the way through to reach thin suspended SiO_2 membrane on the other side. (c) FIB drilling to make 20 μm micropore in SiO_2 membrane. (d) The chip with single micropore is sandwiched between the Teflon blocks. PDMS gaskets are used to avoid leakage. Ag/AgCl electrodes are inserted into the tubing attached to inlet and outlet chambers. Inset shows a sketch of the PDMS gaskets sealing micropore chip.

The resistance of flow of ionic current is given by $R = \rho L/A$, where ρ is the resistivity of the medium (0.85% w/v NaCl solution), L represents thickness of oxide membrane

(length of the micropore) and *A* stands for effective area of micropore. Therefore, any variation to the effective area of the micropore due to physical blockage from the translocating cells was measured as the change in its resistance[26].

The flow rate of cells and the sampling frequency for micropore measurements had to be optimized. A very high flow rate increased the device throughput but decreased the resolution between two different cell types. At low flow rate, the device throughput became too small. Using a very high sampling frequency added too much noise to the system, consequently decreasing the device sensitivity. In contrast, low sampling frequency had less noise but it resulted in missing fast translocation events, again reducing the sensitivity[25]. Taking these two parameters into consideration, experiments were performed at a flow rate of 20 μl/min and sampling rate of 200 KHz.

5.3.2   *Measurements of Cell Diameters*

The U251, U87, D54 EGFRviii, and G55 cells are indicative of the most significant cells in a glioblastoma mass. All of these cells assumed spherical shapes in suspension and were found to be healthy after disaggregation. The optical micrographs of these cell lines and human astrocytes (healthy cells) were taken before running the sample through the micropore as shown in Figure 2(a-e). The cellular diameters were measured in *ImageJ* for each cell line. The statistical analysis of the data was done by an ANOVA test. The variance analysis showed that the effect of different cell types on cell's diameters was significantly different (F $(4, 232)$ = 122.29, *p*-value = 0.0005). The analysis demonstrated that cells from these lines varied in size compared to normal human astrocytes cells. Thus, a size-based discrimination should be feasible to distinguish between cell lines. The box plot of cellular diameters from the optical micrographs of each cell type is shown in Figure 2(f). The average diameters of U251, U87, D54 EGVRviii, G55, and human astrocytes are
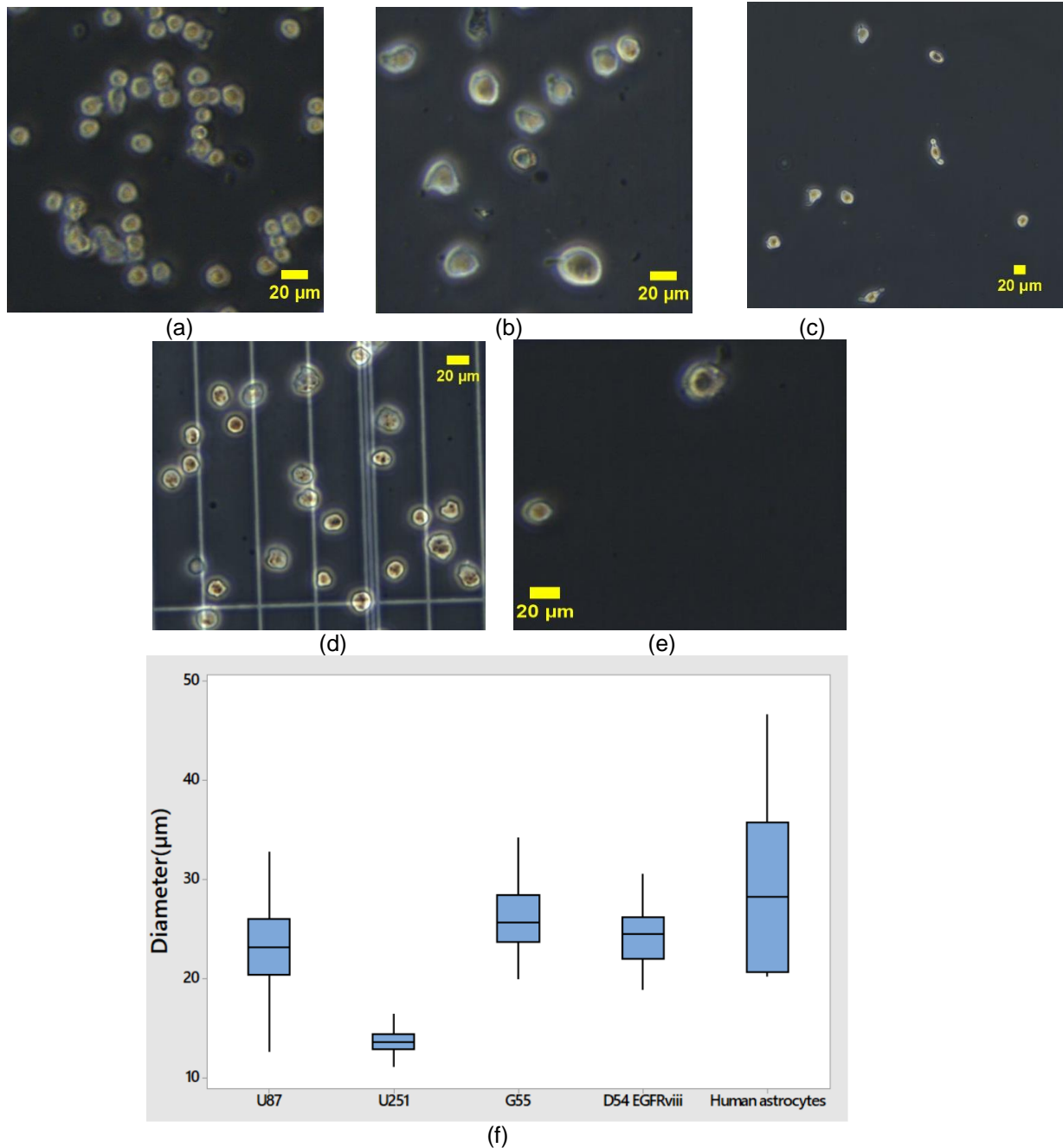
Figure 2. Optical micrographs of cells (a) U251, (b) U87, (c) D54 EGFRviii, (d) G55, and

(e) Human astrocytes. (f) Box plot of cell diameters. The average diameter of U251 was

found to be much smaller than others (p-value = 0.0005)

91

13.73 µm (S.D. 1.20), 23.39 µm (S.D. 4.27), 24.19 µm (S.D. 3.18) 26.77 µm (S.D. 4.73), and 29.35 µm (S.D. 9.28), respectively.

5.3.3   GBM Cell Lines Library

After measuring the average diameter of each GBM cell line, separate solutions were prepared for each cell line by suspending 100,000 cells of each in 10 ml NaCl solution. Each GBM cell line was processed for 15-20 minutes through a 20 µm micropore and data was recorded at the optimized settings. Cells of each type caused significantly distinct current blockage signatures while translocating through the micropore. The experiments were repeated twice per cell line and cells were detected from the acquired pulses.

Analysis of the acquired data showed the distinguishing electrical characteristics between the GBM cell lines. The data showed different translocation profiles for each GBM cell line suspensions as shown in Figure 3(a). Each cell line shows a unique cluster that is distinctive from the clusters recorded for the other cell lines. The unique characteristics of the electrical pulses were displayed in their peak amplitudes and pulse widths (Table I).

Table I Summary of pulse statistics for GBM cell lines through 20 µm micropore

GBM Cell line	Average translocation time (µsec)	Average peak amplitude (µA)
U251	41.06 ± 4.07[a]	0.16 ± 0.03[b]
U87	99.46 ± 9.53[a]	0.16 ± 0.02 [b]
D54 EGFRviii	69.15 ± 7.16[a]	0.17 ± 0.03 [b]
G55	173.63 ± 24.35[a]	0.72 ± 0.11 [b]

[a]$F_{(3, 2352)} = 5713.44$, $p = 0.0005$, [b]$F_{(3, 2352)} = 4874.59$, $p = 0.0005$

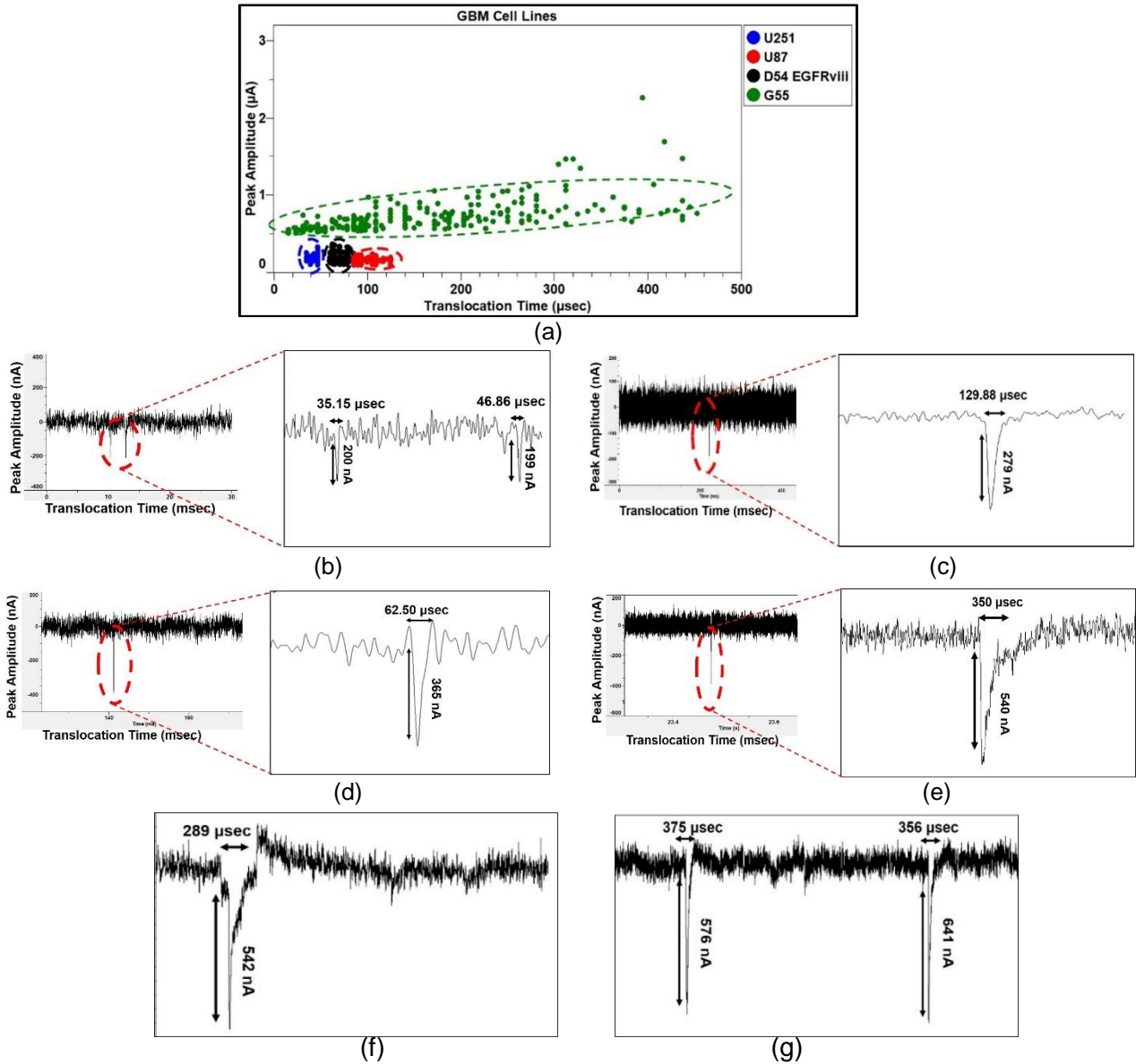Figure 3. GBM cell lines library. (a) Electrical profile of GBM cell lines using 20 μm diameter micropore. Overlaid scatter plot of electrical profile of GBM cell line through micropore shows different profile for each cell line. (b-g) Signature pulses of the four GBM cell lines through 20 μm micropore and the close-up view: (b) U251, (c) U87, (d) D54 EGFRviii and (e) G55. (f-g) closed-up pulses for G55 cell line.

The translocation time width depicted the cell dwell time in the micropore. The representative signature pulses of each cell type are shown in Figure 3(b-g). It was observed that the electrical pulses registered by U251 cells were significantly smaller than those obtained from other GBM cells. U251 pulses had an average peak amplitude of 0.16 μA (S.D. 0.03) and average pulse width of 41.06 μs (S.D. 4.07). One-way ANOVA analysis was used to show that the electrical profiles were significantly different ($F (3, 4) = 0.02$, $p = 0.996$). The differences in peak amplitudes and translocation times of the pulses were sufficient to uniquely identify the GBM cell types from their respective pulses.

5.3.4   *Reproducibility of Electrical Signatures from Micropore Device*

The diameters of the micropore devices used in experiments were measured from optical images taken before experiments (Figure 4(a)). For each GBM cell lines, the experiments were repeated twice. For each experiment run, a new micropore device was used. The average diameter of micropore devices used in the experiments was 20 μm ± 0.02 μm (n = 8). The one-way ANOVA analysis showed that the micropore devices were significantly similar ($F (3, 4) = 0.02$, p-value = 0.996). The micropore device diameter had no effect on the experiments and any change in the electrical profile was solely due to the cells passing through the micropores.

Translocation profile for each GBM cell lines was repeated twice and plotted (Figure 4(b-e)). For each run, fresh cells were suspended in 10 ml 0.85% NaCl solution. These results demonstrate the micropore reliability to recognize GBM cell lines from their unique electrical signatures.
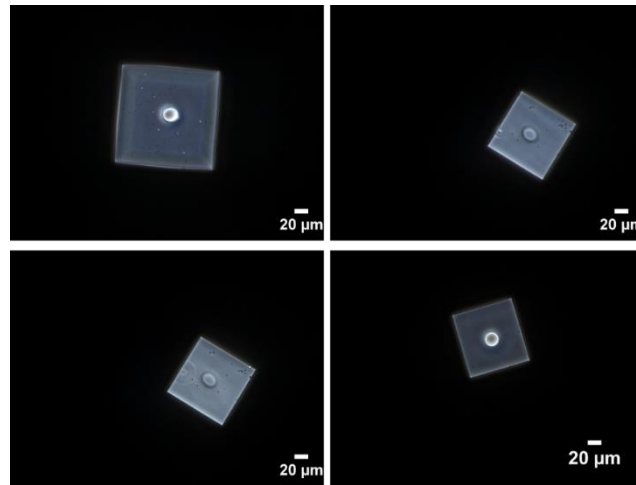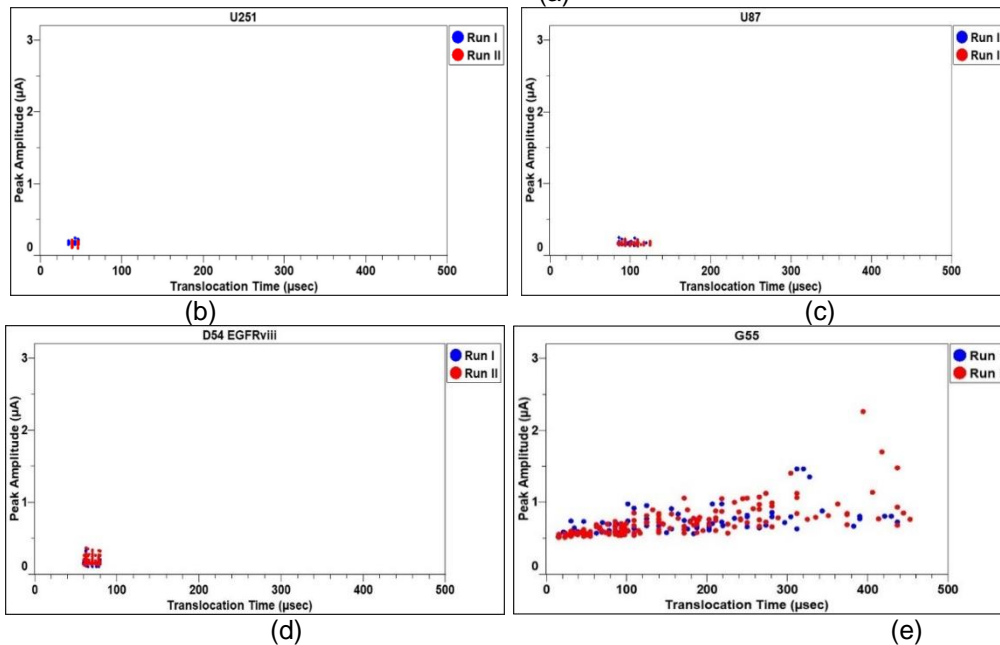
Figure 4. Reproducibility of electrical signatures. (a) Optical images for micropore devices used in the experiments. The average micropore diameter was 20 μm ± 0.02 μm (n = 8). Electrical profile of GBM cell lines using two 20 μm diameter micropores. Data for (b) U251, (c) U87, (d) D54 EGFRviii and (e) G55. The translocation profiles for each GBM cell line are same for the two experiments. This indicates the data is reproducible among the devices.

5.3.5   GBM Cell Detection from Brain Tumor Patient-Derived Samples

Patient-derived samples (10,000 cells) were prepared in 5 ml of 0.85% NaCl and processed through the micropore. Each sample (Case 8, CD133p and Case 25) was processed through a 20 µm micropore for 15–20 min. The cell detection efficiency was 72%, 80%, and 79%, respectively. The electrical profiles of patient-derived samples are shown in Figure 5 (a-c). The four different GBM cell profiles can be readily identified in the representative sample by overlaying the patient's sample profile on GBM library electrical profile (Figure 5 (d-f)). The electrical profile of healthy human astrocyte cells was added to Fig. 5 (d-f). The healthy cells showed unique electrical profiles compared to GBM cells. The registered events associated with a particular cell type profile were counted to determine the number of cells of that cell type present in each sample (Figure 5 (g-i)). This experiment clearly shows that the different subtypes of GBM cells present in patient-derived samples were detected, as well as quantified, and mapped to GBM cell line library with this technology. This differentiation stemmed from their unique biomechanophysical properties.

(a)　　　　　　　　　　　　　　(b)

(c)　　　　　　　　　　　　　　(d)

(e)　　　　　　　　　　　　　　(f)

(g)　　　　　　　(h)　　　　　　　(i)
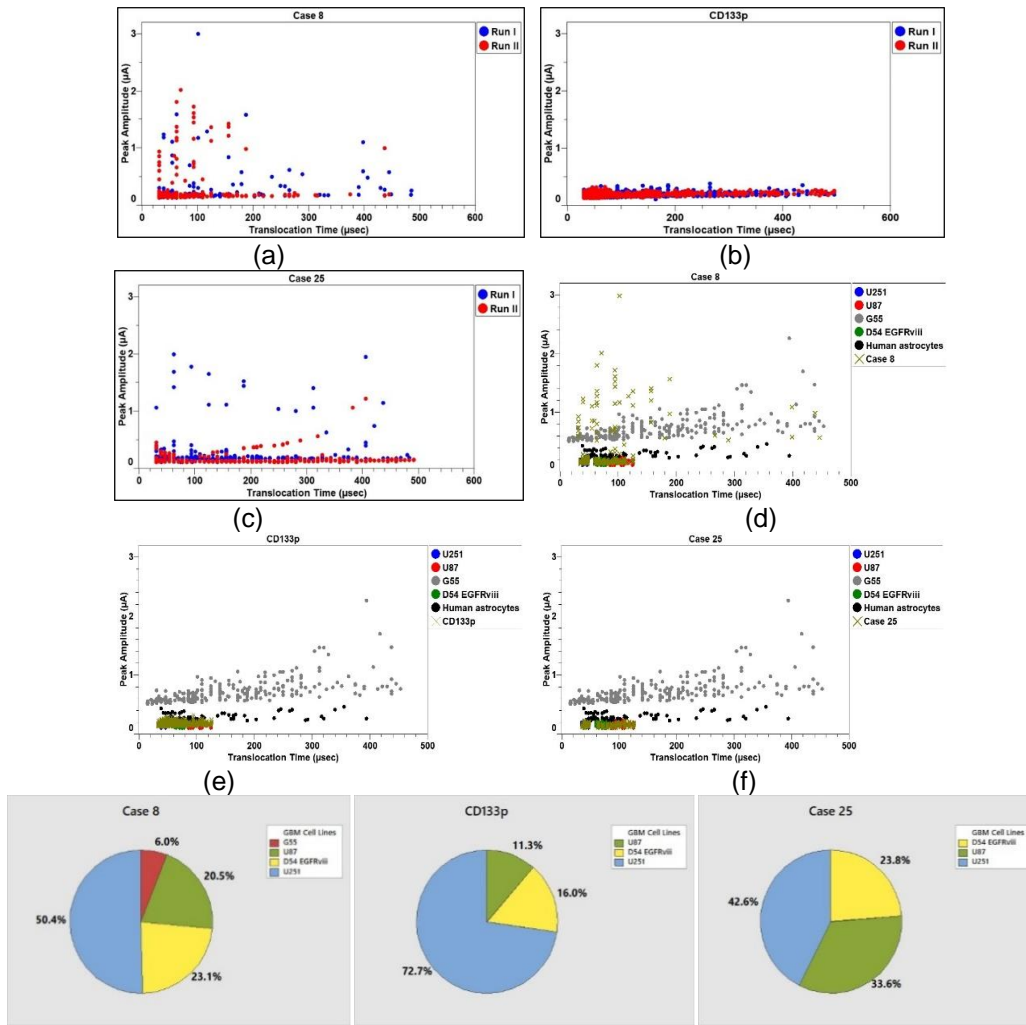
Figure 5. GBM cell detection from brain tumor patient-derived samples. (a-c) Electrical profiles of GBM patient's GBM samples for: (a) Case 8, (b) CD133p, and (c) Case 25. (d-f) The pulse profiles of GBM patient-derived samples overlaid on top of GBM cell lines and healthy human astrocytes: (d) Case 8, (e) CD133p, and (f) Case 25. (g-i) Pie charts show detailed analysis of the cell subtypes detected from the brain tumor patient- derived sample, where the percentage of each GBM cell type pulses was calculated for each patient-derived samples. The analysis shows the heterogeneity of the GBM cells within the patient samples for (g) Case 8, (h) CD133p, and (i) Case 25.

5.4   Discussion

        The development of technical abilities to differentiate between GBM cell lines using micropore technology enhanced the ability to understand brain tumor biology. The brain tumor is known for its widespread heterogeneity. Cancer is a disease of unregulated self-renewal and differentiation, understanding cancer heterogeneity is fundamental to understanding cancer-cell proliferation. GBMs show a highly heterogeneous composition of cells. It is necessary to acknowledge that these cell lines are different in their physical, mechanical and molecular properties. This approach determines the heterogeneity of cancer, which is very important in cancer diagnosis and treatment[27]. The micropore transducer differentiated and quantified the cells from four tumor cell lines and patient's samples. The reproducibility of the data was verified by repeating the experiments twice with separate micropores of the same size, and similar results were observed when processed at same conditions.

        The four cell lines of GBMs are different from each other in their cell attributes[28-30]. The small-sized U251cells were able to translocate easily through the micropore, which caused less hold back from the micropore walls[23]. For U87, D54 EGFRviii and G55 cell lines, the longer translocation times and higher peak amplitudes of the pulses indicated larger sizes and less deformability. Size is the dominant factor and a prime contributor to the translocation profile through the micropore[23], but the elasticity of the cells is also a prime contributor. It has been reported before that that cell deformability is directly linked to the elasticity of the cells[24]. While GBM cells were translocating through the micropore, they were deforming to adjust to the size of the micropore. A lower translocation time was due to the higher elastic deformability and more pliability. This meant the cells took less time to deform and adjusted to the micropore size quickly. On the other hand, longer time to deform due to lower elasticity delayed the ionic flow through the micropore for long,

yielding to higher translocation time. This implies that cell translocation time can be an indirect measure of the cell elasticity. This mechanical difference is important for GBM cell types as this tumor is composed of pathologically heterogeneous mixture of cells. These cells exhibit varying degrees of cellular and nuclear polymorphism. Although this heterogeneity is generally discussed in terms of pathological structures, examining the dynamic heterogeneity at the cellular level is fundamental to understand the origins of the cells[31].

The solid-state micropore with brain tumor patient samples identified the novel potential of the micropore in GBM heterogeneity profiling. The developed GBM library was able to distinguish GBM cell subtypes from brain tumor patient's samples. These results confirm that the patient's tumor samples contained heterogonous and dissimilar morphological subtypes, and we could map the results to each specific subtype. In clinical settings, such matching system can help against extensive heterogeneity of GBM tumor cells from patient's brain tissue to classify the subtype by comparing the data to GBM cell subtype library.

5.5   Conclusion

Discriminating the GBM tumor subtypes is a very important step in disease diagnosis and defining appropriate treatments. A novel approach is presented to detect human brain tumor cells in a sample from a cancer patient using solid-state micropores. The micropore device translated cell properties into electrical profiles to form GBM cells library. Brain tumor patient's samples were processed with the device. We detected cancer cells from patient sample and mapped these to specific cell subtype without any pre-processing, cell staining or beads attachment. The high throughput, rapid detection and faithful mapping made it suitable choice for clinical setups and diagnostic applications.

99

5.6   Acknowledgements

5.7   Author Contributions

M.G.A, Y.T.K. and S.M.I designed the experiments. T.I.A. and M.U.R. setup the current measurement system and analyzed the data. J.D.B and Y.T.K provide and cultured cells. M.G.A. and Y.T.K. performed experiments. S.M.I directed the project and supervised this work. All authors have read and approved the final manuscript.

5.8   Additional Information

Competing financial interests: The authors declare no competing financial interests

5.9　References

1.　T. S. Surawicz, F. Davis, S. Freels, E. R. Laws, Jr. and H. R. Menck, J Neurooncol, 1998, 40, 151-160.

2.　V. Jung, B. F. Romeike, W. Henn, W. Feiden, J. R. Moringlane, K. D. Zang and S. Urbschat, J Neuropathol Exp Neurol, 1999, 58, 993-999.

3.　E. A. Maher, F. B. Furnari, R. M. Bachoo, D. H. Rowitch, D. N. Louis, W. K. Cavenee and R. A. DePinho, Genes Dev, 2001, 15, 1311-1333.

4.　P. Kleihues, D. N. Louis, B. W. Scheithauer, L. B. Rorke, G. Reifenberger, P. C. Burger and W. K. Cavenee, J Neuropathol Exp Neurol, 2002, 61, 215-225; discussion 226-219.

5.　H. Ohgaki and P. Kleihues, Acta Neuropathol, 2005, 109, 93-108.

6.　D. N. Louis, H. Ohgaki, O. D. Wiestler, W. K. Cavenee, P. C. Burger, A. Jouvet, B. W. Scheithauer and P. Kleihues, Acta Neuropathol, 2007, 114, 97-109.

7.　R. Fisher, L. Pusztai and C. Swanton, Br J Cancer, 2013, 108, 479-485.

8.　R. G. Verhaak, K. A. Hoadley, E. Purdom, V. Wang, Y. Qi, M. D. Wilkerson, C. R. Miller, L. Ding, T. Golub, J. P. Mesirov, G. Alexe, M. Lawrence, M. O'Kelly, P. Tamayo, B. A. Weir, S. Gabriel, W. Winckler, S. Gupta, L. Jakkula, H. S. Feiler, J. G. Hodgson, C. D. James, J. N. Sarkaria, C. Brennan, A. Kahn, P. T. Spellman, R. K. Wilson, T. P. Speed, J. W. Gray, M. Meyerson, G. Getz, C. M. Perou, D. N. Hayes and N. Cancer Genome Atlas Research, Cancer Cell, 2010, 17, 98-110.

9.　P. A. Valdes, D. W. Roberts, F. K. Lu and A. Golby, Neurosurg Focus, 2016, 40, E8.

10.　F. Helmchen and W. Denk, Nat Methods, 2005, 2, 932-940.

11.　C. Ricard and F. C. Debarbieux, Front Cell Neurosci, 2014, 8, 57.

12. S. W. Perry, R. M. Burke and E. B. Brown, Ann Biomed Eng, 2012, 40, 277-291.

13. W. R. Zipfel, R. M. Williams and W. W. Webb, Nat Biotechnol, 2003, 21, 1369-1377.

14. C. W. Freudiger, R. Pfannl, D. A. Orringer, B. G. Saar, M. Ji, Q. Zeng, L. Ottoboni, Y. Wei, C. Waeber, J. R. Sims, P. L. De Jager, O. Sagher, M. A. Philbert, X. Xu, S. Kesari, X. S. Xie and G. S. Young, Lab Invest, 2012, 92, 1492-1502.

15. F. K. Albert, M. Forsting, K. Sartor, H. P. Adams and S. Kunze, Neurosurgery, 1994, 34, 45-60; discussion 60-41.

16. W. A. Freije, F. E. Castro-Vargas, Z. Fang, S. Horvath, T. Cloughesy, L. M. Liau, P. S. Mischel and S. F. Nelson, Cancer Res, 2004, 64, 6503-6510.

17. Y. Liang, M. Diehn, N. Watson, A. W. Bollen, K. D. Aldape, M. K. Nicholas, K. R. Lamborn, M. S. Berger, D. Botstein, P. O. Brown and M. A. Israel, Proc Natl Acad Sci U S A, 2005, 102, 5814-5819.

18. A. Murat, E. Migliavacca, T. Gorlia, W. L. Lambiv, T. Shay, M. F. Hamou, N. de Tribolet, L. Regli, W. Wick, M. C. Kouwenhoven, J. A. Hainfellner, F. L. Heppner, P. Y. Dietrich, Y. Zimmer, J. G. Cairncross, R. C. Janzer, E. Domany, M. Delorenzi, R. Stupp and M. E. Hegi, J Clin Oncol, 2008, 26, 3015-3024.

19. C. L. Nutt, D. R. Mani, R. A. Betensky, P. Tamayo, J. G. Cairncross, C. Ladd, U. Pohl, C. Hartmann, M. E. McLaughlin, T. T. Batchelor, P. M. Black, A. von Deimling, S. L. Pomeroy, T. R. Golub and D. N. Louis, Cancer Res, 2003, 63, 1602-1607.

20. H. S. Phillips, S. Kharbanda, R. Chen, W. F. Forrest, R. H. Soriano, T. D. Wu, A. Misra, J. M. Nigro, H. Colman, L. Soroceanu, P. M. Williams, Z. Modrusan, B. G. Feuerstein and K. Aldape, Cancer Cell, 2006, 9, 157-173.

21.   D. R. Smith, J. M. Hardman and K. M. Earle, Cancer, 1969, 24, 270-276.

22.   O. A. Saleh and L. L. Sohn, Rev Sci Instrum, 2001, 72, 4449-4451.

23.   W. Ali, F. J. Moghaddam, M. U. Raza, L. Bui, B. Sayles, Y. T. Kim and S. M.
      Iqbal, Nanotechnology, 2016, 27.

24.   W. Ali, A. Ilyas, L. Bui, B. Sayles, Y. Hur, Y. T. Kim and S. M. Iqbal, Langmuir,
      2016, 32, 4924-4934.

25.   W. Asghar, Y. Wan, A. Ilyas, R. Bachoo, Y. T. Kim and S. M. Iqbal, Lab Chip,
      2012, 12, 2345-2352.

26.   A. Ilyas, W. Asghar, S. Ahmed, Y. Lotan, J. T. Hsieh, Y. T. Kim and S. M. Iqbal,
      Anal Methods-Uk, 2014, 6, 7166-7174.

27.   A. Soeda, A. Hara, T. Kunisada, S. Yoshimura, T. Iwama and D. M. Park, Sci
      Rep-Uk, 2015, 5.

28.   M. Westphal, M. Hansel, W. Hamel, R. Kunzmann and F. Holzel, Acta Neurochir,
      1994, 126, 17-26.

29.   V. L. Jacobs, P. A. Valdes, W. F. Hickey and J. A. De Leo, Asn Neuro, 2011, 3.

30.   M. D. Inda, R. Bonavia, A. Mukasa, Y. Narita, D. W. Y. Sah, S. Vandenberg, C.
      Brennan, T. G. Johns, R. Bachoo, P. Hadwiger, P. Tan, R. A. DePinho, W.
      Cavenee and F. Furnari, Gene Dev, 2010, 24, 1731-1745.

31.   M. Venere, H. A. Fine, P. B. Dirks and J. N. Rich, Glia, 2011, 59, 1148-1154.

32.   O. Tabata, R. Asahi, H. Funabashi, K. Shimaoka and S. Sugiyama, Sensor
      Actuat a-Phys, 1992, 34, 51-57.

33.   W. Asghar, A. Ilyas, J. A. Billo and S. M. Iqbal, Nanoscale Res Lett, 2011, 6.

34.   W. Asghar, A. Ilyas, R. R. Deshmukh, S. Sumitsawan, R. B. Timmons and S. M.
      Iqbal, Nanotechnology, 2011, 22.

35. A. Ilyas, W. Asghar, Y. T. Kim and S. M. Iqbal, Biosens Bioelectron, 2014, 62, 343-349.

36. Y. Wan, M. A. Mahmood, N. Li, P. B. Allen, Y. T. Kim, R. Bachoo, A. D. Ellington and S. M. Iqbal, Cancer, 2012, 118, 1145-1154.

37. Y. Wan, Y. T. Kim, N. Li, S. K. Cho, R. Bachoo, A. D. Ellington and S. M. Iqbal, Cancer Res, 2010, 70, 9371-9380.

Chapter 6

A Facile Microfluidic Approach to Create Microencapsulation for Single Cell

Confinements

6.1   Introduction

Cell encapsulation technology allows for containing living cells in a microenvironment to be isolated from the extracellular environment.[1] The cell is considered encapsulated when entrapped within a semipermeable polymer at the micron scale. Thus, nitrogen and oxygen, as well as electrolytes can be diffused inside the microcapsule through pores of the encapsulating polymer. Consecutively, small molecules produced by the encapsulated cell, such as metabolites and waste can diffuse outside the microcapsule. This way, a microencapsulated cell is immune-isolated, presenting benefits against immunosuppression.

High-throughput encapsulation of cells into drops protect these from cross-contamination, enable the measurements of cellular diversity within samples, prevent dilution of reagents and biomarkers, and amplify signals.[2] The microencapsulation in drops also provides the ability to remerge drops into larger aqueous samples.[3,4] The reduction in dilution implies stronger detection of signals and higher accuracy in measurements, therefore, may have the ability to reduce volume required of the costly sample and reagents.[5] Encapsulation of cells in drops has been utilized to improve detection of proteins,[6] antibodies,[7,8] enzymes,[9] and metabolic activity[10] for high throughput screening, and could be used to improve high throughput cytometry.[11] Additional studies present applications in bioelectrospraying of drops containing cell for mass spectrometry[12] and targeted surface cell coatings.[13]

Generally, polysaccharides are natural polymers commonly used in cell encapsulation. The polysaccharides allow cell encapsulation under relatively mild conditions and do not interfere with the functional survival of the cells.[14,15] Another pertinent reason is that the majority of polysaccharides form hydrogels.[16] Hydrogels have many beneficial properties for cell encapsulation. They are pliable, soft, mechanically stable,[17]

and reportedly associated with minor host responses.[18] Alginate-poly-L-lysine-alginate (APA) microcapsules[19] have been the most widely investigated formulation for live cell encapsulation. However, serious limitations exist regarding their mechanical adequacy and biocompatibility for long-term *in vivo* applications.[20,21,22,23] Membrane instability causes the eruption of the capsules, resulting in undesirable escape of encapsulated cells. Synthetic polymers offer several advantages over natural polymers: (1) these can be readily synthesized in large quantities, (2) these do not have variations from batch-to-batch, (3) these can be easily engineered for desired properties, (4) these can be tailored to improve biotolerability, and (5) these can be reinforced for better mechanical properties.[24] Many synthetic polymers are associated with encapsulation processes that require the application of toxic solvents.[25,26] This implies a loss of viability or loss of cell functions.

It is known that cancer cells produce sets of antigens that are expressed on their surfaces due to mutations present within the genome of tumor cells and not because of the surrounding normal tissue. These antigens have been attractive drug and vaccine targets. However, antigens have not been investigated due to inefficient and complex isolation and sequencing techniques. The presented microencapsulation can be used to study the single cell behavior. The preparation of hollow PLGA microcapsules is presented that used a microfluidic device to encapsulate cells *in situ*.

6.2   Materials and Methods

6.2.1   Chemicals

PDMS was prepared using Sylgard 184 kits purchased from Ellsworth Adhesives (Dow Corning, Midland, MI, USA). The kit contained PDMS base and a curing agent. Poly (D, L-lactide-co-glycolide) 85:15 molar ratio with ester end group was obtained from Resomer® (Darmstadt, Germany) and 1,2-Dichloroethane was purchased from Sigma-Aldrich (St. Louis, MO).

6.2.2   Fabrication of PDMS Microfluidic Device

The microfluidic device was fabricated by embedded template method as described before.[27] Specifically, the design of the microfluidic device was a "diverged Y-shape", which contained three inlets and one outlet port (Figure 1). The outlet of the template was a plastic hollow tube with an outer diameter of 0.7 mm. A small hole was punched through the plastic hollow using a biopsy needle (26 G x 5/8 in.). The distance from one end of the plastic tube to the punched hole was 1 mm. Furthermore, a long straight aluminum wire was introduced through the hole.   This wire was bent at approximately 45° to form a V-shape to template the main inlets. Another wire was attached at the end of the plastic hollow tube. The embedded template was secured on a glass Petri dish using double-sided tape. Finally, the mixture of PDMS pre-polymer and the curing agent (ratio 10:1) were poured to cover the template completely. The whole assembly was put into a vacuum chamber for degassing. The template in the Petri dish was covered with PDMS and cured at 90 °C. The template was then pulled out from the cured PDMS.
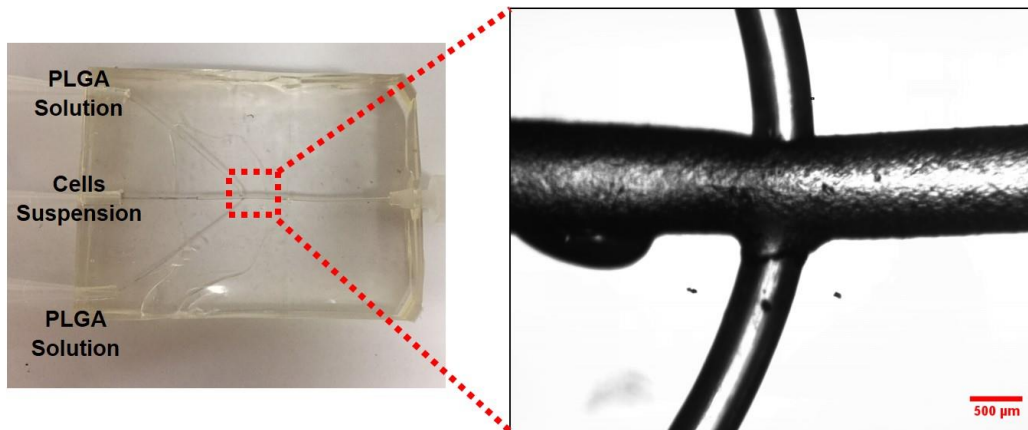

Figure 1 PDMS microfluidic flow channels to synthesize hollow PLGA microcapsules. The zoomed-in optical micrograph of the cross-junction. (Scale bar = 500 µm)

6.2.3 Human Glioblastoma Multiforme (hGBM) Cell Culture

The culture of hGBM cell line has been reported before.[28] The hGBM cells were obtained from consenting patients at the University of Texas Southwestern Medical Center at Dallas, Texas, with the approval of the Institutional Review Board. Briefly, these cells were cultured in DMEM/F-12 (Cellgro) with 10% fetal bovine serum. Gentamycin and L-glutamine (Invitrogen) were added to the cell culture medium and plated at a density of 3 × 10^6 live cells per 60 mm plate.

6.2.4 Synthesis of Hollow PLGA Microcapsules

The PLGA hollow microcapsules were prepared by a single step continuous flow method in a microfluidic device. The dispersed phase consisted of the suspended cells of solution and the continuous phase consisted of the biodegradable PLGA polymer dissolved in an organic solvent. These solutions were pushed inside the device using syringe pumps. The 10% *w/v* PLGA solution was prepared by dissolving 2 g of PLGA in 1, 2-dichloroethane and it was pushed through the side channels as the continuous phase (Q_{PLGA}). The medium solution that consisted of cells was introduced from the central channel as the dispersed phase (Q_{Cell}). Accordingly, the fluids met at the cross-junction (Fig. 7 (b)), where droplets of the dispersed phase formed as the fluids flowed into the main channel to a glass vial at the device outlet. The flow easily controlled the end goal of obtaining spherical or nearly spherical particles by adjusting the flow rates of the continuous and dispersed phases. The relationships between the flow rates and hollow PLGA microcapsules stability was investigated by two sets of experiments: (1) By varying dispersed flow and maintaining continuous flow at 0.10 ml/min, and (2) By varying the dispersed flow while maintaining continuous flow at 0.25 ml/min continuous

6.2.5   Preparation of Hollow PLGA Microcapsules for Imaging

Microcapsules were suspended in PBS and placed on a glass slide for imaging. The sizes of microcapsules were analyzed using *ImageJ* software (National Institutes of Health, Bethesda, Maryland, USA).

6.2.6   hGBM Passive Encapsulation in Hollow PLGA Microcapsules

The principle of passive encapsulation was based on the microcapsule formation by combining two or more streams of immiscible fluids that passed through a small orifice located downstream of the three channels, causing it to break up into discrete microcapsules. The cells were encapsulated in portions of the fluid volumes that were segmented by PLGA flow from the side channels. The encapsulation efficiency (η) was calculated as:

$$\boldsymbol{\eta\% = \frac{Total\ number\ of\ cells\ encapsulated}{Total\ number\ of\ cells\ appears\ in\ an\ image} \times 100\%}$$

The cells were stained with Texas Red; a red fluorescent dye used for cell staining. The cell suspension was centrifuged and the supernatant was removed. Next, 3 ml of DMEM was added to dilute cells to a concentration of 500,000 cells/ml and loaded into a 3 ml plastic syringe, which connected to the device core inlet. The 10% w/v PLGA was prepared and loaded into two 5 ml plastic syringes. The syringes were connected to microfluidic device inlets. The dispersed phase flow rate was set to 0.10, 0.20 and 0.50 ml/min and the continuous phase flow rate was set to 0.10 ml/min on syringe pumps. The samples were collected in glass vials for one minute. After encapsulation, the fluorescence measurements were taken at 560 nm wavelength using a Zeiss confocal microscope. The images were analyzed using *ImageJ.*

6.2.7   hGBM Cells in Microcapsules

After the samples were collected in glass vials, the microcapsules were washed with 5 ml PBS. In a laminar airflow hood, a 500 µl DMEM medium was added and placed in an incubator (95% air, 5% CO_2 and 37 °C). After 24 hours, the samples were observed with an optical microscope.

6.2.8   Post-Encapsulation Cell Viability

Trypan Blue stain was used to discriminate between viable and non-viable cells. A 100 µl of the stain was added to the samples and then incubated for 15 minutes. The stain solution was removed from the samples and washed with 1 ml of PBS three times. Non-viable cells were found blue, while the stain did not get into the viable cells. The cells viability was calculated by dividing the number of viable cells over the total number of viable and non-viable cells

6.3   Results and Discussion

6.3.1   Synthesis of Hollow PLGA Microcapsules

The PLGA hollow microcapsules were generated in a flow-focusing droplet generation microfluidic device with a "diverged Y-shape". The cell suspension was used as dispersed phase flowing through the central channel with the PLGA solution as continuous phase flowing through the two side channels. The PLGA solution was pushed through the side channels as the continuous phase, denoted as Q_{PLGA}. The cell suspension was introduced from the central channel as the dispersed phase. The flow of the suspension was controlled with syringe pumps and denoted as Q_{Cell}. The fluids met at the cross-junction, where droplets of the dispersed phase formed as the fluids flowed into the main channel. Hollow PLGA microcapsules were produced using 10% (w/v) PLGA. The

formed microcapsules exhibited intact spherical surfaces. The ratio between the dispersed and continuous phases played a key role in the stability of microcapsules. The experiments showed that microcapsules were not stable at lower ratios (less than 0.10) between dispersed to continuous. On the other hand, if the ratio was larger than 0.10, microcapsules were stable and intact (Table I). The microcapsules prepared at higher ratios experienced a faster phase separation followed by affinity to stabilize over time.

Table I. Flow rate ratios and microcapsule stability

Continuous Phase Flow Rate (ml/min)	Dispersed Phase Flow Rate (ml/min)	Ratio (Q_{cell}/Q_{PLGA})	Microcapsules intact
0.10	0.01	0.05	No
	0.05	0.25	Yes
	0.10	0.50	Yes
	0.50	2.50	Yes
0.25	0.05	0.10	No
	0.10	0.20	Yes
	0.50	1.0	Yes

6.3.2   Microcapsules Size Analysis

The samples were collected at different Q_{cell}/Q_{PLGA} ratios to study the microcapsule sizes. The continuous phase was maintained at 0.10 ml/min as the dispersed phase was varied. The analysis was done on the optical micrographs (n = 2) of the samples. The *ImageJ* was used to count and determine the diameters of microcapsules. The one-way ANOVA analysis was carried out on the data to ascertain statistical significance.
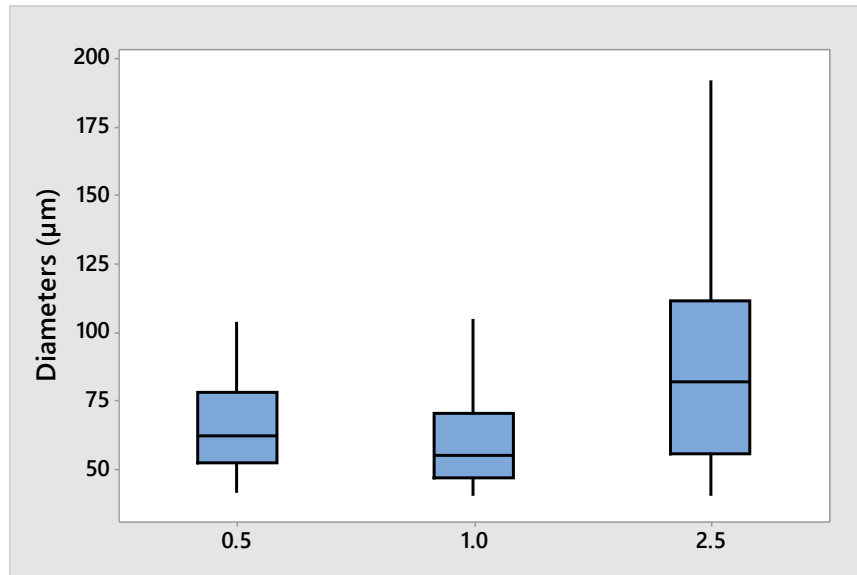
Figure 2 Hollow PLGA microcapsules average diameters box plot analysis using optical images (n = 2). The microcapsules average diameters are reported at three Q_{cell}/Q_{PLGA} ratios of 0.5, 1.0 and 2.5. The larger microcapsule diameters were observed for higher ratio. (N = 348, p-value $\ll 0.05$)

The Figure 2 shows the microcapsule size with respect to the Q_{cell}/Q_{PLGA} ratios at a set continuous phase flow rate of 0.10 ml/min. The microcapsule sizes varied as the Q_{cell}/Q_{PLGA} ratio changed without modifying the microfluidic device geometry and dimensions.

6.3.3   hGBM Passive Encapsulation in Hollow PLGA Microcapsules

For suspended cells traveling through a microfluidic channel, the distribution and the timing of their arrival at the site of encapsulation are random. Passive encapsulation is a method that encapsulates cells by modifying flow rate, cell concentration and channel width. Herein, we regulated the Q_{cell}/Q_{PLGA} ratio to encapsulate hGBM cells (Figure 3). The cells were suspended in the medium solution at the density of 500,000 cells/ml. The
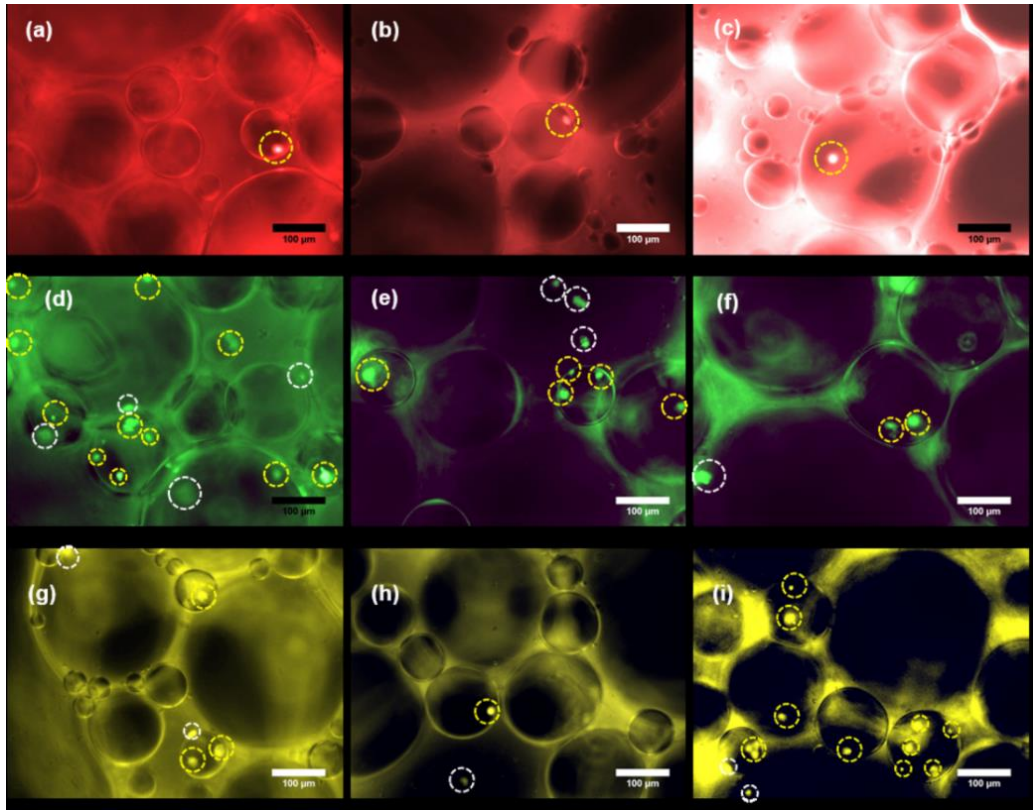
Figure 3 Cells encapsulated in hollow PLGA microcapsule at continuous phase flow rate of 0.10 ml/min and dispersed phase at 0.10, 0.20,and 0.50 ml/min. (a-c) Q_{cell}/Q_{PLGA} = 0.5 (d-f) Q_{cell}/Q_{PLGA} = 1.0 (g-i) Q_{cell}/Q_{PLGA} = 2.5. Yellow circles: cells inside microcapsule, white circles: cells outside microcapsule. (Scale Bar 100 μm)

encapsulation efficiency (η) showed particular profiles when continuous phase flow rate was at 0.10 ml/min and dispersed phase varied at 0.10, 0.20, and 0.50 ml/min. A 100% η was achieved at the lowest Q_{cell}/Q_{PLGA} ratio.
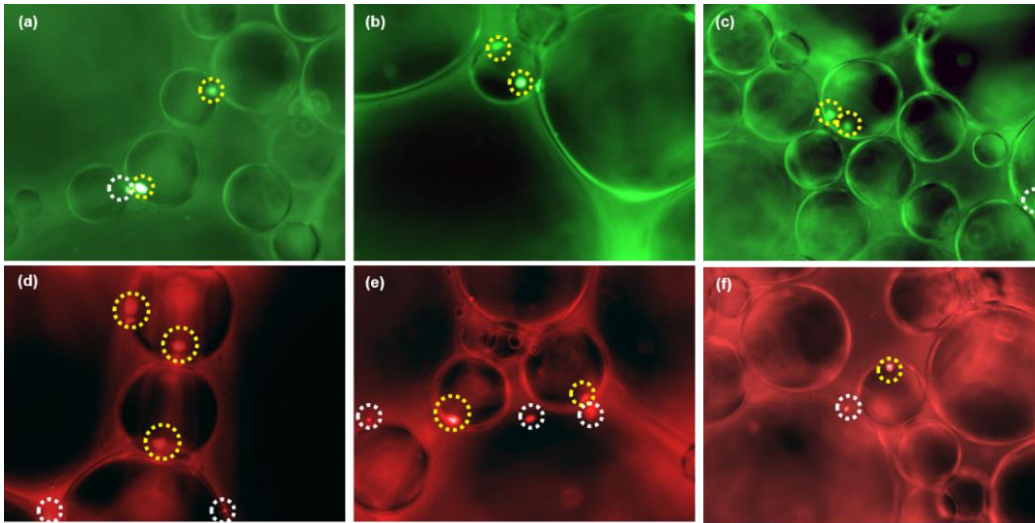
Figure 4 Cells encapsulated in hollow PLGA microcapsule at continuous phase flow rate 0.25 ml/min and dispersed phase varied at 0.30 and 0.50 ml/min. (a-c) Q_{cell}/Q_{PLGA} = 0.6 (d-f) Q_{cell}/Q_{PLGA} = 1.0. Yellow circle: cell inside microcapsule, white circle: cell outside microcapsule

The continuous phase flow rate was then increased by 2.5 times and the Q_{cell}/Q_{PLGA} ratio was maintained at > 0.10 (Figure 4). The η changed when continuous phase flow rate was at 0.25 ml/min and dispersed phase was varied from 0.30 to 0.50 ml/min. The results showed lower η at higher continuous phase flow rate.

In order to understand the relation of continuous phase flow rate and passive encapsulation, the cells per microcapsule were counted and plotted vs. the Q_{cell}/Q_{PLGA} ratio. Table II shows the η and number of cells captured for various encapsulation conditions. For 0.10 ml/min continuous phase flow rate, the analysis showed higher cells per microcapsule at higher Q_{cell}/Q_{PLGA} ratio. Although the η at Q_{cell}/Q_{PLGA} = 2.5 was lower but the tradeoff was that more cells could be encapsulated at higher cell suspension flow rate. By comparing same ratio of Q_{cell}/Q_{PLGA} (= 1.0) at higher continuous phase flow rate (0.25

ml/min), we noticed the η dropped. The data shows both dispersed and continuous flow rates played a key role in cell encapsulation efficiencies and number of cells encapsulated.

Table II.   List of passive encapsulation analysis quantities at different continuous phase flow rate

Continuous Phase flow rate: 0.10 ml/min		
Q_{cell}/Q_{PLGA} Ratio	Average η (%)	Average cells per microcapsule
0.5	100[a]	1 [a]
1.0	68 ± 5[a]	1.5 ± 1 [a]
2.5	64 ± 17[a]	1.8 ± 1.3 [a]
Continuous Phase flow rate: 0.25 ml/min		
Q_{cell}/Q_{PLGA} Ratio	Average η (%)	Average cells per microcapsule
0.6	72 ± 26[a]	1.5 ± 0.6 [a]
1.0	52 ± 13[a]	1.4 ± 0.9 [a]

[a] n = 3

6.3.4   Glass vs. Polystyrene Substrates

Microcapsules were generated using microfluidic device in which PLGA solution and cell suspension met at the cross-junction. The microcapsules were gathered on glass and polystyrene substrate and placed in an incubator (95% air, 5% CO_2, 37 °C). PLGA is a non-polar molecule and provided hydrophobic shell to microcapsules. The hollow PLGA microcapsules maintained spherical shape on the glass but were flattened on polystyrene substrates (Figure 5). Commonly, polystyrene is treated to be hydrophilic for the 2D cell culture applications where cells grow in a planar layer. The hollow PLGA microcapsules maintained their shapes in glass vials and on glass substrates. The hollow PLGA
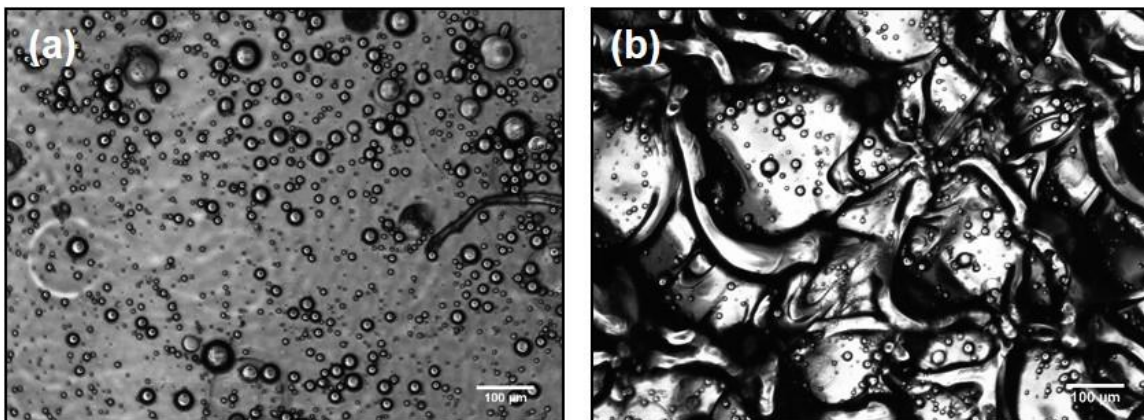
Figure 5 Surface interface comparison of hollow PLGA microcapsules with (a) glass, and

(b) polystyrene substrate. (Scale bar = 100 µm)

microcapsules were thus barriers to the cells environment. The cells this kept their

biochemical and biomechanical properties closer to *in vivo* conditions.[27,28,29]

6.3.5   *Post-Encapsulation Cell Viability*

The encapsulated cells were observed 24-hour post-encapsulation at 3.2X magnification. Figure 6(a) shows cells encapsulated in hollow PLGA microcapsules. Cells appeared as black dots in PLGA microcapsules. In Figure 6(b), a sample was collected from glass vial and methylene chloride was added to it and placed on glass coverslip to observe at higher magnification. The cell viability is calculated as the number of viable cells divided by total number of cells in an image. The average calculated viability of the sample was 78%. The samples were examined immediately under a microscope after Trypan blue staining (Figure 6(c)).
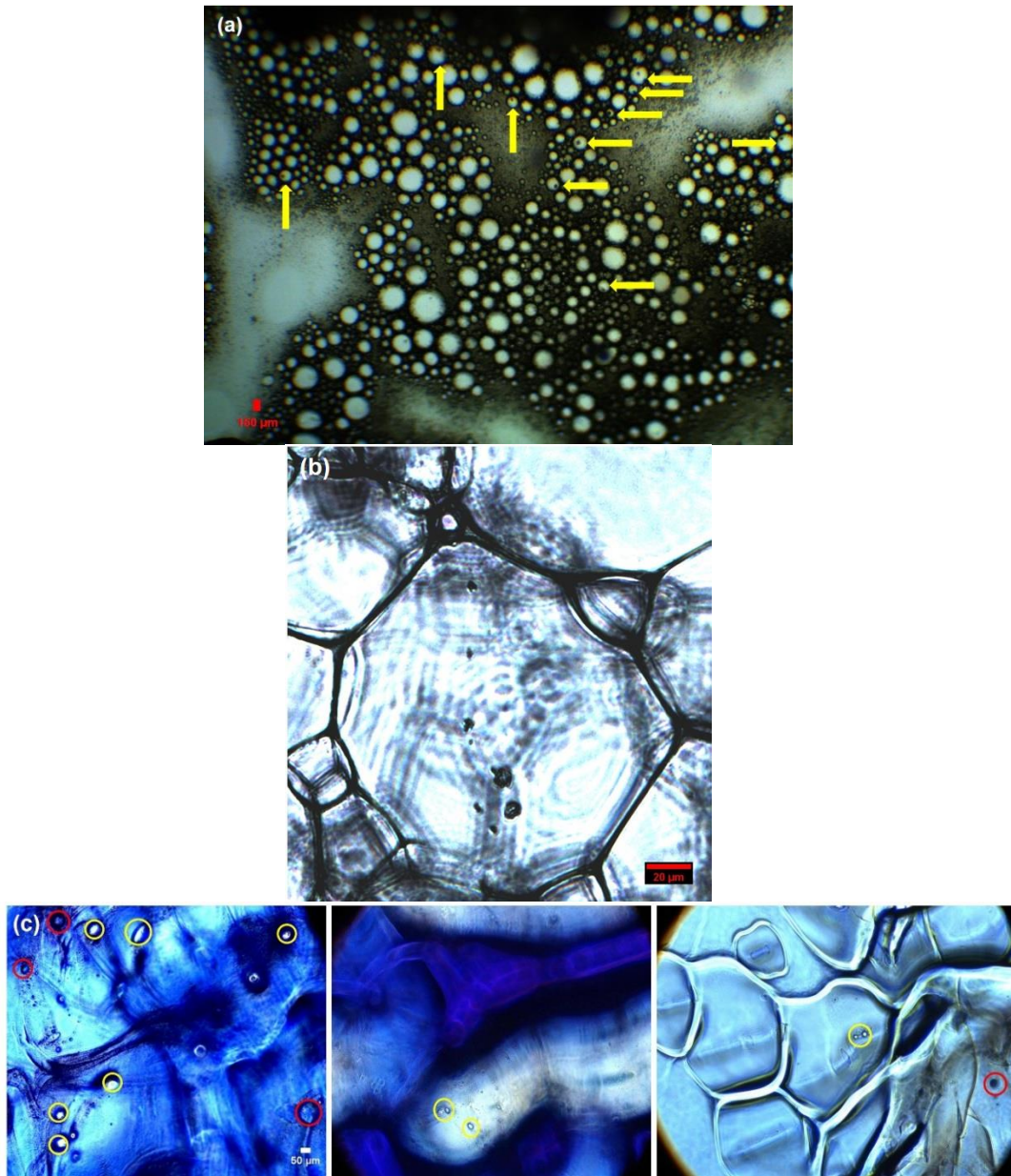
Figure 6 Cells observed 24-hour post-encapsulation with a microscope. (a) Cells at 3.2X magnification. Yellow arrows show encapsulated cells. (b) Cells at 20X magnification. (c) Micrographs after Trypan Trypan blue staining. Yellow circles show healthy cells and red circles show nonviable cells. The average viability is 78% (n =3).

118

6.4   Conclusions

This paper demonstrated a simple, robust and reproducible technology to encapsulate cells in small PLGA microcapsules (average 204 nl). These microencapsulations are perfect to perform single cell analysis and interactions studies. This platform can be used to characterize the genes and proteins of tumorous and other diseased cells comprehensively. Tumors are not homogenous in their mutational profile, i.e., various cells develop new mutations within the tumor, often making them genotypically distinct from their neighbor, one tumor could contain thousands of potential antigens for the immune system to target. This simple encapsulation can provide rapid means to encapsulate cells for tumor profiling at the single cell level, thus providing a complete picture of the disease. The microfluidic approach creates mild conditions, which do not damage the cells. The successful encapsulation of cells is an essential step that can enable the development of a new class of flow cytometry that can be used in noninvasive diagnostics, precision medicine, and next-generation sequencing.

6.5   Acknowledgment

6.6   References

[1]T. M. Chang, *Science 146, 524 (1964).*

[2]T. P. Lagus, J. F. Edd, J. Vis. Exp 64, e4096 (2012).

[3]M. Zagnoni, G. Le Lain, & J.M. Cooper, Langmuir: the ACS journal of surfaces and colloids 26, 14443 (2010).

[4]X. Z. Niu, F. Gielen, J. B. Edel, & A.J. deMello, A.J. A, Nat. Chem. 3, 437 (2011).

[5]M. E. Vincent, W. Liu, E. B. Haney & R. F. Ismagilov, Chemical Society reviews 39, 974 (2010).

[6]A. Huebner, et al. Chemical communications 12, 1218 (2007).

[7]J. C. Love, J. L. Ronan, G. M. Grotenbreg, A. G. van der Veen & H. L. Ploegh, Nature biotechnology 24, 703 (2006).

[8]E. M. Bradshaw, et al. Clin. Immunol 129, 10 (2008).

[9]W. S. Liu, H. J. Kim, E. M. Lucchetta, W. B. Du & R. F. Ismagilov, Lab on a chip 9, 2153(2009).

[10]J. Q. Boedicker, L. Li, T. R. Kline & R. F. Ismagilov, Lab on a chip 8, 1265 (2008).

[11]S. Koster, et al. Lab on a chip 8, 1110 (2008).

[12]R. T. Kelly, J. S. Page, I. Marginean, K. Tang & R. D. Smith, Angew Chem. Int. Ed. Engl. 48, 6832 (2009).

[13]J. Hong, A. J. deMello & S. N. Jayasinghe, Biomedical materials 5, 21001 (2010).

[14]A. M. Rokstad, S. Holtan, S. Strand, B. Steinkjer, L. Ryan, B. Kulseng, G. Skjak-Braek, and T. Espevik, Cell Transplant 11, 313 (2002).

[15]S. Prakash and T. M. Chang, *Biotechnology and Bioengineering 46, 621* (1995).

[16]E. Nafea, A. M. Poole-Warren and P. Martens, *Journal of Controlled Release* 154, 110 (2011).

[17]R. H. Li, *Advanced Drug Delivery Reviews* 33, 87 (1998).

[18]B. V. Slaughter, S. S. Khurshid, O. Z. Fisher, A. Khademhosseini and N. A. Peppas, *Advanced Materials* 21, 3307 (2009).

[19]F. Lim and A. Sun, *Science 210, 908* (1980).

[20]B. Strand, L. Ryan, P. Veld, B. Kulseng, A. M. Rokstad, G. Skjåk-Braek and T. Espevik, *Cell Transplantation 10, 263* (2001).

[21]C. Toso, Z. Mathe, P. Morel, J. Oberholzer, D. Bosco, D. Sainz-Vidal and T. Berney, *Cell Transplantation 14, 159* (2005).

[22]J. M. Van Raamsdonk, R. M. Cornelius, J. L. Brash and P. L. Chang, *Journal of Biomaterials Science, Polymer Edition 13, 863* (2002).

[23]H. Chen, W. Ouyang, M. Jones, T. Haque, B. Lawuyi and S. Prakash, *Journal of Microencapsulation 22, 539* (2005).

[24]E. Piskin, *Journal of Biomaterials Science, Polymer Edition, 6, 775,* (1995).

[25]I. Gill and A. Ballesteros, *Trends in Biotechnology 18*, 282 (2000).

[26]I. Gill and A. Ballesteros, *Trends in Biotechnology 18, 469* (2000).

[27]W. J. Ho, et al., Cancer Science 101, 2673 (2010).

[28]V. S. Nirmalanandhan, et al., Assay Drug Dev Technol 8, 581 (2010).

[29]E. Millerot-Serrurot, et al., Cancer Cell Int 10, 26 (2010): 26.

[27]U. H. Pham, M. Hanif, A. Asthana and S. M. Iqbal, Journal of Applied Physics 117, 214703 (2015).

[28]Y. Wan, M. A. Mahmood, N. Li, P. B. Allen, Y. Kim, R. Bachoo and S. M. Iqbal, Cancer 118, 1145 (2012).

Chapter 7

Future Research Directions

7.1   Introduction

        In this chapter, we are discussing future research directions and potential use of developed single-cell analysis platforms. It includes the scope of more work that would follow the current research work.

7.2   Ion-sensitive Field-effect Transistors with Micropillared gates for Sensing of

        Cancer Cell Ion Exchange as a Biomarker

        Computer simulations provide a bridge between laboratory experiments and the understanding of the physics. This simulation can be used to design and optimize different ion exchange sensors models to study and capture the behavior of cancer cell. The optimization of the micropillar physical dimensions diameter can be done before investing in fabrication processes and laboratory experiments. The next step to advance this work is to design masks and identify critical parameters for the fabrication process. The masks to fabricate this device is shown in Figure 7.
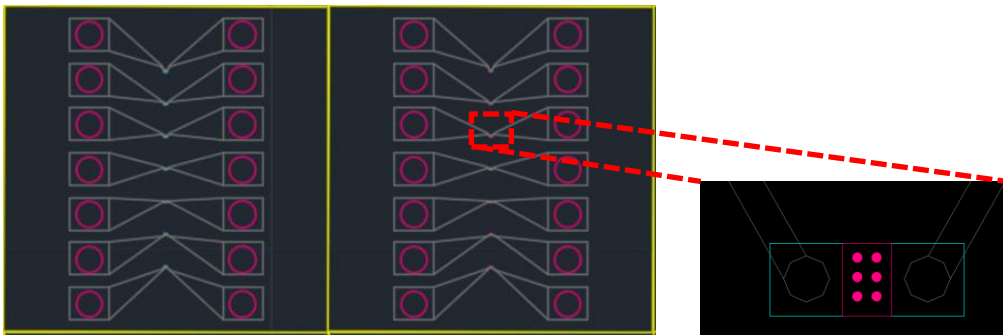

Figure 7.1 Total of four masks have been identified to fabricate the sensor. The image shows the four mask overlaid on top

Four dark field mask have been identified to fabricate this device in a 4 inch, 500 μm thick and n-type silicon wafer. The design size is 5 mm x 5 mm (called a die). There will be total 144 die in one wafer. Each die will have a total of seven devices. Total of 1008 devices per wafer.

The Test and analyze sensor behavior will require to setup semiconductor parameter analyzer tool. Also, a probe card can be used to collect the measurements at different ionic solution concentration.

After well electrical characterization of the device, the experimental setup can be started with different cells type: excitable versus nonexcitble, normal cells versus cancer cells, and different cancer cell type

7.3   Surface Functionalization of Nanoporous PLGA Microparticles

Enhancing surface area of microparticles by introducing nanopores on the surface can increase the density of the functionalization of microparticles. Therefore, we can maximize selectively targeting cancer cell ion channels, which are a potentially advanced therapeutic for cancer. An application of this method can be used to functionalize microparticle with ion channels blockers and study stability, toxicity and the efficacy. Also, study targeting efficiency *in vitro and in vivo*. This approach can be used to design smart nanoporous PLGA microparticles, in which ion channels blockers attached to cancer cell surface and PLGA would be loaded with anti-cancer drug (Figure 7.2)
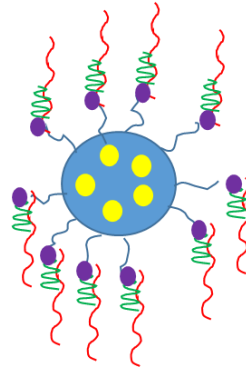
123

Figure 7.2 Smart nanoporous PLGA microparticles

7.4   Glioblastoma Multiforme Heterogeneity Profiling with Solid-state Micropores

These results confirm that the patient's tumor samples contained heterogonous and dissimilar morphological subtypes, and we could map the results to each specific subtype. In clinical settings, such matching system can help against extensive heterogeneity of GBM tumor cells from patient's brain tissue to classify the subtype by comparing the data to GBM cell subtype library (Figure 7.3).
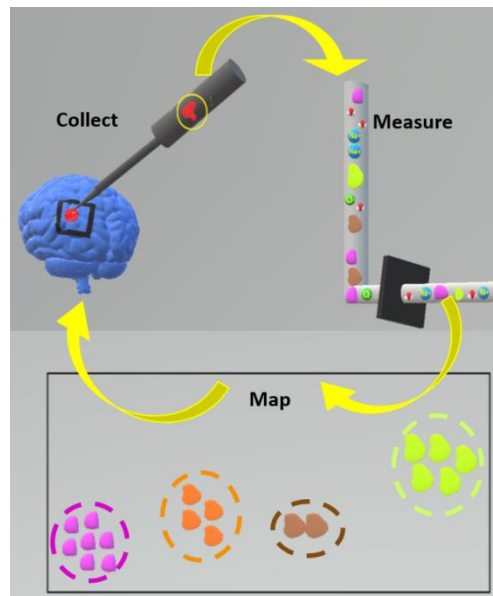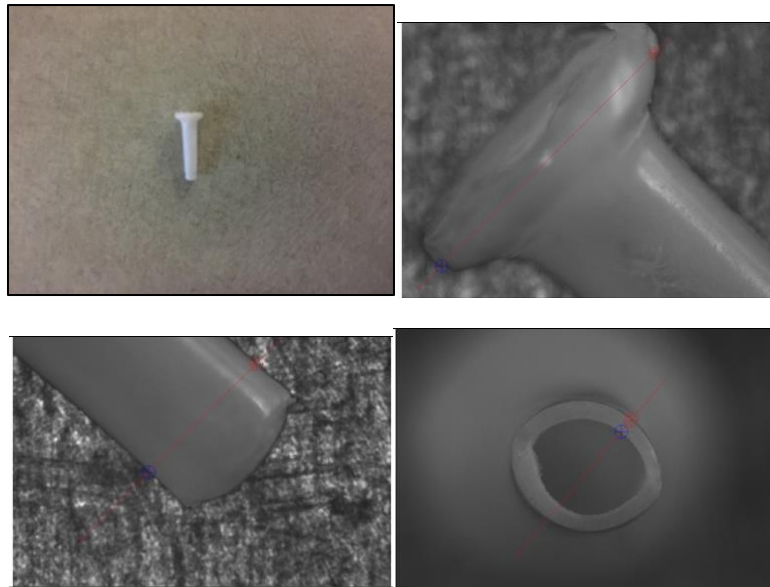

Figure 7.3 GBM cells library

Figure 7.4 Brain cancer proposed device

Herein, we also proposed to develop brain cancer drug reservoir to be implanted in patients during surgery. The device looks like a plug to be inserted and filled with anti-cancer drug (Figure 7.4).

7.5   A Facile Microfluidic Approach to Create Microencapsulation for Single Cell Confinements

This platform can be used to characterize the genes and proteins of tumorous and other diseased cells comprehensively. Tumors are not homogenous in their mutational profile, i.e., various cells develop new mutations within the tumor, often making them genotypically distinct from their neighbor, one tumor could contain thousands of potential antigens for the immune system to target. Characterize genes and protein of cancer cell single cell versus cells culture. This approach can be used for drug screening and multi drug resistance studies, in which identified the specific drug interaction with single cell in very fast, simple and low cost technique.

Appendix A

Permission from co-authors and publishers

To Whom It May Concern

Subject: <u>Permission to request/reprint in preparation/in press/published</u> <u>manuscript in Ph.D. Dissertation</u>

I am a corresponding author on the paper titled "Ion-sensitive Field-effect Transistors with Micropillared gates for Sensing of Cancer Cell Ion Exchange as a Biomarker" I grant permission to Mr. Mohammad G. Abdallah to reuse/reprint this manuscript in his Ph.D. dissertation.

DR. SAMIR IQBAL

Name: _____

Signature: _____

Email: _____SMIQBAL@IEEE.ORG_____

04/24/18

Date: _____

To Whom It May Concern

Subject: <u>Permission to request/reprint in preparation/in press/published manuscript in Ph.D. Dissertation</u>

I am a corresponding author on the paper titled "Glioblastoma Multiforme Heterogeneity Profiling with Solid-state Micropores" I grant permission to Mr. Mohammad G. Abdallah to reuse/reprint this manuscript in his Ph.D. dissertation.

Name: DR. SAMIR IQBAL

Signature: _____

Email: _____ SMIQBAL@IEEE.ORG _____

Date: _____ 04/24/18 _____

To Whom It May Concern

Subject: <u>Permission to request/reprint in preparation/in press/published manuscript in Ph.D. Dissertation</u>

I am a corresponding author on the paper titled "Surface Functionalization of Nanoporous PLGA Microparticles" I grant permission to Mr. Mohammad G. Abdallah to reuse/reprint this manuscript in his Ph.D. dissertation.

DR. SAMIR IQBAL

Name: _____

Signature: _____

Email: SMIQBAL@IEEE.ORG

04/24/18

Date: _____

To Whom It May Concern

Subject: <u>Permission to request/reprint in preparation/in press/published</u> <u>manuscript in Ph.D. Dissertation</u>

I am a corresponding author on the paper titled "A Facile Microfluidic Approach to Create Microencapsulation for Single Cell Confinements" I grant permission to Mr. Mohammad G. Abdallah to reuse/reprint this manuscript in his Ph.D. dissertation.

DR. SAMIR IQBAL

Name: _____

Signature: _____

Email: _____SMIQBAL@IEEE.ORG_____

04/24/18

Date: _____

To Whom It May Concern

Subject: <u>Permission to request/reprint in preparation/in press/published</u>
<u>manuscript in Ph.D. Dissertation</u>

I am a co-author on the paper titled "Surface Functionalization of
Nanoporous PLGA Microparticles" I grant permission to Mr.
Mohammad G. Abdallah to reuse/reprint this manuscript in his Ph.D.
dissertation

Name: _Kim, Young - tae_

Signature: _____

Email: _Ykim @ uta.edu_

Date: _4/24/18_

To Whom It May Concern

Subject: <u>Permission to request/reprint in preparation/in press/published manuscript in Ph.D. Dissertation</u>

I am a co-author on the paper titled "Ion-sensitive Field-effect Transistors with Micropillared gates for Sensing of Cancer Cell Ion Exchange as a Biomarker" I grant permission to Mr. Mohammad G. Abdallah to reuse/reprint this manuscript in his Ph.D. dissertation

Name: _Kim, Young-tae_

Signature: _____

Email: _ykim @ uta.edu_

Date: _~~4/23~~ 4/24/18_

To Whom It May Concern

Subject: <u>Permission to request/reprint in preparation/in press/published manuscript in Ph.D. Dissertation</u>

I am a co-author on the paper titled "A Facile Microfluidic Approach to Create Microencapsulation for Single Cell Confinements" I grant permission to Mr. Mohammad G. Abdallah to reuse/reprint this manuscript in his Ph.D. dissertation

Name: _Kim, Young-tae_

Signature: _____

Email: _Ykim @ Uta. edu_

Date: _4/24/18_

To Whom It May Concern

Subject: Permission to request/reprint in preparation/in press/published manuscript in Ph.D. Dissertation

I am a co-author on the paper titled "Glioblastoma Multiforme

Heterogeneity Profiling with Solid-state Micropores" I grant permission

to Mr. Mohammad G. Abdallah to reuse/reprint this manuscript in his

Ph.D. dissertation.

Name: _Kim, Young-tae_

Signature: _____

Email: _xkim@ Uta.edu_

Date: _4/24/18_

To Whom It May Concern

Subject: <u>Permission to request/reprint in preparation/in press/published manuscript in Ph.D. Dissertation</u>

I am a co-author on the paper titled "Surface Functionalization of Nanoporous PLGA Microparticles" I grant permission to Mr. Mohammad G. Abdallah to reuse/reprint this manuscript in his Ph.D. dissertation

Name: _Muhammed Yousufuddin_

Signature: _Muflal_

Email: _myousuf@untdallas.edu_

Date: _4/23/18_

To Whom It May Concern

Subject: <u>Permission to request/reprint in preparation/in press/published manuscript in Ph.D. Dissertation</u>

I am a co-author on the paper titled "Glioblastoma Multiforme Heterogeneity Profiling with Solid-state Micropores" I grant permission to Mr. Mohammad G. Abdallah to reuse/reprint this manuscript in his Ph.D. dissertation.

Name: _Turki Almugaiteeb_

Signature: _Turki_

Email: _turki.almugaiteeb@UTA.edu_

Date: _04.23.2018_

To Whom It May Concern

Subject: <u>Permission to request/reprint in preparation/in press/published manuscript in Ph.D. Dissertation</u>

I am a co-author on the paper titled "Surface Functionalization of Nanoporous PLGA Microparticles" I grant permission to Mr. Mohammad G. Abdallah to reuse/reprint this manuscript in his Ph.D. dissertation

Name: Serkan YAMAN

Signature: _Serkan Yaman_

Email: serkan.yaman@mdvs.utd.edu

Date: 04-23-2018

To Whom It May Concern

Subject: <u>Permission to request/reprint in preparation/in press/published manuscript in Ph.D. Dissertation</u>

I am a co-author on the paper titled "Ion-sensitive Field-effect Transistors with Micropillared gates for Sensing of Cancer Cell Ion Exchange as a Biomarker" I grant permission to Mr. Mohammad G. Abdallah to reuse/reprint this manuscript in his Ph.D. dissertation

Name: _Rayan Khan_

Signature: _RayanKhan_

Email: _rayan.Khan@mavs.uta.edu_

Date: _4/5/2018_

To Whom It May Concern

Subject: <u>Permission to request/reprint in preparation/in press/published</u>
<u>manuscript in Ph.D. Dissertation</u>

I am a co-author on the paper titled "A Facile Microfluidic Approach to
Create Microencapsulation for Single Cell Confinements" I grant
permission to Mr. Mohammad G. Abdallah to reuse/reprint this
manuscript in his Ph.D. dissertation

Name: _____Rayan Khan_____

Signature: _____Rayan Khan_____

Email: _____rayan.Khan@mavs.uta.edu_____

Date: _____4/5/2018_____

To Whom It May Concern

Subject: <u>Permission to request/reprint in preparation/in press/published</u>
<u>manuscript in Ph.D. Dissertation</u>

I am a co-author on the paper titled "Surface Functionalization of
Nanoporous PLGA Microparticles" I grant permission to Mr.
Mohammad G. Abdallah to reuse/reprint this manuscript in his Ph.D.
dissertation

Name: _Bayan Khan_

Signature: _Bayankhan_

Email: _rayan.khan @mavs.uta.edu_

Date: _4/5/2018_

To Whom It May Concern

Subject: <u>Permission to request/reprint in preparation/in press/published</u>
<u>manuscript in Ph.D. Dissertation</u>

I am a co-author on the paper titled "Glioblastoma Multiforme

Heterogeneity Profiling with Solid-state Micropores" I grant permission

to Mr. Mohammad G. Abdallah to reuse/reprint this manuscript in his

Ph.D. dissertation.

Name: Muhammad Usman Raza

Signature: _____

Email: raza.muhammadusman@mavs.uta.edu

Date: 04/25/2018